Resistance Welding of Automotive Fuel Tank Grade Steel

A DISSERTATION SUBMITTED IN PARTIAL FULFILMENT
OF THE
REQUIREMENT FOR THE AWARD OF THE DEGREE

Of

Master of Technology in Material Engineering
Department of Metallurgical and Material Engineering
Faculty of Engineering and Technology
Jadavpur University Kolkata 700032
Session: 2017-2019

by

Md Tahsin Akhtar
Exam Roll no: M4MAT19003
Registration no: 140913 of 2017-2018

Under the Guidance
Of

Dr. Amrita Kundu
Assistant Professor
Department of Metallurgical
and Material Engineering
Jadavpur University

Dr. Mahadev Shome
Industrial Supervisor
Head
Material Welding and Joining group
Research and Development
Tata Steel Limited

Jadavpur University

Kolkata 700032

2019

FACULTY OF ENGINEERING AND TECHNOLOGY

Department of Metallurgical and Material Engineering

Declaration of Originality and Compliance of Academic Ethics

I hereby declare that the work **"Resistance welding of Automotive Fuel Tank Grade Steel"** contains literature survey and original research work by the undersigned candidate, as a part of his Master of Technology in Material Engineering studies. All information in this document have been obtained and presented in accordance with academic rules and ethical conduct. I also declare that, as required by these rules and conduct, I have fully cited and referenced all material and results that are not original to this work.

Place: Kolkata

Date:

Md Tahsin Akhtar

Examination Roll Number: M4MAT19003

Registration Number: 140913 of 2017-18

Certificate of Approval

This thesis is hereby approved as a creditable study of an engineering subject carried out and presented in a manner satisfactory to warrant its acceptance as a prerequisite to the degree for which it has been submitted. It is understood that by this approval the undersigned do not necessarily endorse or approve any statement made opinion expressed or conclusion drawn therein but approve the thesis only for the purpose for which it is submitted.

(SIGNATURE OF EXAMINERS)

COMMITTEE ON FINAL EXAMINATION FOR

EVALUATION OF THE THESIS

Acknowledgements

I express deep sense of gratitude and thankfulness to my supervisor **Dr. Amrita Kundu**, Assistant Professor, Metallurgical and Material Engineering Department, Jadavpur University. This work would not have been possible without her guidance, cooperation and constructive criticism. Her unflinching courage and conviction always inspired me and enriched my growth from a casual science student to a scientific researcher. I feel blessed in every way to have been under her tutelage and I would be ever grateful to her for her untiring efforts. I had privilege of imbibing many valuable attributes from Amrita Ma'am like dedication, will power, faith in oneself, self-dependence and a burning desire to achieve one's goal. Dear Ma'am, I have no words to express my feeling, but I would like to thank you from the bottom of my heart for picking me up as a research student and guiding me so meticulously and providing unconditional support and keeping a strong faith in me during my hard times.

I am indebted to **Dr. Akshay Kumar Pramanick**, HOD, Metallurgical and Material Engineering Department, Jadavpur University for providing me valuable guidance and allowing me to utilize the facilities in his laboratory.

I owe my deepest gratitude to **Dr. Mahadev Shome**, Head, Material Characterization and Joining Research Group, Research and Development, TATA Steel limited for his detailed review, constructive remarks and excellent advice during my research period.

My words are falling short to express my gratitude to **Soumyajit Koley**, Principal Researcher, Research and Development, TATA Steel limited for his guidance, advice and enthusiasm. Besides his academic brilliance and infectious passion on engineering which has helped me to formulate, design and execute the work, my biggest takeaway is to be associated with his which has benefited me immensely in many aspects of life. Dear Sir, I am indebted to you for your Belief Perseverance on me and consistence motivation.

I would like to thank **TATA Steel India** for providing the essential research facilities.

I would like to give special thanks to **TATA steel staff** for helping me to utilize the facilities in the laboratory. Moreover, I would like to thank all staff and respected teachers and professors of Metallurgical and Material Engineering Department, Jadavpur University for their valuable guidance and cooperation.

Words cannot express my deepest gratitude towards **my dear parents**. They raised me, supported me and allowed me to live in my own way. My bundle of acknowledgement will always have a special place for my seniors and friends. They were always with me in my ups and downs.

I highly acknowledge **All India Council for Technical Education (AICTE)** for the scholarship without which it would have been very difficult to perform this study.

Tahsin

CONTENTS

Abstract

Present thesis addresses two important aspects of resistance spot welding (RSW) and resistance seam welding (RSeW). First part of the thesis focusses on developing a data-centric prediction model for critical nugget diameter while the second part addresses the electrode life estimation.

Critical nugget diameter (Φ_C) indicates the diameter of weld nugget at which the failure mode changes from brittle interfacial failure (IF) to pull-out failure (PF). Pull-out failure is preferable as it signifies higher energy absorption capacity. Thereby critical nugget diameter plays an important role for approval of a new steel grades. Hence predicting Φ_C without carrying out real welding experiments is an important subject. The work done in this area is not comprehensive. The present thesis is concerned about creation and validation of a data centric model based on spot welding data collected from 60 published literatures. Multivariate regression analysis has been found suitable for modelling small subset (i.e., 8 number of the observation) and hence was not pursued. An artificial neural network (ANN) based model has been developed which can predict the Φ_C from steel properties (such as thickness, chemistry (C, Mn, Si content), mechanical properties (YS, UTS and %El) and coating type) for the complete dataset (i.e., 100). The model has been validated against experimental data. However, the effect of welding parameter (electrode force, welding current and time) on Φ_C could not be modelled owing to the higher uncertainty associated with the published data.

The present thesis also addresses an important issue of estimating electrode life of standard Copper based electrodes during welding of primary coated (zinc based) and secondary coated (organic/inorganic) steels. Typically, these steels are commercially produced for automotive fuel tank applications where RSW and RSeW are used. However, there is limited literature on the electrode life estimation. RSW and RSeW experiments were done to generate weldability process window and corresponding mechanical properties for 0.8 mm thick secondary coated galvannealed interstitial free (IF-GA steel. This information was subsequently used for determining the parameters for electrode endurance tests. Commercially available Cu-Cr-Zr alloy based electrodes were selected for the study. It was found that the electrode can withstand up to 1500 number of RSW spots without loss in nugget quality which is acceptable. It was observed that 20 m of continuous RSeW can be done without affecting the weld quality in terms of the mechanical properties and the leak performance.

LIST OF ABBREVIATIONS

RSW	Resistance Spot Welding
RSeW	Resistance Seam Welding
IF	Inter Facial failure
PF	Pull-out Failure
PIF	Partial Interfacial Failure
H_{WN}	Weld Nugget Hardness
H_{FL}	Failure Location Hardness
BHN	Brinell Hardness Number
YS	Yield Stress
UTS	Ultimate Tensile Strength
EL/ ε	Elongation
$\emptyset_{cr}$	Critical nugget Diameter
ANN	Artificial Neural Network
IF steel	Interstitial Free Steel
GA Steel	Galvannealed Steel
BM	Base Metal
HAZ	Heat Affected Zone
FZ	Fusion Zone
MFDC	Medium Frequency Direct current
AC	Alternating Current
Dc	Direct Current
TS	Tensile Shear
CT	Cross Tension
CP	Coach Peel
AWS	American Welding Society
JIS	Japanese Industrial Standard
BS	British Standard
DP	Dual Phase
TRIP	Transformation Induced Plasticity
TWIP	Twinning-Induced Plasticity
AHSS	Advanced High Strength Steel
HSLA	High Strength Low Alloy Steel
PLC	Programmable Logic Controller
CE	Carbon Equivalent
ppm	Parts per million
Zn	Zinc

List of Figures

List of Tables

Part I: Prediction of Critical Nugget Diameter in Resistance Spot Welding

Chapter 1: Introduction

1.1 Background

Resistance welding (RSW) is widely used in the fabrication of sheet metal assemblies in automotive and aerospace industries. In a spot welding process, two or three overlapped or stacked components are welded together due to the result of the heat, created by the electrical resistance, at the interface between the workpieces held together under pressure between two electrodes. Materials, such as steel, aluminum, titanium and copper alloys, are commercially used in spot welding [1]. The main advantages of spot welding are the high speeds and adaptability for automation in high-volume production. Typically, a vehicle body contains several thousands of spot welds joining sheets of different thickness. The design of spot welded joints and their mechanical integrities are critical to the performance of the vehicle in service [1], [2]. One important design factor is the optimum strength of the spot weld, as it controls the performance of the welds under tension, bending and torsion modes of loading and influences the durability, structural integrity and safety of the vehicle.

For bonded structures, the extent of the deformation is governed by the interaction between the geometry of the joint, the constitutive material properties, and the performance of the actual bond itself. The welding process is a complex thermal and mechanical process. The finished assembly consists of regions with significantly different microstructure and properties (e.g. the nugget and the HAZ). For IF steel grade of 0.8 mm, the weld nugget formed by the fusion zone, consists of a martensitic structure due to the high cooling rate while the HAZ is a mixture of tempered structure [3]. These microstructure variations result in gradient mechanical properties within the welding zones, thus making it difficult to predict the final joint strength. Current practice involves using simplified material properties due to difficulties in measuring the localized material properties (softening effect in heat affected zone of advance strength steel) which could not accurately represent the material behavior. A more thorough approach is needed to incorporate the detailed material properties.

The failure mode of spot welds is a qualitative measure of the weld reliability. Spot welds fail in two modes: interfacial and pullout. Failure mode of RSWs can significantly affect their load carrying capacity and energy absorption capability. Spot welds that fail in nugget pullout mode provide higher peak loads and energy absorption levels than spot welds that fail in interfacial and partial interfacial fracture modes [4]. To

ensure reliability of spot welds during vehicle lifetime, critical diameter of fusion is important as it is defined as the minimum nugget diameter to ensure the performance of the welds. Previous study on spot weld critical diameter reveled that lot of focused was made but no general correlation was made as shown in table 2.1

1.2 Objectives

Since steel sheets that are made for the use in the automotive industry are eventually spot-welded in the production process, weldability of the steel must be assessed before application. In most cases, higher strength in strong steels comes from enhanced alloying element concentrations such as carbon, manganese, silicon and mechanical properties such as yield stress, ultimate tensile stress and elongation. This may bring about a reduction in weldability because of an increased carbon equivalent [5]. It becomes clear that when conducting an alloy design, not only mechanical properties of the steel but also its spot weldability should be taken into account [5].

Existing models for prediction of critical nugget diameter are not suitable for any grade of steel. Instead, these models are valid only within a small range. For example, a model developed for DP600 grade of steel can't be extended for other high strength grades such as DP800. Also, these models can accommodate only few input parameters such as thickness, yield strength and hardness. Effect of steel chemistry or coating type on critical nugget diameter can't be studied. Hence, in the present work, an attempt has been made to develop a generalized model for prediction of critical nugget diameter using various inputs e.g. thickness, steel chemistry, mechanical properties and coating characteristics.

Chapter 2: Literature Review

2.1 Resistance Spot Welding Overview

Resistance spot welding process is a joining process where coalescence of material is produced at the faying surfaces by the heat generated due to contact resistance and joule effect when an electric current is passed through the work piece. Electrode force is applied before, during and after the application of current so that problem of arcing/expulsion at faying surface is prevented. Major parameters that control RSW process are welding current, weld time, electrode force[6], [7]. The dependence of the above-mentioned parameters leads to the complex interaction of electrical, thermal, mechanical and metallurgical phenomena. Due to such interaction, heterogeneous structure is developed in and around the fusion zones which are categorically distinct into three zones [8]:

i. Fusion zone or nugget (first melted and then recrystallized)
ii. Heat affected zone (HAZ), a region which is not melted but recrystallized due to heat dissipated from the faying zone
iii. Base material (BM), a region which is neither melted nor recrystallized during the process of welding, also called as work piece (Figure2.1).

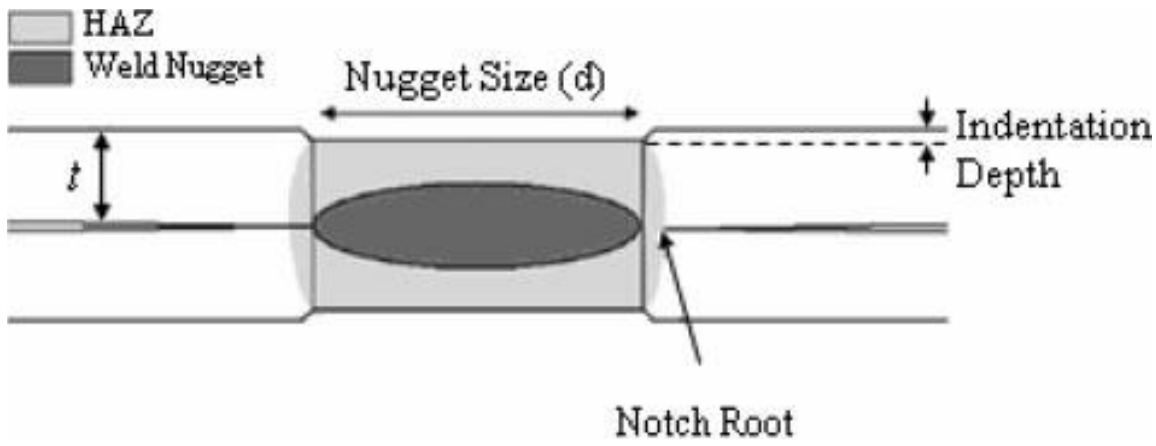

Figure 2.1. Schematic of spot weld microstructure [4]

Spot welds are not free from defects, which can be largely categorized into two groups; external and internal discontinuities [9]. External discontinuities defects appear on the weld surface. They usually can be

observed by bare eyes or with the aid of low magnifying microscope as shown in figure 2.2 (a). The prevention of external defects in most cases comes from the adjustment of welding parameters [9]. Internal discontinuities are found inside of the welds and revealed only by means of metallographic examination of weld cross sections or non-destructive tests as shown in Figure 2.2 (b), gaseous bubbles from the fusion stage, as the nugget solidifies, leads to porosity due to solidification shrinkage. This does not however pose a threat as long as such voids confined in the center of the nugget because it is at the heat affected zone where the most strain is concentrated [9].

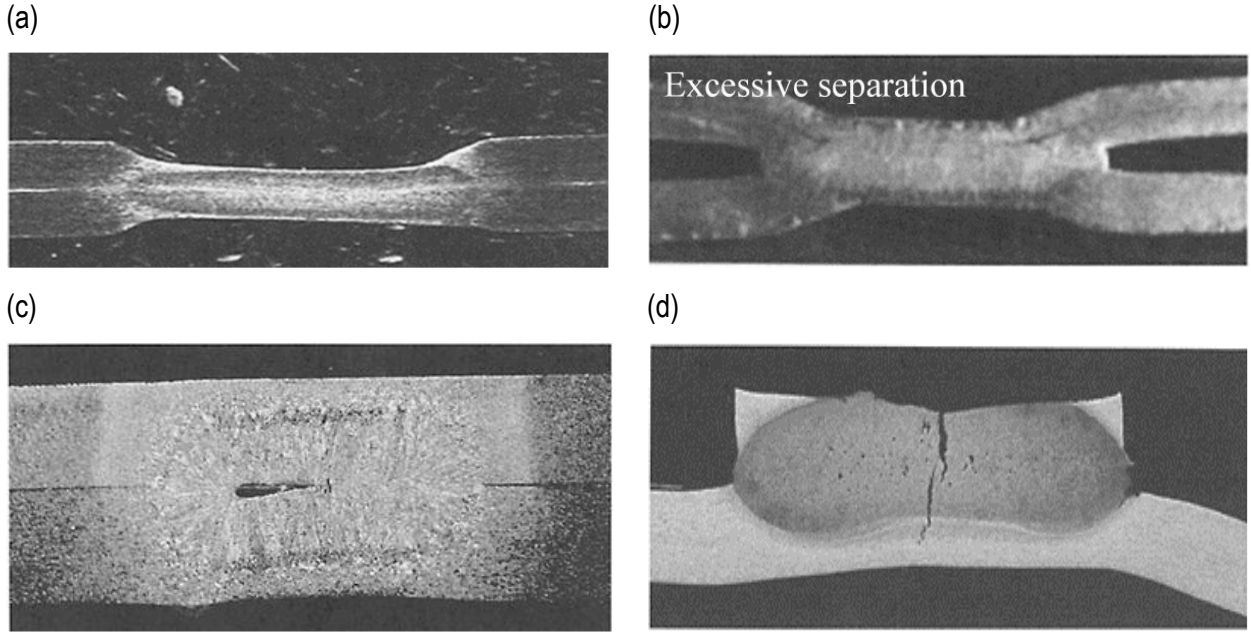

Figure 2.2. Examples of External discontinuities such as (a) Excess indentation (b) Excess separation; Internal discontinues such as (c) Voids (d) Weld crack in RSW [16]

RSW is called as solid-state welding because no traces of melting in the nugget of weld is developed. Spot welding joins two or more pieces of metal. The pieces of metal which are to be joined are pressed together with the help of two continuously water cooled electrodes on either side through a small spot as shown in Figure 2.3.

The material of electrode should have higher electrical and thermal conductivities with sufficient strength to sustain high pressure at elevated temperatures. Commonly used electrode materials are pure copper and copper base alloys. Copper base alloys may consist of copper as base and alloying elements such as cadmium or silver or chromium or nickel or beryllium or cobalt or zirconium or tungsten. Since copper is soft metal and steel is hard metal therefore their impacts leads to the deformation of copper metals, in order to

prevent deformation of copper electrode, some amount of chromium is added to increase strength and hardness to great extent. Zirconium is added to enhance the life of electrode by increasing corrosive resistant. The temperature of nugget weldment during welding is around 900^0C and melting point of zinc is 419.6 ^{0}C coated on steel, at that elevated temperature low melting point metal is highly reactive to different metals leads to the reaction with copper to form brass results in widen the width of electrode in the form of mushroom, when current start to pass during welding, current density ($\frac{I}{A}$) reduces because of increase in area due to increase in width of electrode leads to impaired nugget formation. Although electrode is water cooled copper made by cold worked having fine kiked structure after certain time during welding, it will reach the recrystallization temperature due to which very fine polygonal grain nucleate. As pancaked structure is more mechanically stronger and high hardness than recrystallized polygonal structure leads to softening of electrode is the another factor in developing mushroom [10].

Resistance generated during RSW can be attributed to the contact resistance at the electrode sheet interfaces (R2) and sheet faying surfaces (R1) and bulk resistance of the sheet (R3) [11]. Both the contact resistance and bulk resistance are usually not constant.

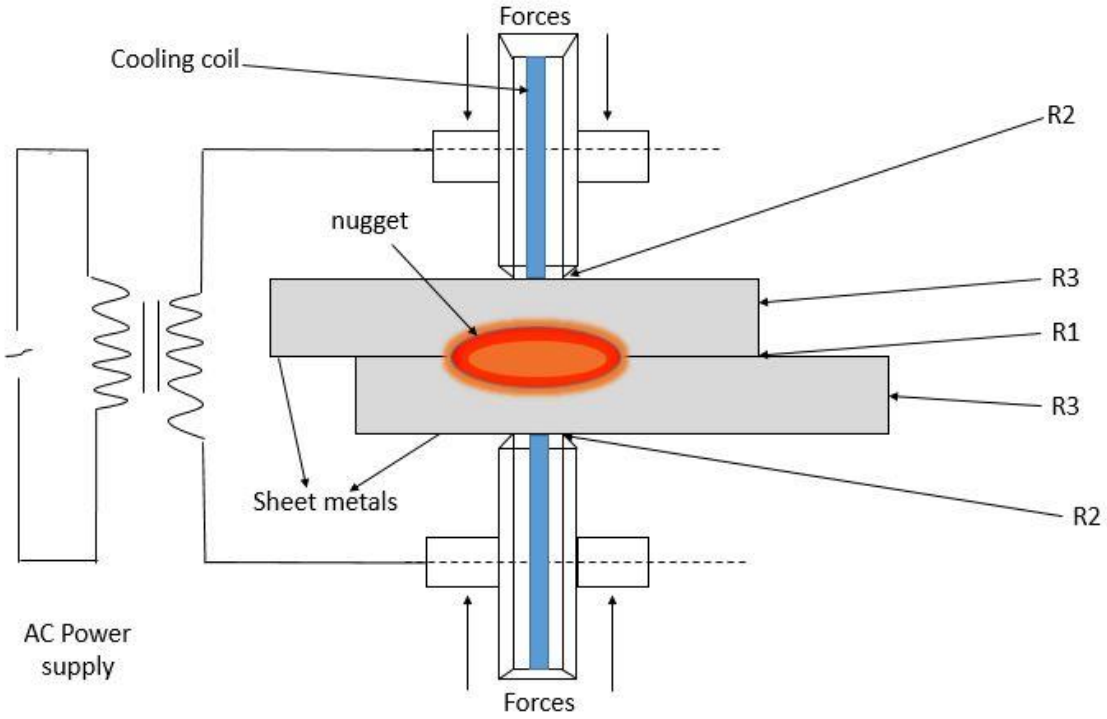

Figure 2.3. Schematic diagram of RSW Process [12]

The Contact resistance is strongly influenced by temperature and pressure while bulk resistance changes with only temperature. The heat generated during the RSW process due to interface contact resistance and bulk resistance is given by the following equation[10][13]:

$$Q = i^2RtK \quad \text{..... (2.1)}$$

Where, Q is the total heat produced to weld the work pieces, i is the welding current passing through electrodes, R the total circuit resistance produced along interface, t is the total weld time taken and K is process efficiency (constant for a particular setup).

Commercialization of RSW in automotive industry is due to its low cost, robustness and less time. Spot welding can also be used for attaching braces, pads or clips with cases, bases and covers which are mainly product of sheet metal forming. Moreover, the aircraft industries rely greatly of spot welding these days [14]. Moreover, RSW is the dominant metal sheet joining process in the automotive industry because of minimum skill requirements, inexpensive equipment, ease of control, its versatility, high operating speeds, repeatability, suitability for automation or robotization and inclusion in high-production assembly lines. Moreover, the process can be used to join most metals provided suitable welding conditions are applied [15]. Typically, there are about 2000–5000 spot welds in a modern vehicle. The quality, structural performance, durability, safety design, stiffness, strength and integrity of a vehicle depend not only on the mechanical properties of the sheets, but also on the quality of resistance spot welds [16][17] [18].

2.2 Effect of Electrical Properties

During welding, molten zone at the contact sheet surface becomes the weld nugget, so if more heat can be generated, a larger volume of metal can be melted, resulting in a bigger nugget. Larger weld nuggets are generally good for weld performance [2], [19]. The weld nugget size should be large enough for better impact property as well as preferable weld failure mode [2].

2.2.1 Current

In RSW, the generated heat is proportional directly to the weld current. Two types of current wave forms are available for conventional RSW processes; they are AC (alternating current) and DC (direct current) wave forms. In the automotive industry, the spot welding process with single-phase AC has been predominant [20]. DC systems can be used by rectification of single-phase or multi-phase AC into DC. Inverter equipped spot welders can provide very high frequency (2000 Hz) DC, which is effective in terms of energy use [20]. Also, DC system-based spot welding usually requires more equipment, thus bringing reliability problems, and is costlier [21], but it minimizes the heat loss and provides uniform heat flow. In a single-phase AC there is

an inevitable energy loss because of a series of current zero points, while DC systems provide reliable uniform heat flow. Many investigations on the differences that may come from different power systems, AC or DC, have been conducted by many authors [20].

2.2.2 Resistance

Resistance is very important to understand the effect on weldability in RSW. It can be observed that there are two major types, bulk resistance (R3) and contact resistance (R1 and R2) as shown in figure 2.3. The total is then the sum of all the resistance values which are in series. Bulk resistance largely is the characteristic of the sheet material that is spot welded. For most metals, it increases with temperature.

Contact resistance is significantly affected by pressure and surface condition. In the case of AC welding, resistance drops rapidly at the initial stage because of the decreased contact resistance from the high current peak that is absent in DC. Highly concentrated current generates great heat and brakes down the contact surface, destroying possible oxide phases on surface that can act as insulators [20]. As a result, heating efficiency in spot weld process can be compromised for AC welding. Later, because of the fact that bulk resistance increases in proportion to temperature, the overall resistance of AC eventually approaches to that of DC.

2.3 Effect of Weld Parameters

2.3.1 Weld time

Spot welding process generally consists of 4 steps, which are squeezing, welding, holding and final releasing [7]. In AC systems, the weld time is expressed in cycles (one cycle is 1/60 of a second in a 60 Hz power system), while millisecond is used for DC systems. During squeeze time, metal sheets are placed in position and clamped by electrodes. When the electrode force has reached the desired level, welding proceeds by the application of current. During this time, melting and joining occurs. Weld time should be determined according to material type, weld quality as well as productivity. The current is shut off during the hold time, so the nugget is allowed to cool. Finally, the metal is released, and the next welding sequence begins. The time for each step should be set according to the material, thickness and the coating conditions [22].

2.3.2 Electrode force

Electrode force is applied on electrodes to press and secure metal sheets in position. Electrode force F is expressed as below on the basis of shear stress at sheet/sheet interface can be approximated using following relation:, where F is the applied force and D is the weld nugget size [23].

$$\tau = \frac{4F}{\pi D^2} \quad \text{..... 2.2}$$

According to the above equation, stronger steels will require greater electrode force. If the force is insufficient to push the two metal sheets tight, a small contact diameter results, which alters the amount of heat that is generated, according to equation 2.1.

Electrode life of resistance welding is defined as the number of welds that can be made, without dressing the electrode tips, before the weld size falls below an acceptable level or reducing weldability. Electrode tip wear, resulting in electrode tip face growth, are the dominant process that limits electrode life in RSW of Zn coated steel [24], [25].

2.3.4 Weld Lobe

Fig. 2.4 demonstrates the general type of weld-lobe curve diagram. This diagram simply shows the window of operation within which weld quality can be guaranteed. Although many variations of the lobe diagram can exist, the electrode force is customarily set constant, and the diagram is drawn on the basis of current versus time. The lower boundary in the graph is determined at the condition in which the weld current is not high enough, so weld nugget size would not grow as big as minimum weld nugget size, which is $4\sqrt{t}$ (t=metal sheet thickness). Criteria for the minimum nugget size may vary depending on the standards and applications for example $5\sqrt{t}$ for more severe condition. Sun et. al [26] explained that the conventionally suggested minimum weld nugget size $4\sqrt{t}$ is insufficient to guarantee spot weldability for 800 grade high steels. Marya came up with a new and stricter criterion for determining minimum weld size, and it is expressed as [19].

$$\emptyset = 2.7d + 1.6 \text{.....2.3}$$

Where φ is a weld nugget diameter in mm, and d is the sheet thickness in mm.

The upper boundary is drawn from the points over which expulsion occurs. Expulsion is one kind of a weld defect and leads to the loss of metal, so it is detrimental to weld quality [27]. Different materials have different weld conditions, so different lobe curves. For weld quality, welding should be done within the range of two boundaries.

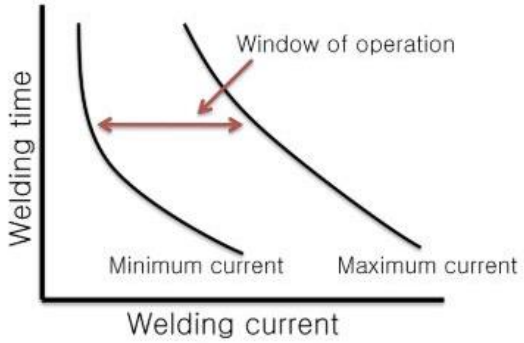

Figure 2.4. An example of weld lobe diagram [28].

2.4 Weldability of Interstitial Free Steels

2.4.1 Suitable Weld Condition

The lobe curve diagrams are a useful tool to see suitable welding conditions of certain materials. Since a larger process window allows flexibility during the production process, a broad range between the minimum and maximum weld current is appreciated in industry. A comparison of weld lobe curves of mild steel and IF (interstitial free) steel is illustrated in figure 2.5, the latter is hardly alloyed and hence requires more current value. The addition of alloying elements in steel increases its bulk resistance, so that heat generated from welding process increases [7]. Therefore, for an IF steel to acquire the same nugget size as mild steel, it requires the current to be maintained for a longer period. Figure 2.6 shows the weld nugget growth graph for three different steel alloys. The more alloyed steel, 590TRIP steel, has the suitable weld current range that is overall lower than other alloys by the same principle.

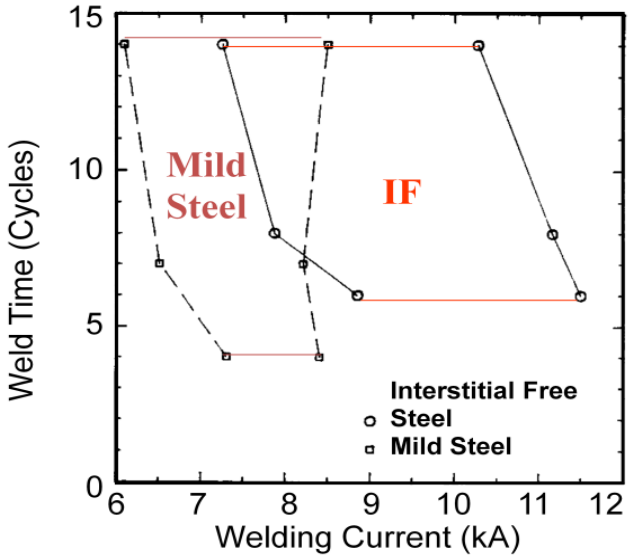

Figure 2.5 Weld lobe curves for mild steel and IF steel [48]

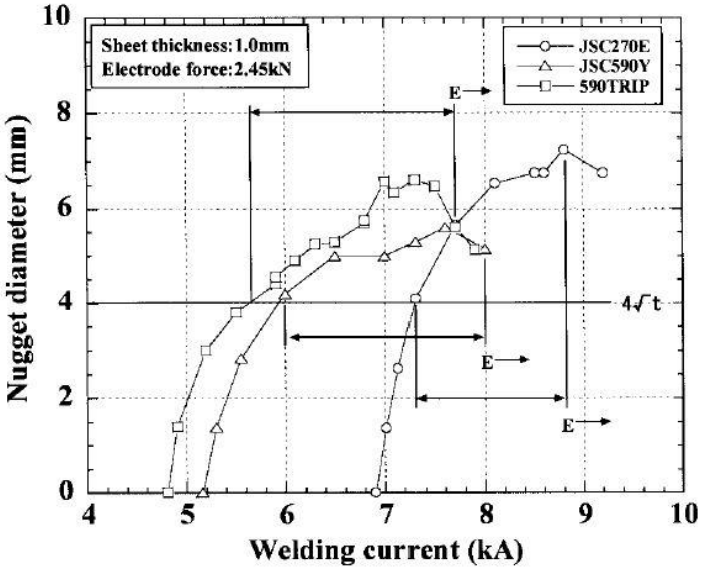

Figure 2.6 Effect of weld current on nugget diameter [5]

2.4.2 Carbon equivalent

In typical resistance spot weld process, cooling rate is very rapid ranging from 1,000-10,000 K s^{-1} because of the quenching effect from the copper electrodes [49, 50]. As a result, martensite forms at the fusion zone, increasing hardness around weld compared with the base metal. When considering weldability, the carbon equivalent is important because it is closely related to hardenability around the weld zone. Typically, highly alloyed steels have the high value of carbon equivalent. Many different empirical equations have been published for determining carbon equivalent [5], [29] , of which are listed below.

- **Yurioka** carbon equivalent; CE = C+ A(c) (5B + $\frac{Si}{24}$ +$\frac{Mn}{6}$ + $\frac{Cu}{15}$ + $\frac{Ni}{20}$ + $\frac{Cr+Mo+v}{5}$)

  Where, A(c) = 0 .75 + 0.25tanh [20(C-0. 12)]
- **Nippon** carbon equivalent; CE = C + $\frac{Si}{30} + \frac{Mn}{20} + 2P + 4S$ (Non-AHSS spot welds)

  Where symbols having usual meaning

2.5 Metallurgical characteristics:

Due to complex thermal cycle, introduction of rapid heating and cooling made the microstructural change in resistance spot welds resulting in significant variations in hardness profile throughout base metal to fusion zone. Depending on the chemical composition and initial microstructure of the BM, hardness profile of spot welds of carbon steels may exhibit hardening in FZ and HAZ as well as softening in the HAZ. To

describe the degree of hardening in FZ and softening in HAZ, two parameters, hardening ratio and softening ratio, are defined as follows [30][31]:

$$Hardening\ ratio = \frac{H_{FZ}}{H_{BM}} \quad \text{.....2.4}$$

$$Softening\ ratio = \frac{H_{min}}{H_{BM}} \quad \text{.....2.5}$$

where H_{BM}, H_{FZ} and H_{min} are BM hardness, FZ hardness and minimum hardness in HAZ respectively.

Microstructure evolution in FZ is governed by chemical composition and cooling rate during RSW process. The chemical composition of the FZ is affected by the chemical composition of the BMs involved in the joints and the mixing of them. In the case of dissimilar metal welding or dissimilar thickness welding, the melting ratio is different for each sheet [32]. Sheet with higher electrical resistivity or higher thickness exhibits higher bulk electrical resistivity resulting in higher contribution in the volume of melted zone [11].The heating and cooling rate of RSW process is significantly higher than conventional arc welding and laser welding processes [33]. The time to cool from 800 to 500 ^{0}C which is recognized as the most important temperature range in determining phase transformation of steel welds for 0.8 mm thick sheet spot welds is reported to be ≈ 0.06 s [28]. This high cooling rate can significantly affect the phase transformation during RSW. The cooling rate during RSW is governed by the heat dissipation from molten FZ to the surrounding via two mechanisms: heat dissipation through water cooled electrode in axial direction and radial heat dissipation through adjacent cold base metal [34],[35].

Kim et al. [28] have shown that the ratio of axial heat loss rate to the redial heat loss rate is proportional to the electrode diameter divided by the square of sheet thickness. Therefore, the most effective mechanism depends on the sheet thickness and electrode diameter (and weld nugget size). Cooling mechanism for small welds (i.e. with a weld nugget diameter smaller than the electrode tip diameter) and thin sheet thickness is dominated by heat loss in axial direction via water cooled electrode. However, large welds (i.e. the weld nugget diameter exceeding the electrode tip diameter) and thick sheets will be cooled by conduction of heat to the rest of the material [28].

Cooling rate during steel RSW depends on the following parameters: sheet thickness, electrode face thickness, welding parameters. In comparison to the arc welding process in which increasing sheet thickness increases the cooling rates, in RSW process, increasing sheet thickness reduces the cooling rate due to increasing the distance of liquid pool from the water-cooled electrode with increasing sheet thickness. Increasing electrode face thickness, decreases the cooling rats as a result of decreasing heat dissipation

from hot nugget through the water-cooled electrode. Increasing heat input (via increasing welding current and welding time and decreasing the electrode force) reduces the cooling rate.

Gould et al.[36] developed a simple analytical model predicting cooling rates of resistance spot welds. They proposed the following relationship to estimate cooling rate during RSW:

$$\frac{\partial T}{\partial t} = -\left(\frac{\alpha\pi^2}{4t_s}\right)\left(\frac{T}{T_P}\right)\left\{T_{TP} - \frac{T}{1+\left(2/\pi\right)\left(\frac{K_E}{K_S}\right)\left(t_S/t_E\right)\cos\left[\left(\frac{\pi}{2t_S}\right)x\right]}\right\} \quad \text{.....2.6}$$

where α is thermal diffusivity of the steel sheets, T_P is the maximum temperature experienced in FZ during welding process, t_S is the sheet thickness, t_E is the electrode face thicknesses (i.e. the distance of water cooled hole to the electrode surface), k_S and k_E are thermal conductivity of steel and electrode respectively and x is the position through the spot weld in sheet thickness direction.

2.6 Mechanical Properties of Resistance Spot Welds

In an automotive structure, spot welds experience both shear loading due to the relative displacement or rotation of the adjacent sheets and tensile loading due to the separating forces applied between adjacent sheets in a direction normal to the sheets [37]. The mechanical performance of spot welds is normally considered under quasi-static and dynamic loading conditions. Tensile-shear (TS), cross-tension (CT) and coach peel (CP) tests are examples of tests conducted under quasi-static loading conditions. Impact and fatigue tests are examples of tests conducted under dynamic loading conditions [19]. Figure 2.7 schematically illustrates sample geometry for TS, CT and CP tests. Due to simplicity in preparing samples for tensile–shear (TS) test, it is widely used to determine the strength of resistance spot welds [38]. In this test, load bearing capacity (peak load) and failure energy are the two most important parameters used to describe the performance of the joint. The peak load and failure energy are extracted from the load–displacement curve obtained from the test [39].

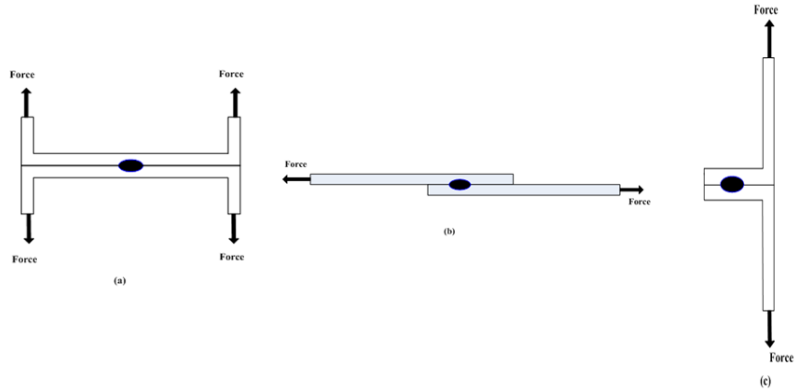

Figure 2.7. Specimen geometry for (a) CT, (b) TS and (c) CP tests [40]

2.6.1 Different failure modes in RSWs

Interfacial Failure Mode (IF)

In Interfacial failure mode, the joint fails through the weld nugget centerline and the fracture surface is relatively smooth [41][42]. Cracks usually initiate from a sharp notch and then propagate through the weld nugget as shown in figure 2.8. IF mode is accompanied by little plastic deformation and has a detrimental effect on the crashworthiness of the vehicles results in weak weldability [43]. For a given sheet thickness, decreasing $\frac{H_{WN}}{H_{FL}}$ increases possibility of interfacial failure mode where H_{WN} is the hardness of weld nugget and H_{FL} is the hardness of failure location in BHN [4].

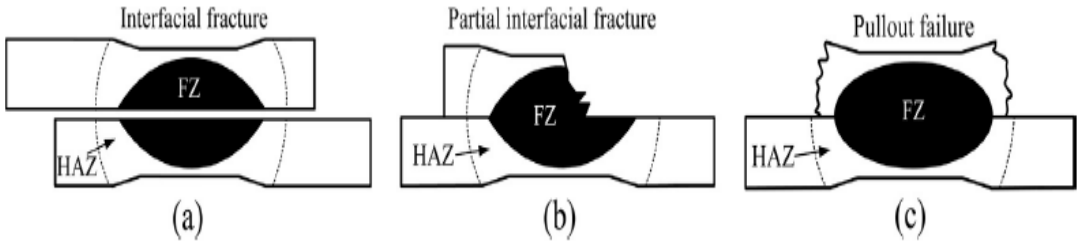

Figure 2.8. Schematic representation of three failure modes observed in tensile shear test: (a) interfacial, (b) partial interfacial, and (c) pullout [18]

Partial Interfacial Failure (PIF)

In this mode which is shown in Figure 2.8 (b), a fraction of the weld nugget is removed. The crack first propagates in the weld nugget, then redirects perpendicularly to the centerline towards one of the sheets.

Pullout Failure (PF) Mode

PF occurs by withdrawal of the weld nugget from one sheet, as shown in Figure 2.8 (c), Fracture may initiate in the base metal (BM), HAZ or HAZ/FZ, depending on the metallurgical and geometrical characteristics of the weld zone and the loading conditions. Spot welds that fail by PF mode have higher peak loads and energy absorption levels than those that fail through IF or PIF failure modes. PF is the most preferred failure mode especially for automotive industry due to wide range of plastic deformation and energy absorption results in vehicle crashworthiness and hence process parameters should be adjusted so that the

pullout failure mode is established [44]. Load carrying capacity and energy absorption capability for those welds fail under interfacial mode, are much less than those which fail under pullout mode which is shown in figure 2.9

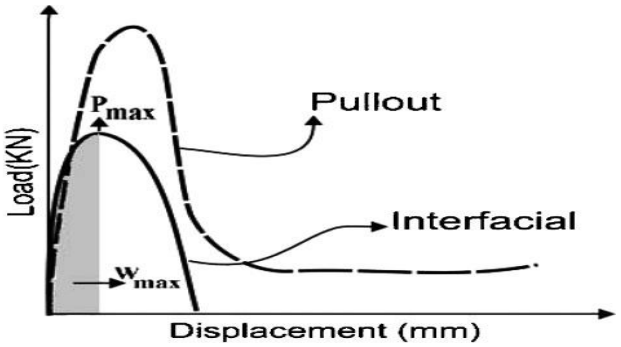

Figure 2.9. Load displacement diagram for both failure modes[4]

2.6.2 Different Loading Conditions in RSW

During TS test, the driving force for the IF mode is the shear stress at the sheet/sheet interface which depends on the area of the weld nugget in the sheet/sheet plane. The resistance against the IF of the spot welds with a given FZ size is determined by the FZ hardness. An increase in the FZ hardness decreases the tendency to fail in the IF mode [45]. The driving force for the PF mode is tensile stress which is mainly induced by the bending moment as a result of overlapping of the two sheets and rotating of the weld nugget. The resistance against the necking initiation (i.e. PF mode) of the spot welds with a given FZ size is determined by the hardness of PF location (BM or HAZ). A decrease in the hardness of PF location decreases the tendency to fail in the IF mode [45]. Since, there is a competition between shear plastic deformation in FZ and necking in base metal as seen in figure 2.10 (a), Therefore, the tendency to fail in the pullout mode is proportional to the ratio of the hardness of the FZ to the hardness of the pullout failure location (PFL) [46]–[48]

$$(D_c)_{\mathrm{TS}} = \frac{H_{PFL}}{H_{FZ}} \quad \text{.....2.7}$$

During CT test, the driving force for the IF mode is the tensile stress at sheet/sheet interface as shown in figure 2.10 (b). Depending on the hardness and degree of brittleness of the FZ, the controlling factor is different. For HAZ and weld nugget of relatively high alloyed DP or TRIP steels, the stress intensity factor is the driving force of the failure and the driving force of the material having soft fusion zone is tensile stress [49]. The fracture surface in IF mode exhibits near equiaxed dimples, indicating that a ductile fracture

occurred under tensile stress [50]. When the FZ is hard, the tendency to fail in the pullout mode in the CT loading is proportional to the ratio of the fracture toughness of the FZ to the shear strength of the HAZ

$$(D_c) = H_{HAZ} + H_{FZ} \quad \text{.....2.8}$$

when the FZ is soft, the tendency to fail in the pullout mode in the CT loading is proportional to the ratio of the tensile strength of the FZ to the shear strength of the HAZ

$$(D_C) = \frac{H_{FZ}}{H_{HAZ}} \quad \text{.....2.9}$$

During CP test, the driving force for IF mode is the tensile stress at sheet/sheet interface as shown in figure 2.10 (c). This is justified by SEM images which showed that the fracture surface of a spot weld failed near equiaxed dimples [51]. For PF mode, bending moment is the driving force which is justified by SEM image which showed that fracture exhibited near elongated dimples [51]. The tendency to fail in the pullout mode in the CP loading of carbon steel resistance spot welds increased as the FZ and HAZ harnesses increase.

$$(D_C)_{CP} = H_{HAZ}H_{FZ} \quad \text{.....2.10}$$

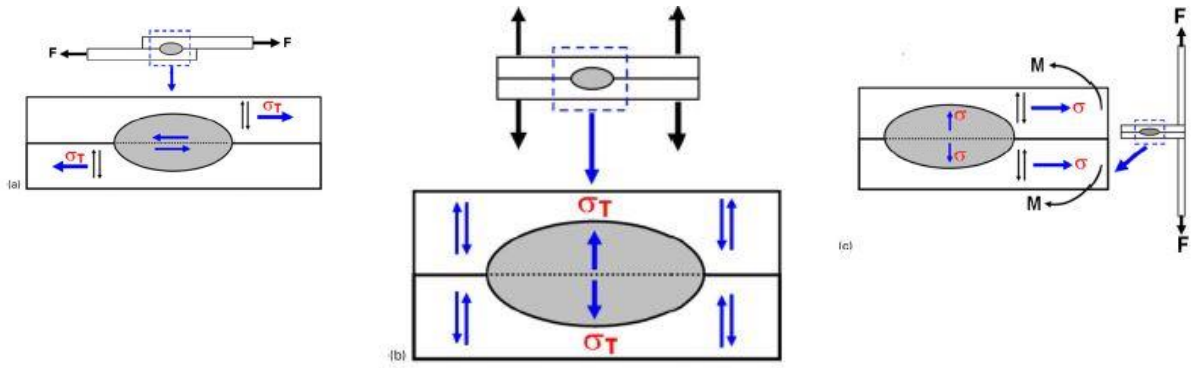

Figure 2.10. Simple models describing stress distribution at the interface and circumference of a weld nugget during (a) TS[18] (b) CT[50]and (c) CP tests [52]

The importance of weld nugget size should be emphasized because the size (or diameter) of the welds controls the weld tensile strength. Studies done at the laboratory on several high-strength steel grades and at various sheet thickness have shown a strong dependence of the fracture appearance (or mode) on weld size in spot weld shear-tension tests [53]. It was found through modeling of actual test results that the failure load for a full-button pullout is given by the amount of force required to cause failure is equal to the product of the strength of the material and the failed area of cross section. Based on this, the following equations were derived to predict failure loads, F_{PO} and F_{IF}, for pullout and interfacial failure modes, respectively:

$$F_{PO} = K_{PO} \times \sigma_{UT} \times d \times t \quad \text{.....2.11}$$

$$F_{IF} = K_{IF} \times \sigma_{UT} \times d^2 \quad \text{.....2.12}$$

K_{PO} (~2.2) and K_{IF} (~0.6) are constants; $\sigma_{UT}$is the ultimate tensile shear strength of the base material, d is nugget diameter, t is the sheet thickness.

The equation (2.11) is not valid for every steel because high strength steel is more sensitive to the occurrence of expulsion of weld metal as compared to low-strength, drawing-quality steels [54].

2.7 Existing Models for Prediction of Critical Nugget Diameter

The response of resistance spot welds to mechanical loading is significantly different from that of BM, due to microstructural/properties gradient in FZ and HAZ as well as geometrical stress concentration induced by spot welding. It has been reported that the joint efficiencies (weld TS strength to BM tensile strength) for resistance spot welds ranged from 29 to 54% [55]. Quasi-static mechanical properties (i.e. load bearing capacity and energy absorption capability) of resistance spot welds depend on several factors which can be summarized as follows:

The peak load of RSW increased in order of CP, CT and TS loading conditions [56],[57]. It has been shown that increasing the loading angle (i.e. angle between load application line and the centre line of the specimen) decreases the load bearing capacity [58]. It has also been found that energy absorption capability of spot welds is increased in order of CP, TS and CT tests [56].

The weld nugget diameter controls the mechanical performance and failure mode of resistance spot weld. Small nugget diameter often results in interfacial failure (IF) mode while a large one normally leads to pullout failure (PF) mode [16]. The transition from IF mode to PF mode is generally related to the increase in the size of the FZ above a minimum value. The minimum FZ size to avoid interfacial failure is called critical weld nugget diameter. Various industrial standards have recommended a minimum weld size for a given sheet thickness

AWS/ANSI/AISI [59] weld button sizing to ensure that the weld size was large enough to carry the desired load, is expressed by equation

$$D = 4t^{0.5} \quad \text{.....2.13}$$

Marya et al. [2] show that conventional recommendation of equation AWS is not sufficient to obtain pullout failure mode of DP600, DP780 and DP980 resistance spot welded. Also, Sun et al. [48] showed that $4\ t^{0.5}$

rule could not guarantee pullout failure mode of advanced high strength steel including DP800 and TRIP800. Therefore, it seems that metallurgical factors (e. g. weld microstructure) should be considered to more precisely analyze and predict the RSWs failure mode, in addition to sheet thickness.

According to Japanese JIS Z3140 [60] and the German DVS 2923178 standards, the required weld size is specified according to equation

$$D = 5t^{0.5} \quad \text{.....2.14}$$

In automotive industry, sizing of spot welds in most cases is based on the $4t^{0.5}$ rule[56],[61],[62]. However, this criterion does not always give the best result. In some cases, (particularly for AHSS welds), in order to ensure the PF mode, a bigger weld nugget diameter than the value recommended by $4t^{0.5}$ rule is required [47],[4],[31]. It has been shown that no direct relationship can be proposed between critical weld size and sheet thickness [28]. This confirms the fact that in addition to sheet thickness, the critical weld size is also affected by material's properties. Therefore, it seems that in addition to sheet thickness, metallurgical factors should be considered to precisely analyze and predict failure mode of resistance spot welds[62].
Van den Bossche et al. [63]. A weld sizing criterion was developed based on the premise that the fracture will happen in the region that first yields (BM or FZ). The following equation describes the resulting criterion for PF

$$\left(\frac{D}{t}\right)_c = \left[1.5\left(\frac{\sigma_{y\,BM}}{\sigma_{y\,FZ}}\right)\left(\frac{w}{t}\right)\right]^{1/2} \quad \text{.....2.15}$$

where $\sigma_{y\,BM}$ is tensile yield strength of the BM, $\sigma_{y\,FZ}$ is tensile yield strength of the FZ and w is the specimen width.

Different researchers have developed an empirical relation as summarized in table 2.1 to calculate critical diameter of resistance spot weld. A detail review on previous study of experimental critical nugget diameter as reported in 57 published paper along with Steel Grade, Coating, Welding Process, Characterization, Chemical composition (wt.%), Loading condition and References is shown in table 2.2. Figure 2.11 shows the comparison between critical nugget diameter calculated by different researcher as shown in table 2.2 with AWS and Japanese standard.

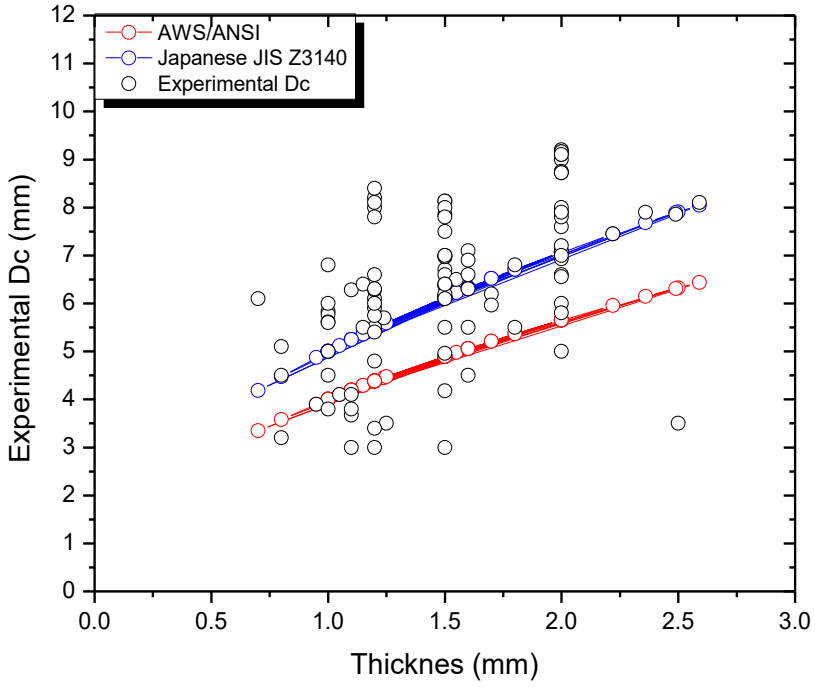

Figure 2.11. Variation of experimental critical nugget diameter reported from reviewed literature (table 2.3) with AWS and JIS standard.

Table 2.1. Empirical relation of critical nugget diameter

Empirical relation	Steel Grade	Loading condition	Limitation	References
$D = 4\sqrt{t}$	All	NA	AHSS Steel specially DP and TRIP	[59]
$D = 5\sqrt{t}$	All	NA	AHSS Steel specially DP and TRIP	[60]
$D_c = 4t$	AHSS	TSS	BM, HAZ and FZ properties were assumed to be homogeneous	[64]
$D_c = 3.41t^{4/3}$	Mild steel	CT	Considered fracture toughness of HAZ and BM	[65]
$D_c = 2.7d + 1.6$	AHSS	TSS/CT	DP600	[19]
$\left(\frac{D}{t}\right)_c = \left[1.5\left(\frac{\sigma_{y\,BM}}{\sigma_{y\,FZ}}\right)\left(\frac{w}{t}\right)\right]^{1/2}$	All	TSS/CT	Not for CP test	. [63]
$D_c = 0.53t^{3.22} + 8.48\left(\frac{H_{max}}{H_{min}}\right)^{-1.24}$	AHSS	TSS	Specific steel grade	[66]
$D_C = \frac{4t}{Pf}\left(\frac{H_{PFL}}{H_{FZ}}\right)$	low carbon steels, HSLA steels, DP and TRIP steels	TSS	Porosity factor is approximated	[48]
$D_C = 2.93\left(\frac{\tau_{BM}}{K_C^{FZ}}\right)^{2/3} t^{4/3}$	Mild steel	CT	τ_{BM} and K_C^{FZ} can be obtained from experimental data.	[67]
$(D_C)_{CT} = 4t\frac{f \times H_{PFL}}{H_{FZ}}$	LCS/AISI 304	CT	For dissimilar welding	[42]
$(D_c)_{TS} = \frac{H_{PFL}}{H_{FZ}}$	All	TSS	Definition from TSS test	[46]–[48]
$(D_C) = \frac{H_{FZ}}{H_{HAZ}}$	All	CT	Definition from CT test	[50]
$(D_C)_{CP} = H_{HAZ}H_{FZ}$	All	CP	Definition from CP test	[51]

where t is the sheet thickness (mm), H_{max} and H_{min} are maximum and minimum hardness values in the HAZ, P is the porosity factor, f is the ratio of shear strength to tensile strength of the FZ and H_{FZ} and H_{PFL} are hardness values (HV) of the FZ and PF location respectively. τ_{BM} is the shear strength of the BM and K_C^{FZ} is the fracture toughness of FZ. τ_{BM} and K_C^{FZ} can be obtained from experimental data.

Table 2.2. Database created from literature

Sl. No.	Steel Grade	Coated / Bare	Welding Process		Characterization	Chemical composition (wt.%)			Loading condition	Critical diameter	References
			Joint Configuration	Type of power source	Thickness (mm)	C	Mn	Si		Dc (mm)	
1	DP780	Bare	Similar	MFDC	1.8	0.157	1.89	0.52	TS	6.8	[43]
2	DP500EG/CRS	Electro Galvanized	Similar	MFDC/AC	0.7	0.14	1.6	0.4	TS	6.1	[68]
3	DP600	Galvanized coating	Similar	MFDC	1.8	0.13	1.4	0.4	TS	5.5	[2]
	DP600	Galvanized coating	Similar	MFDC	2	0.11	1.5	0.1	TS	6	
4	DP600	Galvanized coating	Similar	MFDC	0.95	0.096	1.5	0.1	TS	3.9	[2]
	DP600	Galvanized coating	Similar	MFDC	2.22	0.096	1.5	0.1	TS	7.45	
5	DP600	Bare	Similar	AC	1.7	0.08	1.8	0.01	TS	6.2	[16]
6	M130 martensitic sheet	Bare	Similar	AC	2	0.093	1.56	0.16	TS	9.2	[13]
7	DP780	Bare	Similar	AC	2	0.12	1.45	0.4	CT	6.6	[69]
	DP780	Bare	Similar	AC	2	0.098	1.58	0.198	CP	7.9	
8	DP600	Bare	Similar	AC	1.5	0.07	1.83	0.015	TS	6.37	[47]
	DP780	Bare	Similar	AC	1.5	0.079	1.52	1	TS	8.13	
	DP980	Bare	Similar	AC	1.5	0.11	0.53	0.07	TS	6.97	
9	TWIP	Bare	Similar	MFDC	1.5	0.16	0.67	0.24	TS	3/4.8	[70]
10	DP600	Bare	Similar	AC	1.7	0.16	0.67	0.24	TS	5.967	[71]
11	DP600	Bare	Similar	AC/MFDC	2	0.1	1.4	0.14	TS	9	[72]
12	MS1400	Bare	Similar	AC	1.5	0.12	1.3	0.18	TS	6.7	[73]
13	DP780	BARE	Dissimilar	AC/MFDC	1.2	0.14	1.7	0.08	TS	6.1	[74]
	DP600				1.5	0.06	0.16	0.04	TS	6.1	
14	DP600	Bare	Dissimilar	AC	2	0.03	1.1	0.35	TS	7.1	[44]
	Low Carbon Steel	Bare			2	0.51	22.4	--	TS	7.1	
15	DP600	Bare	Dissimilar	AC	2	0.08	1.52	1	TS	5.8	[17]
	LCS	Bare			2	0.08	1.52	1	TS	5.8	

16	DP600	HDGI	Dissimilar	AC	1.2	0.16	1.13	0.18	CP	5.5	[75]
	DP780	GA			1.15	0.065	2.04	0.01	CP	5.5	
17	DP780	HDGI	Dissimilar	AC	1.2	0.036	1.528	0.048	TS	6.6	[76]
	DP600	HDGI			1.5	0.35	1.28	0.388	TS	6.6	
18	DP600	GI	Dissimilar	MFDC/AC	1.6	0.065	0.204	0.095	TS	4.5	[77]
	DC54D	Bare			1	0.135	1.28	0.308	TS	4.5	
19	HSLA350	GA	Dissimilar	MFDC/AC	1.55	0.065	0.204	0.095	CT	6.5	[78]
	DP600	GA			1.55	0.099	0.1523	0.157	CT	6.5	
20	DP600	Bare	Similar	AC	2	0.113	0.1523	0.036	TS	8.75	[32]
	DP600	Bare	Dissimilar	AC	2	0.065	2.04	0.01	TS	6.925	
	LCS	Bare			2	0.036	1.528	0.048	TS	6.925	
	LCS	Bare	Similar	AC	2	0.1	0.4	0.14	TS	7.6	
21	DP600	Bare	Similar	AC	2	0.002	0.16	--	TS	9.1	[49]
	DP600	Bare	Dissimilar	AC	2	0.05	0.6	0.05	TS	7.2	
	LCS	Bare			2	0.1	1.5	0.19	TS	7.2	
	LCS	Bare	Similar	AC	2	0.135	1.28	0.388	TS	7.9	
22	DP600	Bare	Similar	AC	1.5	0.135	1.28	0.388	TS	6.4	[79]
	DP780	Bare	Similar	AC	1.5	0.065	0.204	0.095	TS	7.85	
	DP980	Bare	Similar	AC	1.5	0.065	0.204	0.095	TS	7	
23	HIF	GA	Similar	AC	1.6	0.135	1.28	0.388	TS	5.5	[80]
24	Austenitic stainless steel	Bare	Dissimilar	AC	1.2	0.135	1.28	0.388	TS	6.28	[15]
	Galvanized Low carbon steel	GI			1.1	0.065	0.204	0.095	TS	6.28	
25	DP600	HDGI	Similar	AC	1.24	0.065	0.204	0.095	TS	5.695	[81]

	DQSK	Bare	Similar	AC	1.5	0.1	1.4	0.14	TS	4.96	
	DP600	Bare	Similar	AC	1.5	0.12	1.3	0.18	TS	6.37	
	DP780	Bare	Similar	AC	1.5	0.14	1.7	0.01	TS	8.13	
26	DP980	Bare	Similar	AC	1.5	0.004	0.53	0.104	TS	6.97	[30]
	AISI304	Bare	Similar	AC	1.5	0.035	1.08	0.388	TS	11.41	
	TRIP (AT)	Bare	Similar	AC	1	0.065	0.404	0.095	TS	5.83	
27	RIP (AST)	Bare	Similar	AC	1	0.08	1.91	0.004	TS	5.77	[82]
	TRIP (ST)	Bare	Similar	AC	1	0.12	2.13	0.08	TS	5.61	
28	Low Carbon Steel	GI	Similar	AC	1.1	0.16	1.9	0.85	TS	3.67	[83]
	HSLA	GI	Similar	AC	1	0.19	1.63	1.62	TS	6	
	590R	GA	Similar	AC	1.2	0.065	0.404	0.095	TS	5.9	
29	DP600	HDGI	Similar	AC	1.2	0.06	0.64	0.24	TS	5.4	[22]
	DP780	GA	Similar	AC	1.15	0.13	1.599	0.12	TS	6.4	
	TRIP780	HDGI	Similar	AC	1	0.1	1.523	0.157	TS	5.6	
30	HSLA420	Bare	Similar	AC	1.5	0.113	2.082	0.036	TS	6.2	[84]
31	LCS	Bare	Similar	AC	2	0.188	1.631	1.618	TS	8.72	[85]
	HSLA	Bare	Similar	AC	2	0.08	0.72	0.14	TS	9.16	
32	TRIP700	Electroplated zinc	Similar	AC	1.05	0.14	0.6	--	TS	4.1	[86]
	DP600	HDGI	Dissimilar	AC	0.8	0.06	0.64	0.24	TS	4.5	
33	LCS	BARE	Similar	AC	0.8	0.31	1.54	0.29	TS	3.2	[4]
34	LCS	Bare	Similar	AC	0.8	0.12	1.58	0.19	TS	5.1	[87]
35	LCS	Bare	Similar	AC	1.5	0.045	0.189	0.032	TS	6.1	[57]
	LCS	Bare	Similar	AC	1.5	0.045	0.189	0.032	CP	5.5	
36	DP600	Bare	Dissimilar	AC	2	0.04	0.21	0.03	TS	7	[88]
	LCS	Bare			2	0.04	0.21	0.03	TS	7	
37	TRIP800	Bare	Similar	AC	1.5	0.135	1.28	0.388	TS	7.5	[89]
	TRIP800	GI	Similar	AC	1.5	0.065	0.2	0.095	TS	8	

38	TWIP	Bare	Similar	AC	1	0.2	1.69	1.66	TS	5	[90]
	TWIP	Bare	Similar	AC	1	0.2	1.69	1.66	TS	6.8	
39	DP980	Bare	Similar	AC	2	0.024	32	2.36	TS	7.8	[91]
40	LCS	Bare	Similar	AC	2	0.024	32	2.36	TS	8.72	[92]
	HSLA	Bare	Similar	AC	2	0.13	1.326	0.13	TS	9.16	
41	DP980	Bare	Similar	AC	2	0.065	0.2	0.095	TS	8	[93]
42	LCS	Coated	Similar	AC	1.1	0.06	0.64	0.24	TS	4.1	[94]
43	LCS	Bare	Dissimilar	AC	1.25	0.13	1.326	0.13	TS	3.5	[95]
	LCS	Bare			2.5	0.05	0.2	0.05	TS	3.5	
44	DP980	Bare	Similar	AC	1.5	0.08	0.21	0.01	TS	7	[96]
45	M 130	Bare	Similar	AC	2	0.05	0.2	0.05	TS	9.1	[97]
	M 130	Bare	Dissimilar	AC	2	0.14	1.7	0.08	TS	5	
	LCS	Bare			2	0.11	0.53	0.07	TS	5	
	LCS	Bare	Similar	AC	2	0.11	0.53	0.07	TS	7.9	
46	LCS	Coated	Similar	AC	1.1	0.065	0.204	0.095	TS	3.8	[98]
	LCS	Coated	Dissimilar	AC	1.1	0.065	0.204	0.095	CP	3	
	SS	Bare			1.2	0.065	0.404	0.095	CP	3	
	SS	Bare	Similar	AC	1.2	0.065	0.404	0.095	TS	5.75	
47	Mn-Mo-Cb	Bare	Similar	AC	2.49	0.035	1.08	0.388	TS	7.86	[63]
	V-N	Bare	Similar	AC	2.36	0.035	1.08	0.388	TS	7.9	
	SAE 1008	Bare	Similar	AC	2.59	0.05	1.14	0.18	TS	8.1	
48	Rephosphorized Steel	Bare	Similar	AC	1	0.09	1.06	0.27	TS	3.8	[99]
49	Austenitic stainless steel	Bare	Similar	AC	1.2	0.04	0.25	<.005	CT	3.4	[50]
	Austenitic stainless steel	Bare	Similar	AC	1.2	0.06	0.45	--	TS	6	
50	AISI304 FSS	Bare	Dissimilar	AC	1.5	0.03	1.2	0.4	TS	4.18	[100]
	DQSK LCS	Bare			1.5	0.03	1.2	0.4	TS	4.18	
51	DP800	GI	Similar	AC	1.6	0.024	0.513	0.383	CT	7.1	[31]

	TRIP800	Bare	Similar	AC	1.5	0.044	0.202	0.001	CT	6.4	
52	Austenitic stainless steel	Bare	Similar	AC	1.2	0.15	1.5	0.5	TS	4.8	[40]
53	Mild Steel	Bare	Similar	AC	1.2	0.2	1.69	1.66	CT	8	[101]
		GI (both side)	Similar	AC	1.2	0.035	1	0.388	CT	8.2	
		GI (both side)	Similar	AC	1.2	0.05	0.014	0.014	CT	8.4	
		Bare	Similar	AC	1.2	0.04	0.016	0.017	CT	7.8	
		GI (both side)	Similar	AC	1.2	0.05	0.013	0.015	CT	8.1	
		GI (both side)	Similar	AC	1.2	0.05	0.014	0.014	CT	8.1	
54	304L	Bare	Dissimilar	AC	1.2	0.04	0.016	0.017	TS	6.3	[102]
55	DP780	HDGA	Similar	AC	1.6	0.05	0.013	0.015	TS	6.9	[54]
	DP 780	HDGA	Similar	AC	1.6	0.025	1.48	0.34	CT	6.6	
	DP780	HDGI	Similar	AC	1.6	0.11	0.57	0.62	CT	6.3	
56	304 ASS	Bare	Similar	AC	2	0.113	2.082	0.036	TS	6.558	[103]

Chapter 3: Methodology

The following methodology was followed:

1 **Database creation -** A database of the critical diameter of steels was compiled from the published literature as shown in table 2.3. Database contains 122 data points having thickness of steel sheets, chemical composition, mechanical properties, type of coatings, welding process, testing condition of the spot welding and corresponding critical nugget diameter.

2 Database characterization – Before fitting, the collected data initially checked for its suitability. Scatter plots with critical nugget diameter on 'y' axis and different potential input parameters such as, thickness, chemical composition and mechanical properties on 'x' axis. These simple plots help to identify existing trend and outlier points.

3 Multivariate regression analysis - Regression analysis was used to model variability of critical nugget diameter as a function of different inputs such as thickness of steel sheets, chemical composition, mechanical properties, type of coatings, welding process.

4 Artificial neural network based model- ANN is a tool which can help in analyses non-linear relationships in complex systems within a data framework. This network works on the basis of assigning *'weight'* and '*bias*' to the input till they match with target value through MATLAB parameters such as adoption learning function, number of neuron and hidden layer with transfer function.

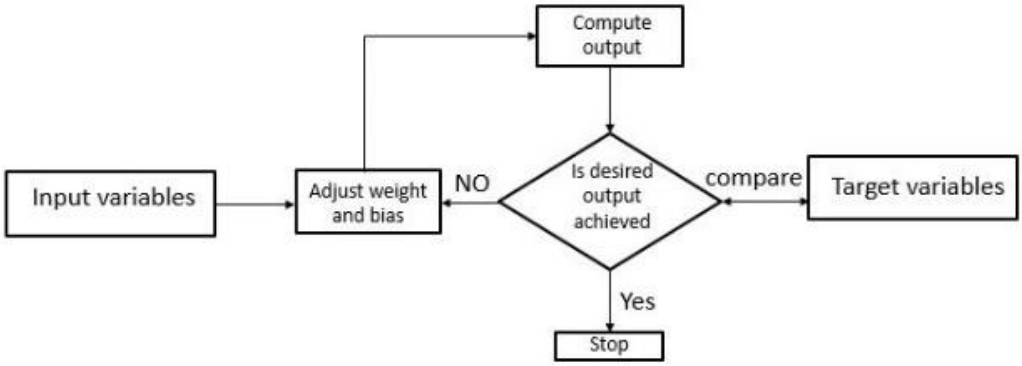

Figure 3.1: A schematic diagram showing the working of ANN tools and how they learn by comparing with target value.

5 Model validation - Experimental data of secondary coated IF steel, IFHS-GA, DP600, DQ and EIF steel were used to validate a trained artificial neural network.

Chapter 4: Results and Discussion

4.1 Database Extraction

Data extracted from sixty published papers out of one hundred fifty articles. Figure 4.1 illustrate the histogram of type of steels reported along with number of occurrence and the year of publishing that very journal.

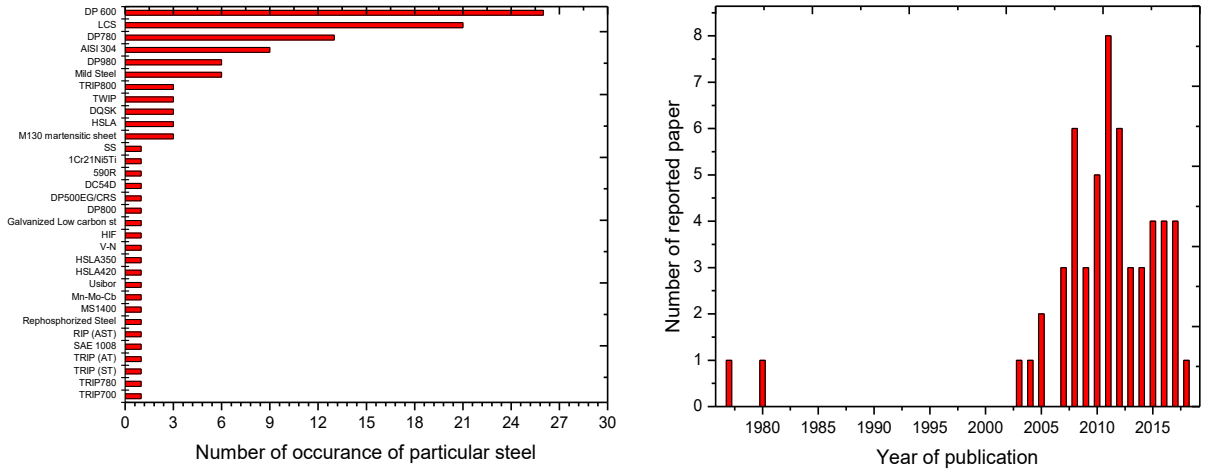

Figure 4.1. Bar diagram showing number of occurrence of a particular steel grade in the collated information from published literature and year of publication.

As seen in figure 4.1, majority of the paper related to the critical diameter of the spot welding were from last 10 years. The highly researched grade steels were advanced high strength steel (such as DP600, DP780, DP980, TRIP and TWIP), followed by low carbon steel and austenitic stainless steel because of the use in the automotive industry in wide range.

4.2 Database Characterization

The objective of database characterization is: to identify a set of input elements dependence on the output and to establish the relation between them, to determine ordering relationships as quantitative, ordinal, or nominal. These characterizations can also be helpful for judging how to group and integrate relations.

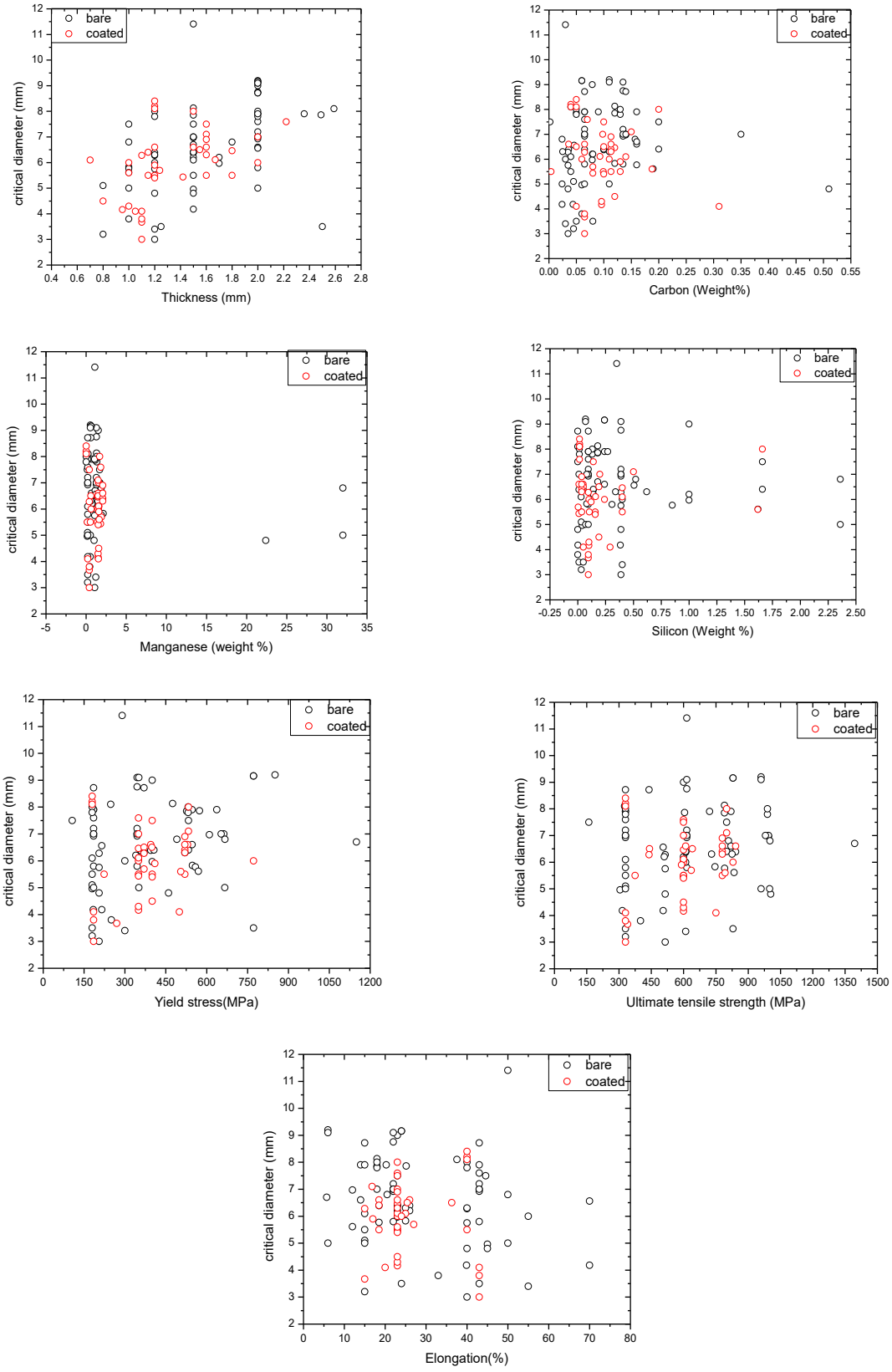

Figure 4.2. Distribution of different input variables in the database.

Figure 4.2 illustrates the range and the distribution of the variables plotted against critical diameter of the spot welds reported in different journals. There is a greater spread in the commonly used chemical composition of the steel such as carbon, manganese, base material hardness and mechanical properties such as ultimate tensile strength, yield strength and elongation including the most important variable i.e., steel thickness and coating of the steels having higher quality of prediction.

The database comprising uniform distribution of thickness, carbon content, amount of manganese; ultimate tensile strength, yield strength, elongation of steel etc. Therefore, the thesis is focused to model accordingly by varying these variables. Any effect resulting from the variation of these parameters could therefore be reflected as large uncertainty in the predictions.

The graphical presentation identifying a single element from a set of possible values, can be called as database characterization. Several characteristics of a set are relevant to choose an appropriate graphical technique. One characteristic is determining ordering relationships as quantitative, ordinal, or nominal. Another identifies whether an element is a coordinate [104]. A third feature may determine if sets can belong to the different domains. This information helps to preserve subtle stylistic conventions, such as using a horizontal axis for thickness coordinates and a vertical axis for critical diameter of resistance spot welding. These characterizations can also be helpful for judging how to group and integrate relations within pictures. The database contained sporadic data for the usually small amounts of phosphorus and silicon. Sufficient number of examples was no available to model the action of these two inputs reasonably.

4.3 Regression Analysis

A standard multivariate regression analysis algorithm was followed to correlate carbon, manganese, silicon in wt. %; yield stress, ultimate tensile strength in MPa, elongation and welding parameters such as electrode force in kN, welding current in kA and welding time in ms, along with coating index to critical diameter of resistance spot welding as seen in table 2.1. The analysis was carried out using standard spreadsheet. The regression statistics such as intercepts; coefficients of different variants are presented in Table 4.1. Near unity value of regression coefficient 'R^2' and 'adjusted R^2' (for multivariate regression) indicates that the sets of data have been fitted well to the equation [105]. As shown in the table 4.1, the adjusted r square of similar welding of low strength bare steel and similar welding of high strength coated steel were 0.91 and 0.83 when thickness, carbon, manganese, silicon and welding parameters were taken into account. On the contrary, when welding parameters were not taken in to consideration, the adjusted r

square of similar welding of low strength bare steel and similar welding of high strength coated steel were 0.93 and 0.99. This happened because database extracted from different published papers.

Approach 1: Without considering welding parameters

To predict the best fitted equation as shown in the equation 4.1, multivariate linear regression analysis was used. The equation is in the form:

$$\emptyset_{cr} = \boldsymbol{b_0}+\boldsymbol{b_1} \times (\boldsymbol{t}) + \boldsymbol{b_2} \times (\mathbf{C})+\boldsymbol{b_3} \times (\boldsymbol{Mn}) + \boldsymbol{b_4} \times (\boldsymbol{Si}) + \boldsymbol{b_5} \times (\boldsymbol{YS}) + \boldsymbol{b_6} \times (\boldsymbol{UTS}) + \boldsymbol{b_7}(\boldsymbol{\epsilon}) \quad \textbf{(4.1)}$$

Where b_0 is the intercepts and $b_1,\ b_2,\ b_3,\ b_4,\ b_5,\ b_6,\ b_7$ are the slopes of the equation having inputs variants as a thickness in mm, chemical composition such as carbon (C), manganese (Mn) and silicon (Si) by wt.%, Mechanical properties such as yield stress (YS), ultimate tensile stress (UTS) in MPa followed by elongation (ϵ). Output variant is critical diameter ($\emptyset_{cr}$) in mm.

Table 4.1. Sub classes of Resistance spot welding with adjusted R^2 without considering welding parameter.

Sl.NO.	Sub class	Observation	Intercept	Coefficient							Adjusted R^2
				Thickness (mm)	C	Mn	Si	YS (MPa)	UTS (MPa)	Elongation (%)	
1	Similar and dissimilar welding of bare and coated steel	122	2.912	1.66	-2.65	-0.049	0.377	0.001	0.001	0.006	0.236
2	Similar welding of bare and coated steel	88	1.999	1.99	-4.41	-0.071	0.306	0.000	0.003	0.019	0.357
3	Similar welding of bare steel	58	2.366	2.23	-5.11	-0.041	0.104	-0.001	0.003	0.003	0.408
4	Similar welding of high strength bare steel	43	2.794	2.27	-5.87	-0.030	0.045	-0.001	0.003	-0.001	0.344
5	Similar welding of low strength bare steel	15	-12.790	1.76	-12.2	-20.307	25.30	0.044	0.036	-0.018	0.926
6	Similar welding of caoted steel	30	0.362	1.13	-6.62	-2.244	0.11	-0.012	0.019	0.030	0.318
7	Similar welding of high strength coated steel	22	2.316	1.34	-3.76	2.173	1.41	0.013	-0.010	-0.039	0.677
8	Similar welding of low strength coated steel	8	6.776	0.0001	9.35	-2.158	0.001	-0.286	0.253	-0.773	0.998

Graphs shown in figure 4.3, Similar and dissimilar welding of bare and coated steel, similar welding of bare steel and coated steel, similar welding of low strength bare steel and similar welding of low strength coated steel having adjusted r^2 of 0.23, 0.35, 0.92 and 0.98 respectively. As the number of input data are decreased, adjusted r^2 are improved but not found the basis of exact fitting.

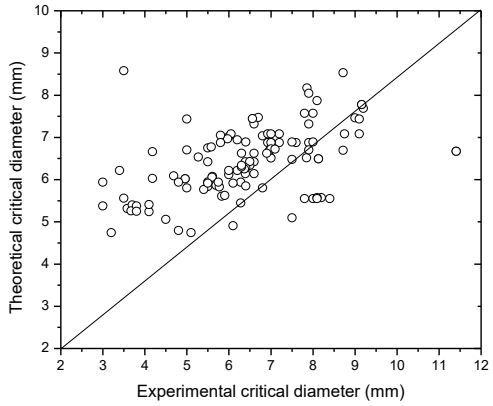

(a) Similar and dissimilar welding of bare and coated steel

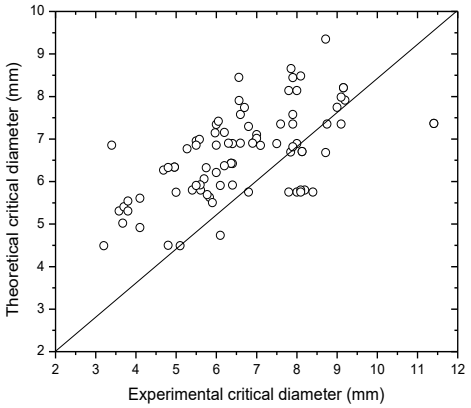

(b) Similar welding of bare steel and coated steel

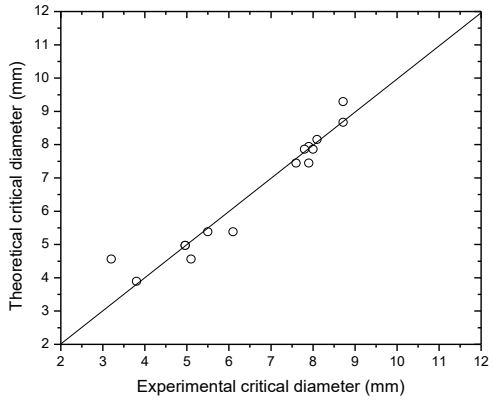

(c) Similar welding of low strength bare steel

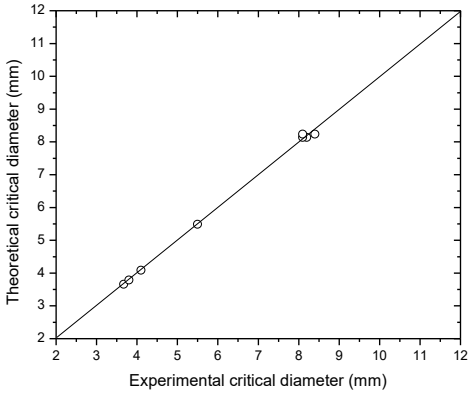

(d) Similar welding of low strength coated steel

Figure 4.3. Graph showing fitted model of different sub classes of resistance spot welding.

Approach 2: Considering welding parameters

Another attempt has been made to predict the best fitted equation as shown in the equation 4.2, multivariate linear regression analysis was used. The equation is:

$$\emptyset_{cr} = \boldsymbol{b_0}+\boldsymbol{b_1} \times (\boldsymbol{t}) + \boldsymbol{b_2} \times (\mathbf{C})+\boldsymbol{b_3} \times (\boldsymbol{Mn}) + \boldsymbol{b_4} \times (\boldsymbol{Si}) + \boldsymbol{b_5} \times (\boldsymbol{YS}) + \boldsymbol{b_6} \times (\boldsymbol{UTS}) + \boldsymbol{b_7}(\boldsymbol{\epsilon}) + \boldsymbol{b_8} \times (\boldsymbol{F})+\boldsymbol{b_9} \times (\boldsymbol{i})+\boldsymbol{b_{10}} \times (\boldsymbol{\tau}) \quad \textbf{(4.2)}$$

Where b_0 is the intercepts and $b_1,\ b_2,\ b_3,\ b_4,\ b_5,\ b_6,\ b_7,\ b_8,\ b_9,\ b_{10}$ are the slopes of equation having Inputs variants as thickness in mm, chemical composition such as Carbon (C), Manganese (Mn) and Silicon (Si) by wt.%, mechanical properties such as yield stress (YS), ultimate tensile stress (UTS) in MPa followed by elongation (ϵ). Welding parameters such as welding current (i), welding time (τ) and electrode force (F) as the function of critical diameter ($\emptyset_{cr}$) in mm.

Table 4.2. Sub classes of Resistance spot welding with adjusted R^2 considering welding parameters.

S.No.	Sub Class	observation	Intercepts	Coefficients										Adj. R^2
				t (mm)	C (wt.%)	Mn (wt.%)	Si (wt.%)	YS (MPa)	UTS (MPa)	ϵ (%)	F (kN)	i (kA)	τ (ms)	
1	Similar and dissimilar welding of bare and coated steel	122	0.19	1.7	-2.39	-0.03	0.61	-0.001	0.003	0.007	0.044	0.21	-0.001	0.21
2	Similar welding of bare and coated steel	88	-1.0	1.52	-3.21	-0.03	0.04	-0.001	0.003	0.019	0.065	0.28	0.003	0.33
3	Similar welding of High strength bare steel	43	0.74	1.1	-2.86	-0.01	0.4	-0.001	0.001	0.006	0.063	0.4	0.001	0.2
4	Similar welding of low strength bare steel	15	-22.74	2.86	-6.59	-21.35	-0.76	0.027	0.059	-0.01	0.795	0.24	-0.003	0.91
5	Similar welding of bare steel	58	1.65	1.45	-2.33	-0.08	.03	-0.002	0.001	0.001	0.021	0.12	-0.003	0.398
6	Similar welding of coated steel	30	1.65	1.56	-6.93	-0.82	0.93	-0.004	0.006	0.031	0.251	0.12	-0.004	0.47
7	Similar welding of high strength coated steel	22	5.2	2.01	-10.81	0.05	1.32	0.001	0.001	-0.046	-0.029	0.07	-0.004	0.83
8	Similar welding of low strength coated steel	8	-14.4	0.001	-5.99	-10.71	0	0.012	0.053	0.095	-1.172	0.51	-0.005	0.90

Since the adjusted R^2 as shown in table 4.2 is almost lower than that of first approach, therefore no any combination suited the basis of modelling in that case. Moreover, because of following reason, welding parameters were not considered in the ANN analysis:

1) The credibility of the welding parameters reported in different literature paper were doubtful.
2) The setup of laboratory across the world pertains different operating conditions
3) Most of the literature published had not mentioned welding parameters, therefore these data were reported through experiments of similar steel sheets
4) Selected steel sheets for experimental procedure were not having exact chemical composition and mechanical properties

4.4 Neural network

A general method of regression which avoids these difficulties is neural network analysis, illustrated at first using the familiar linear regression method. A network representation of linear regression is illustrated in Figure 4.3 The inputs x_i such as chemical composition (C, Mn, Si), mechanical properties (YS, UTS, %EL) and coating index define the input nodes, the critical nugget diameter the output node. Each input is multiplied by a random weight w_i and the products are summed together with a constant bias θ give the output $y = \sum_i^n w_i x_i + \theta$. The summation is an operation which is hidden at the hidden node. Since the weights and the constant θ were chosen at random, the value of the output will not match with experimental data. The weights are systematically changed until a best-fit description of the output is obtained as a function of the inputs; this operation is known as training the network [106].

To construct the modelling through ANN tools, input data set having thickness in mm, carbon (wt.%), manganese (wt.%), silicon (wt.%), yield stress (MPa), ultimate tensile stress (MPa) and elongation and the output/ target data set contained Critical diameter (mm) were first trained and then validated. In this case, training data were taken as 70% of all data, validation and test data were 15% each of all data which was selected arbitrarily by the ANN tools [107]. Since ANN compare the output value to the target value by assigning weight and bias and continues till it gets fully justified. ANN works with the help of following basic characteristic coefficient such as adoption learning function, number of layers, transfer function and number of neuron [108].

4.4.1 Effect of ANN on Similar welding of bare and coated steel without considering welding parameters

Table 4.3 shows the results of the neural network which was developed for the similar welding of bare steel by changing characteristic coefficient parameters of ANN tools through MATLAB. The best network developed when the adoption learning function was Learn GDM, number of neurons and layers were 10 with log sigmoidal as a transfer function. The adjusted R^2 is 0.938 shows the model is best fitted than that of other as shown in figure 4.4.

Table 4.3. Coefficient characteristics of ANN modelling network without considering welding parameter.

Network	Adoption learning feature	No. of layer	Transfer function	No. of Neuron	R value
1	Learn GDM	2	Tan sigmoidal	10	0.601
2	Learn GDM	2	Tan sigmoidal	20	0.811
3	Learn GDM	2	Tan sigmoidal	30	0.633
4	Learn GDM	2	Tan sigmoidal	40	0.601
5	Learn GDM	2	Log sigmoidal	10	0.938
6	Learn GDM	2	Log sigmoidal	20	0.741
7	Learn GDM	2	Log sigmoidal	30	0.803
8	Learn GDM	2	Log sigmoidal	40	0.084
9	Learn GD	2	Tan sigmoidal	10	0.908
10	Learn GD	2	Tan sigmoidal	20	0.442
11	Learn GD	2	Tan sigmoidal	30	0.488
12	Learn GD	2	Log sigmoidal	10	0.591
13	Learn GD	2	Log sigmoidal	20	0.901
14	Learn GD	2	Log sigmoidal	30	0.471
15	Learn GD	2	Log sigmoidal	40	0.544
16	Learn GD	3(20+10)	Tan sigmoidal	10+10	0.644
17	Learn GD	3(20+10)	Log sigmoidal	20+10	0.59

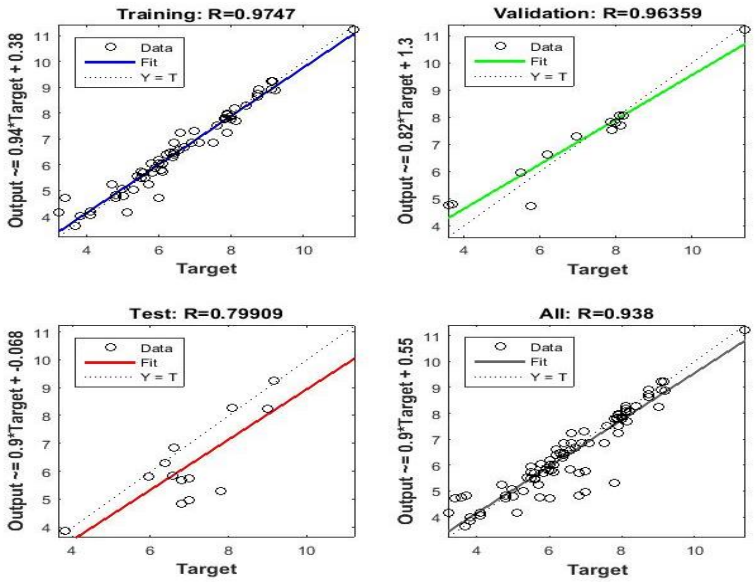

Figure 4.4. Graphs shows the magnitude of R for a similar welding of steel grades using ANN tool.

As shown in figure 4.4, the graph shows the best fitted training data R as 0.97. This shows that among all the inputs subsets, the training data is almost best fitted for this case and trained significantly at the fixed MATLAB parameters. The inputs subsets were arbitrarily selected as 70% of all data. The validation plot shows R of 0.96

4.4.2 Effect of ANN on Similar welding of bare and coated steel considering welding parameters

Table 4.4 shows the results of the neural network which was developed for the similar welding of bare steel by changing characteristic coefficient parameters of ANN tools through MATLAB. The best network developed when the adoption learning function was Learn GDM, number of neurons and layers were 10 with tan sigmoidal as a transfer function. The magnitude of R is 0.81 shows the model is best fitted than that of other as shown in figure 4.4 when welding parameters were considered. The welding parameters reported in different literature papers were not exactly reported. In most of the cases, it is assumed with reference to the other literature having same experimentation.

As shown in figure 4.5, the graph shows the best fitted training data R as 0.93. This shows that among all the inputs subsets, the training data is almost best fitted for this case and trained significantly by fixing the MATLAB parameters. The inputs subsets were arbitrarily selected as 70% of all data. The validation plot shows R of 0.70 of 15% of all data and the remaining data were randomly selected for testing. The R value for testing data is 0.34 made the result very less reliable.

Table 4.4. Coefficient characteristic of ANN modelling network considering welding parameters.

Network	Adoption learning feature	No. of layer	Transfer function	No. of Neuron	R value
1	Learn GDM	2	Tan sigmoidal	10	0.69
2	Learn GDM	2	Tan sigmoidal	20	0.3
3	Learn GDM	2	Tan sigmoidal	30	0.55
4	Learn GDM	2	Tan sigmoidal	40	0.81
5	Learn GDM	2	Log sigmoidal	10	0.35
6	Learn GDM	2	Log sigmoidal	20	0.6
7	Learn GDM	2	Log sigmoidal	30	0.69
8	Learn GDM	2	Log sigmoidal	40	0.47
9	Learn GD	2	Tan sigmoidal	10	0.61
10	Learn GD	2	Tan sigmoidal	20	0.48
11	Learn GD	2	Tan sigmoidal	30	0.77
12	Learn GD	2	Tan sigmoidal	40	0.47
13	Learn GD	2	Log sigmoidal	10	0.46

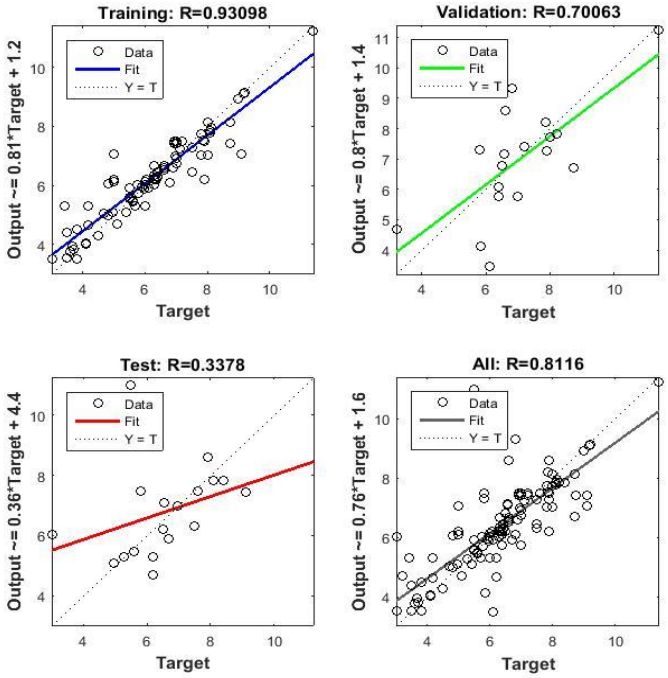

Figure 4.5. Graphs shows the magnitude of R for a similar welding of steel grades considering welding parameters.

Validation of ANN modelling

Validation of ANN model was done by carrying out experiment works on the secondary coated IF steel, IFHS-GA, DP600, DQ and EIF steel grades manufactured by Tata Steel Limited. The chemical composition, mechanical properties, coating index and corresponding critical diameter are shown in table 4.5

Table 4.5. Validation input data of steel grades.

Thickness (mm)	C (Wt.%)	Mn (Wt.%)	Si (Wt.%)	YS (MPa)	UTS (MPa)	EL (%)	Coting Index	Critical diameter	Steel Grades
0.8	0.0022	0.067	0.005	195	360	38	1	4.5	GA-IF (secondary coating)
1.6	0.04	0.53	0.104	224	375	40	1	5.6	IFHS GA
2	0.009	1.63	0.12	403	617	29.5	1	7	DP600 GA
1.5	0.07	0.4	0.04	290	390	30	0.5	7	DQ
1.2	0.07	0.4	0.04	300	400	30	0.5	5.5	DQ
1.2	0.0035	0.15	0.015	160	305	49	0.5	4.6	EIF

Figure 4.6, describes the variation of predicted critical nugget diameter on the y- axis and the experimental critical diameter on the x- axis. It is found that the prediction is better for primary coated steel grades, e.g. IFHS GA, DP600, DQ and EIF with thickness in excess of 1.2 mm. Since the ANN based model is developed by considering primary coated steel grades, therefore secondary coated. IF steel showed more scatter.

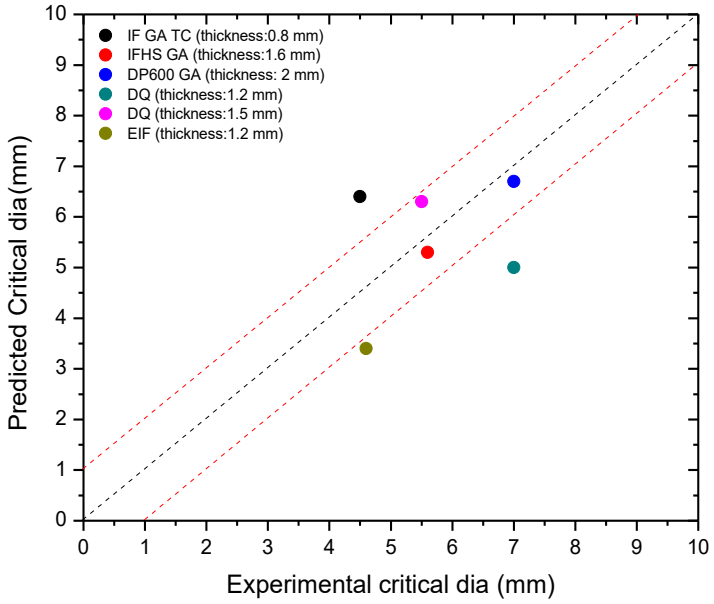

Figure 4.6 Validation of experimental critical diameter with the critical diameter.

Chapter 5: Conclusions

The ANN model development work for critical nugget diameter has led to the following conclusions:

1. An extensive database comprising of data from 122 welding experiments has been constructed, collected from 60 published literatures. This database contains information of steel properties (e.g. thickness, chemistry, YS, UTS, %El), coating type, welding parameters, joint configuration and critical nugget diameter. This database is the source of training/fitting data in subsequent analysis.

2. As in first approach, multivariate linear regression where carried out with (1) thickness and chemistry of steel (C, Mn and Si), mechanical properties (YS, UTS, %El) and coating type as inputs and critical nugget diameter as an output. However, this technique was not found suitable for modelling incorporating the entire dataset. Good correlation between input and output was observed when small subset of data was used. For example, for similar welding of low strength coated steel the magnitude of adjusted R^2 was 0.998. As the dataset contained only 8 data points and the result could not be generalized.

3. ANN based approach were subsequently conceived to model with data of: (1) chemistry (C, Mn and Si) of steel, mechanical properties (YS, UTS, %El) and coating type as inputs and critical nugget diameter as output. A neural network consisting of single hidden layer with 10 neurons and log-sigmoidal transfer function was used to successfully model the complete dataset. This model was validated against experimental data and the prediction was found to be within ±10% error band.

4. Inclusion of welding parameters (electrode force, welding time and current) in the input matrix of both regression analysis and ANN model revealed poor correlation and resulted in to poorer adjusted R^2 for complete dataset as well as smaller subsets. The higher degree of uncertainty factors associated with the welding parameters reported in the literature seems to be responsible for poor prediction performance.

Part II: Electrode Life Determination for Resistance Spot and Seam Welding of Automotive Coated Steels

Chapter 6: Introduction, Objective and Literature Survey

6.1 Electrode Life

Electrode life of resistance welding is defined as the number of welds that can be made, without dressing the electrode tips, before the weld size falls below an acceptable level or reducing weldability. Electrode tip wear, resulting in electrode tip face growth, are the dominant process that limits electrode life in RSW of Zn coated steel [24]. The extensive use of interstitial-free (IF) steels in the automotive industry makes their resistance spot welding (RSW) metallurgy important. Competition between materials and environmental legislation are driving the big trend for lighter automobile. The exploitation of formable steels commonly used in automotive industry due to excellent deep drawability, owing to its ultralow carbon and nitrogen[109].

Resistance spot welding has been used for various fields from an auto industry to a medical area. In the automotive industry, galvannealed (GA) steel sheet is used for both exposed and internal body parts because of its superior corrosion resistance and its good weldability and printability [110]. Galvannealed coatings are essentially diffusion layers containing Fe-Zn intermetallic phases formed between molten Zn and steel substrates at annealing temperatures around 500 ^{o}C.

IF steel is essentially a single-phase bcc steel with ductility. IF steels have been developed by achieving ultra-low carbon and nitrogen levels for lower yield strengths and higher work hardening exponents (n-values) [109]. These steels have more stretchability than Mild steels. Phosphorus is added to increase the strength and are widely used for both structural and closure applications. In order to achieve optimum formability and also to compensate for the loss in strength due to their ultralow carbon content, strong carbonitride forming elements such as titanium and niobium during production stage are added when the steels are in molten state by the process of degassing [111]. As this type of steel is not so strong rather it formed shape easily when pressed so it is used easily in automobile to make parts easily. IF steel is termed as ‘clean steel’ as the total volume fraction of precipitates is very less. In spite of this, the precipitates appear to have a very significant effect on the properties of IF steels. properties of these types of steels extending their application in the automotive industry are their stretcher-strain (St-St) pattern inexistence and antiaging property due to the negligible amount of solute C and N atoms [112]. Furthermore, the low yield strength of these steels leads to the disappearance of surface deflection (orange peel effect) at the outer face of the automobile [113].

Therefore, due to these distinct characteristics of IF steels, they are frequently used as rear and front door inners, side panels, spare wheel wells, oil pans, and rear floor pans [114].

6.2 Objective

Researchers have already reported works on electrode life determination for resistance spot welding. However, most of these works focused on working with either galvanized or galvannealed steel sheets. There is hardly any work discussing the effect of organic/inorganic based secondary coating on electrode life. Also, for electrode life determination in resistance seam welding there is no comprehensive information available. In this work, attempts have been made to determine the life of commercially available electrodes when welding is done on a 0.8 mm thick secondary coated galvannealed steel sheets. Electrode life for both resistance spot and seam welding have been determined.

6.3 Literature Survey

Resistance seam welding (RSeW) is also called as solid-state welding as no traces of melting is observed. The principle of seam welding is same as that of spot welding rather it produces a series of overlapping spots coalescence in the form of continuous line rather than a point unlike spot welding. Here the electrodes used, are revolving in nature as shown in figure 6.1 [115], [116]. RSeW is mainly suited in very thin sheets with the help of two wheel electrodes. During welding, these electrodes first exert a necessary pressure called as squeeze pressure with appropriate time called as squeeze time to maintain a base metal in close contact followed by transmitting electric current to the closed contacted sheet. The resistance seam welding depends on the electrode force, electrode characteristics, welding current, current on/off timing and welding speed [117]. The electric current used in seam welding is usually pulsating in nature. Spots overlapping depends on the electric current frequency and welding speed. For a constant welding current, when welding speed increased, the nugget overlap decreases [118]. Moreover, Girth weld is possible in rectangular or square or even in circular shapes. Due to high welding speed the process is efficient, non-polluting. It does not require any filler metals to perform suitable welds. The welding process is restricted to a straight line or uniformly curved line. The metals sheets having thickness more than 3 mm can cause problems while welding. The design of the electrodes may be needed to change to weld metal sheets having obstructions. Seam welding is mostly applied in manufacturing of containers, radiators and heat exchangers and fuel tanks for two wheelers [119].

M. D. Tumuluru et al.[120] investigated procedure development and practice considerations for seam welding. Peel test and tensile tests were carried out to evaluate mechanical strength of weld. This paper elaborates seam welding of ferrous materials like low carbon steel, stainless steel and nonferrous materials like Al, Cu, Bronze etc. The paper concludes that if the indentation is properly controlled, the welded joint will have a tensile strength of 80 to 100% of the parent metal.

J. Saleem et al. [121] have been done 3 dimensional finite element simulation of seam welding process. Appropriate parameters selection for welding sheets of different thicknesses depends on trial and error methods. They prove that a three-dimensional model with accurate material properties for the seam welding could prove to be a good tool for understanding the difference between applying different frequency/mode input signals and in checking their effect on the seam weld nugget growth.

Alireza Khosravi et al. [118] concluded that increasing current for low welding speeds results in the decreases nugget size. It also increases joining zone thickness in each galvanized and electro galvanized sheet when higher current used. With the increase of welding speed keeping current constant, nugget size decreased and thickness of joining zone increased. Maximum hardness always was in the centre of the weld.

Inoue Tomohiro et al. [122] investigated an electric resistance welding (ERW) line pipe technique with a high performance weld seam developed by JFE Steel. An analytical model of the ERW seam was constructed by finite element analysis. Improved seam mechanical properties were achieved by the development of this homogeneous heating technology.

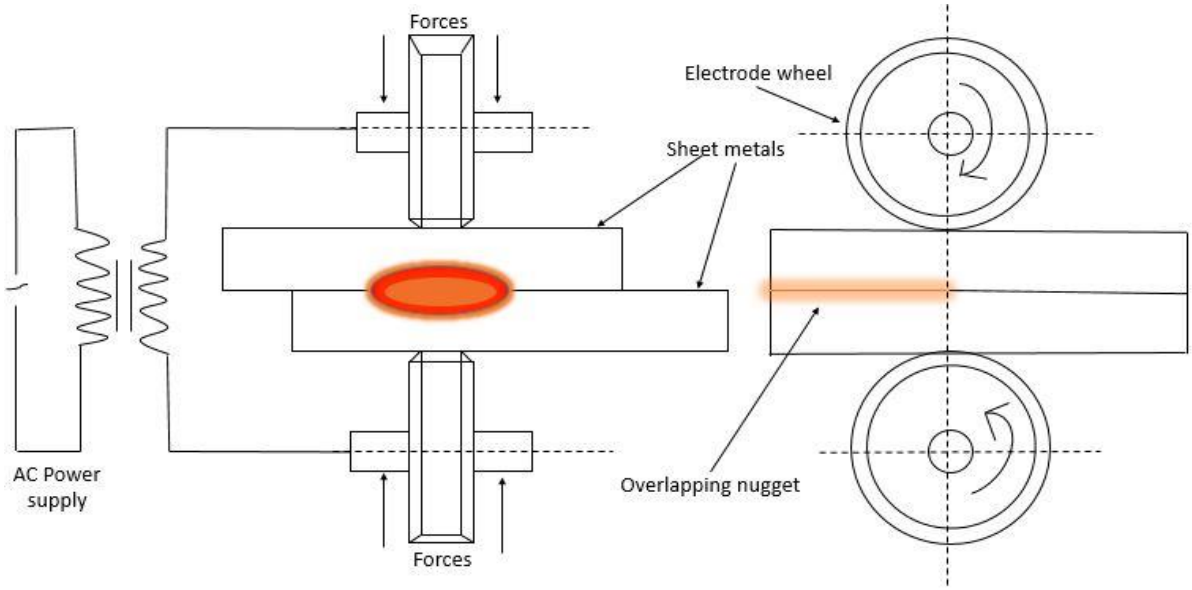

Figure 6.1. A Schematic diagram of RSeW Process.

Table 6.1. Electrode life of resistance welding

Welding type/ configuration	Type of steel	Life of electrode	Remark	References
RSW/similar	Nickel coated Mild steel	TiC composite coating increased the tip lives of Cu-Cr-Zr and Cu-Al_2O_3 electrodes by about 70 %	Improvement in tip life due to the use of Cu-Al_2O_3 electrode was relatively small compared to the Cu-Cr-Zr electrode (only 15%)).	[123], [124]
RSW/similar	Fe coated GA steel	Electrode life increased by two-fold when Fe content increased from 8 to 10 mass% and further increased when Fe increased to 13 mass%	Experiment stopped at 10,000 number of weld so exact improvement was not made.	[125]
RSW/similar	GA steel	electrode life increased by 110% when Fe was 11.4 mass%, while electrode life remains same when Fe coating ranges from 7.6 to 9.6 mass %	Higher Fe content in coating leads to higher hardness and contact resistance reduces the current to obtain the same weld	[126]
RSW/similar	Aluminum sheet	The increase in Relative radius and Edge concentration led to a decrease in weld shear strength	Applicable for Ac life test	[127]
RSW/similar	Zinc coated IF steel	The adjustment in welding parameters favors an increase in the lifetime of conventional copper electrodes, ensuring an improvement in the quality of the welds.	The hardness results at the end of the useful lifetime of the electrode were lower in all regions because of formation of brass.	[128]
RSW/similar	High strength steel with Zn coating	The Al was found on the surface of the tungsten insert. The presence of aluminium is most likely in the form of aluminium oxides, and also the presence of Al-tungsten phases	Tungsten insert in copper alloyed electrode is through sintering technique to remove the possibility of cracking.	[129]
RSW/similar	Zinc coated steel grade	The predicted rate of liquid Zn penetration into Cu was 500 times more than the rate of solid-state diffusion.	Model suggested that the life of resistance spot welding electrodes can be increased by enhancing their softening resistance rather than their absolute strength	[130]

Chapter 7: Materials and Experimental Procedure

7.1 Materials

The materials used in the present study were commercially produced grade interstitial free steel with coating from TATA Steel LTD., Jamshedpur, India. The steel was in the form of sheet having nominal thickness of 0.8 mm. The chemical composition of the steel in wt.% is given in table 7.1.

Table 7.1. Chemical composition of coated IF steels (wt.%)

Sheets	Coatings	C	Mn	Si	Cr	P	Ni	Nb	Ti	N (ppm)
IF steel	GA + secondary (organic)	0.0022	0.067	0.005	0.016	0.015	0.021	0.012	0.028	25
IF steel	GA	0.003	0.064	0.004	0.018	0.011	0.019	0.013	0.03	22

7.2 Resistance Welding

Before resistance welding (RSW), the specimens were thoroughly cleaned with ethanol so that surface asperities effects and expulsion during welding due to impinges of the dust particles can be avoided.

7.2.1 Resistance Spot Welding

The sample configuration is shown in figure 7.1 to ensure proper alignment during spot welding. The dimensions of the samples were 240 mm×120 mm. The sample were automatically welded for continuous number of weld in the same manner as marked with “S” and end with “E”. The spot welding was performed using a 120 kVA AC pedestal-type resistance spot-welding machine operating at 50 Hz, controlled by a programmable logic controller (PLC) as shown in figure 7.2. The welding was conducted using a 45^{o} truncated-cone RWMA Class-2 electrode with a 5 mm face diameter. The electrode was Copper based alloy having 0.8 wt.% chromium 0.08 wt.% zirconium.

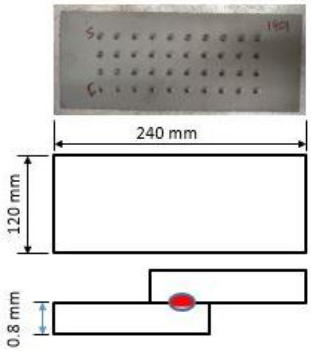

Figure 7.1. Configured sample of spot weld

Figure 7.2. Arrangement of spot welding

7.2.2 Resistance Seam Welding

The sample configuration is shown in figure 7.3 to ensure proper alignment during spot welding. The dimensions of the samples were 240 mm×120 mm. The seam welding was performed using a 120 kVA AC pedestal-type resistance seam-welding machine operating at 50 Hz, controlled by a programmable logic controller (PLC) as shown in figure 7.4. The welding was conducted using a circular Copper based alloy electrode wheel with a 30 cm diameter having trade wheel of 6.19 mm width.

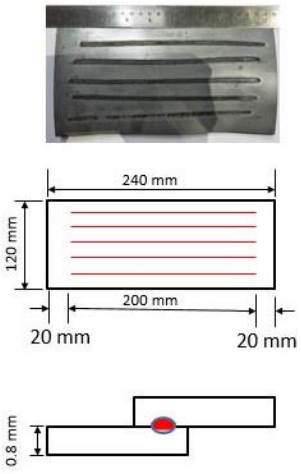

Figure 7.3. Configured sample of seam weld

Figure 7.4. Arrangement of Seam welding

7.3 Tensile Shear Test

Uniaxial shear tensile tests were carried out at room temperature using an Instron 5582 machine at a constant strain rate of 5 mm/min. Spot and seam welds sample were tested for each parameter combination. This tests were done to know the failure mode (such as IF, PF, PIF), maximum load, extension at maximum load, energy at maximum load. The schematic drawing of the specimen for spot and seam welding is presented in figure 7.5 and 7.6 respectively.

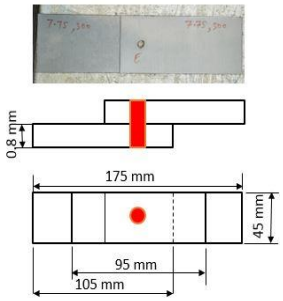

Figure 7.5. Schematic weld joint design of spot welding for TS test

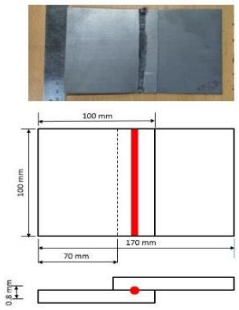

Figure 7.6. Schematic weld joint design of seam welding for TS test.

7.4 Cross Tension Test

Cross tension tests were carried out at room temperature using Instron 5582 machine at a constant strain rate of 5 mm/min. Since vehicles also exerts a bending stress in addition to tensile stress, therefore this type of test is necessary to determine the buckling stress or bending strength of the weld nugget. These tests were possible only in case of resistance spot welding. The schematic drawing of the specimen is presented in figure 7.7.

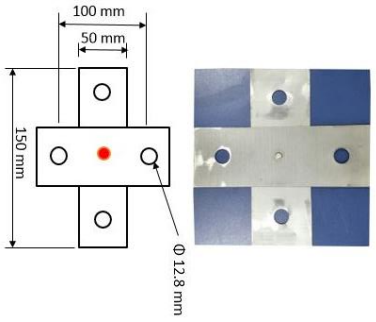

Figure 7.7. Schematic weld joint design of spot welding.

7.5 Heat Generation Measurement

Heat generated during resistance spot as well as seam welding were calculated from the Miyachi instrument which directly measures welding current in “kA” and welding voltage in “v” corresponding to total time in a cycle. In spot welding heat generated during single spots were calculated in kJ and in seam welding, it is calculated in the form of kJ/cm because of peripheral velocity of electrode wheels.

7.6 Optical Metallography

The transverse cross sections of welds nuggets were prepared by a standard metallographic procedure which were: cutting each of the samples cross section wise through EDM machine and using an Al_2O_3 abrasive disc in a PRESI Mecatome T180 abrasive cutter, molding with a nonmagnetic powder through black epoxy with a “Mecapress 3”, polishing in such a way that no scratches and pits were available followed by two step modified etching which were: 4 % Picral etchents (2 gm of picric acid mixed with 50 ml of ethanol) and 2 % Nital solution (1 ml of nitric acid mixed with 50 ml of ethanol). Optical examination of specimens was carried out using a Leica optical microscope (LEICA DM 6000 M), Gemini supra 25 type SEM microscope.

7.7 Electrode imprints and images

Electrode imprints and images were taken after every 120 number of spots and after every five meter of continuous seam welds to expose the variation in the width of electrode and to explore the damage occurred during welding either in the form of deposition or break of up of zinc layer from the electrodes. Electrode imprints were done through carbon paper. Images were taken from stereo microscope in case of spot welds and camera in case of continuous seam welding.

Chapter 8: Results and Discussion

Approach 1: Resistance Spot Welding

The material for this study was chosen as 0.8 mm thick galvannealed interstitial free (IF-GA) steel with thin organic secondary coating (2±1 μm). The standard RWMA Class-II type electrodes with truncated dome geometry and made of Cu - 0.8% Cr-0.08% Zr were chosen. The weldability lobe was generated using BS 1140:1993 standard. The TSS and CTS tests were also carried out to confirm the mechanical performance and failure modes of the weld. The welding parameters for electrode endurance test were decided with the help of weldability lobe. For example, welding current for endurance test was selected as 0.25 kA less than the expulsion current. Expulsion current was found to be 8 kA from the weldability lobe.

For performing endurance test, weld lobe was constructed to obtain the range of welding parameters such as welding current and welding time. Welding current of (According to BIS 1140:1913; $I_{Expulsion} - 0.25$) 7.75 kA, welding time of 300 ms and electrode force of 3.2 kN were used. For endurance test, weldability of steel sheets was evaluated by performing welding of 1440 number of continuous spot welds. This was done to prepare the test samples for tensile shear test, cross tension test, peel test for evaluating the maximum tensile strength, maximum cross tension strength and nugget diameter and the failure location starting from the no weld condition (initial) to 1440 number of welds at an interval of 120. Microstructure of eight welded specimens with varying welding current and welding time were prepared to assess the quality of welds. Stereo images of the tip of electrodes at the initial and final condition were taken to know the condition of electrode.

8.1 Construction of Weld Lobe

The weld parameters such as welding current and time were varied with the constant electrode force of 3.2 kN to construct the weld lobe. The effect on the weld nuggets starting from 5 kA (no weld) to 8.5 kA. The expulsion was noticed during welding when the current exceeds the permissible range leads to the arcing between sheet-electrode interference or between sheet-sheet interference [27]. The welding currents were increased with a step size of 0.25. The welding time for each of the given current were 150 ms, 200 ms, 250

ms and 300 ms.

Figure 8.1 shows the undersize, weaker nuggets were generated (no weld condition) between 4.5 to 5.0 kA weld current at a welding time of 150 milliseconds due to the scarcity of welding current to develop nugget and thus heat generated at the faying surface decreases [80]. The right limit of weld lobe was established as the nugget weldments are large. This can result in severe expulsion which decreases the weld strength. Pouranvari et al. [27] reported that expulsion did not reduce the load carrying capacity of spot welds. It reduced their energy absorption capability due to the change of failure location. Excessive electrode indentation is responsible for this. When welding current and welding time are high, the spot weld will also have intensive heat. This will affect the nugget size and strength of the weld joint [131], [132]. In the present study, weld strength is used as a criterion to assess the weld quality.

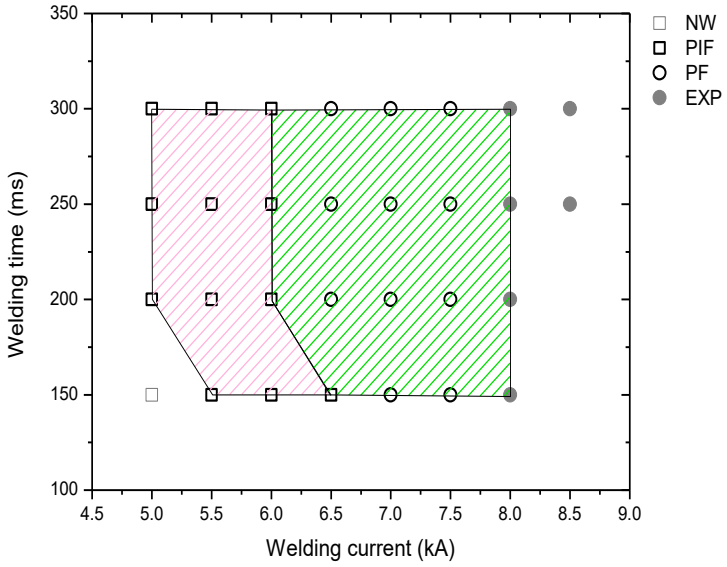

Figure 8.1 Weld Lobe at constant electrode force of 2.2 kN.

8.1.1 Tensile shear (TS) performance of the spot welds

The effects of the welding parameters such as welding current and welding time on the, nugget diameter, tensile shear strength and failure mode of the nugget were investigated. As the welding current increases, plug or nugget diameter increases due to heat generation increases

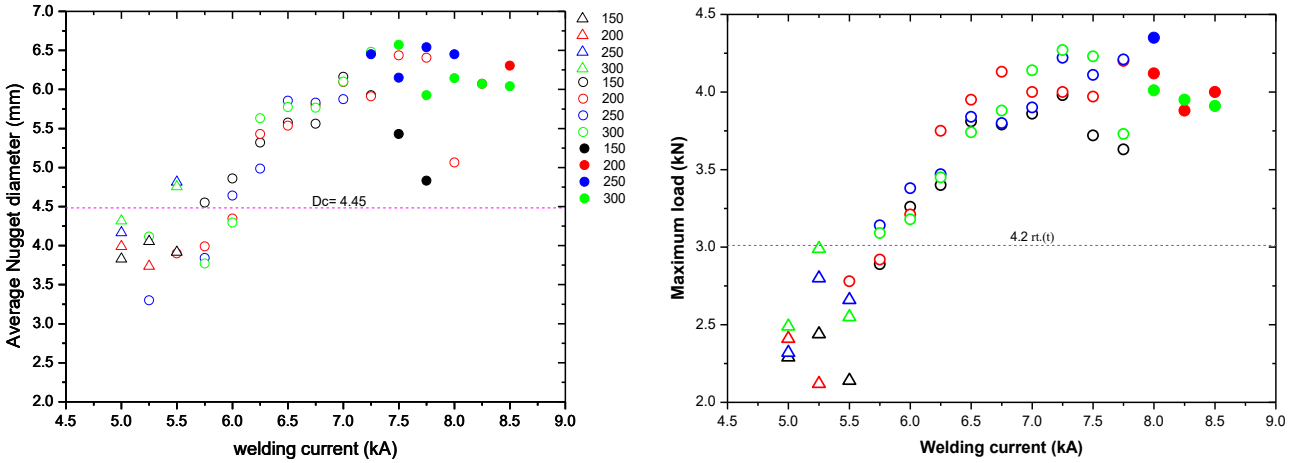

Figure 8.2. Variation of Nugget diameter and the tensile strength as the function of welding current and time at constant electrode force of 3.2 KN

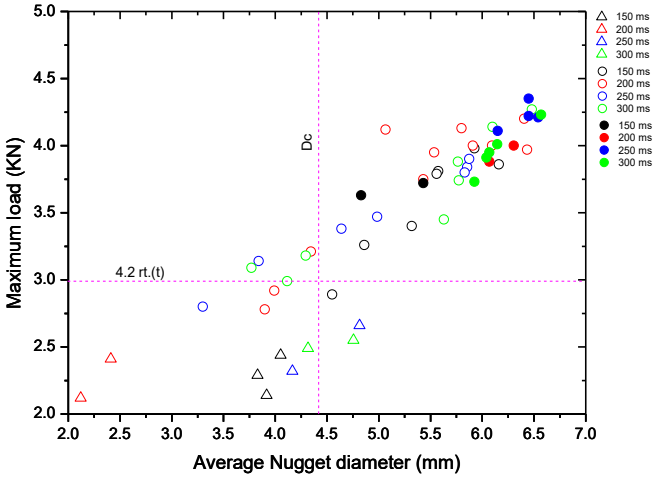

Figure 8.3. Variation of maximum tensile strength as the function of average nugget diameter at constant electrode force of 3.2 KN by varying welding current and time.

The tensile shear strength of the weldments improves by increasing the heat input associated with the welding current and the welding time. The maximum tensile shear strength for the welded sample 4.35 kN at the welding current of 8 kA and welding time of 250 ms. However, it resulted in expulsion as discussed earlier. The acceptable maximum tensile strength was therefore being 4.27 KN with welding current of 7.25 kA and welding time of 250 ms.

The failure modes of the test samples were examined. An interfacial failure mode was assessed till 5.5 kA welding current for all welding times (Figure 8.2 and Figure 8.3). The interfacial fracture mode can be avoided by either reducing the fusion zone hardness or alternatively increasing the nugget diameter for a given sheet

thickness [86]. Increasing the heat input, enabled a joining of larger area, resulting in a desired pullout failure mode. An expulsion was evaluated with welding current of 8 to 8.5 kA for all welding times due to high heat input. There is a critical heat input which results in a PIF type failure [89]. In between IF and PIF mode, the PF mode is assessed with the range of welding currents of 5.5 to 7.75 kA. With the increase of the welding current, the mode of failure changes. This is due to the increase in the nugget diameter [133]. The nugget diameter for IF mode was 4.8 mm (tensile load: 2.67 KN). The maximum nugget diameter in which expulsion was started is 6.45 mm (tensile load:4.35 KN).

8.1.2 Cross Tension (CT) performance of the spot welds

As the welding current increases, the nugget diameter increases to 6.5 mm at 7.75 kA and then due to expulsion, nugget diameter start decreasing because of arcing in the form of molten metal due to maximum heat generated. The maximum cross tension load also increases with the increase in nugget diameter. The failure mode initially PIF, then PF having maximum CT an TS strength and then expulsion with decreasing trends.

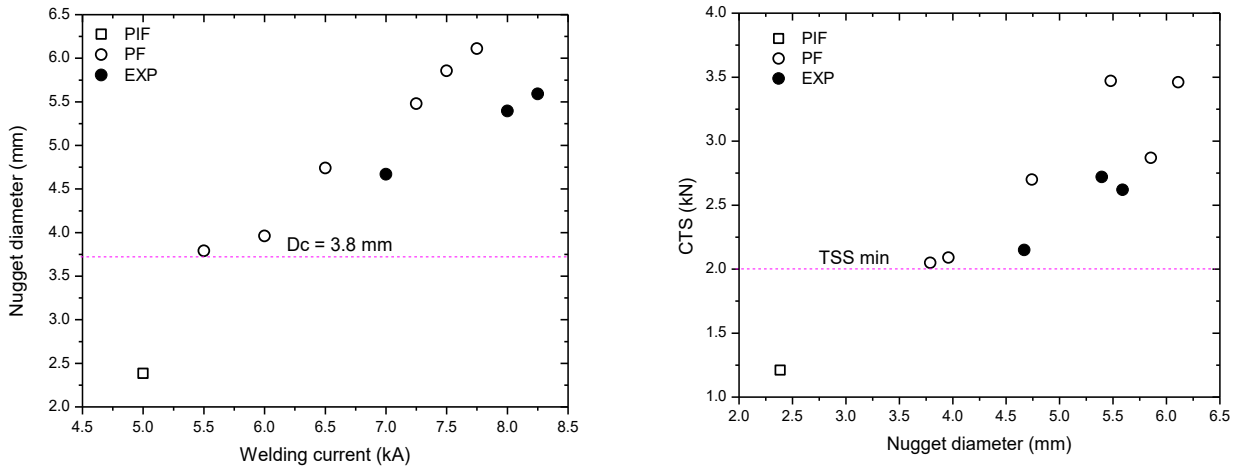

Figure 8.4. Effect of welding current and nugget diameter on the cross-tension strength of the spot weld.

As seen in figure 8.4, minimum critical diameter where nugget fails via pull out failure is 3.75 under cross tension test at 5.5 kA. The failure mechanism for pullout failure is proportional to the ratio of the tensile strength of the FZ to the shear strength of the HAZ [40]. The critical diameter in cross tension test decreases as compared to the tensile shear test.

8.2 Endurance test

8.2.1 Effect of Heat input on number of spot weld

Nugget diameter shows almost constant trends with all the diameter above $4\sqrt{t}$ and $5\sqrt{t}$ as described by AWS and Japanese standard (Figure 8.5 (a,b)). The energy was calculated using the equation (4.3):

Energy input per spot = $\int_0^t v(t).I(t).dt$.....(8.1)

Where t is the welding time required to complete cycle in ms, v is voltage in v and I is the current in kA. These data were directly taken from the Miyachi instrument during welding.

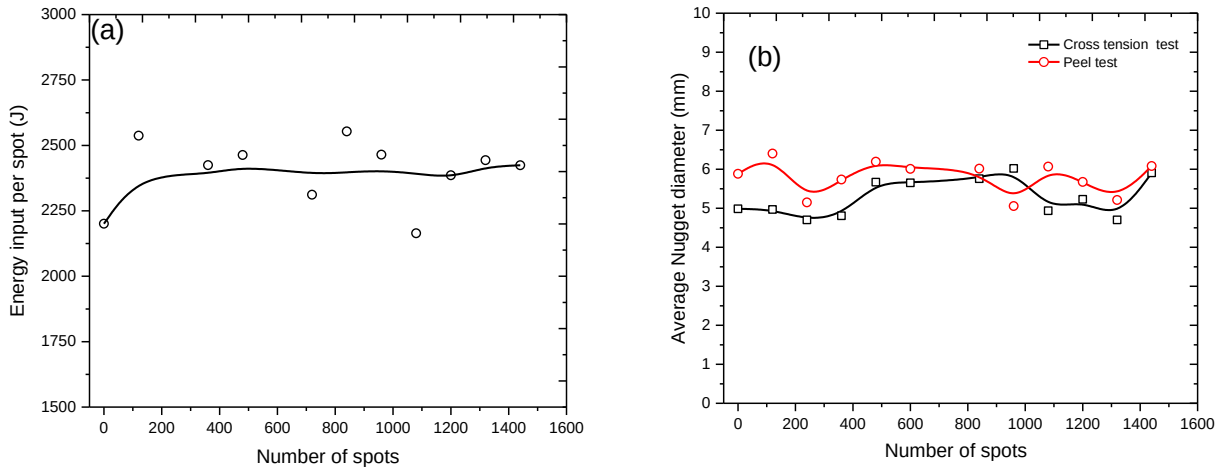

Figure 8.5. Variation of energy with the number of welds under cross tension test and (b) The effect of the number of spot welds on nugget diameter.

8.2.2 Effect of mechanical performance on number of continuous spot welds

Maximum load and extension at maximum load decrease with the increase in number of continuous spot welds. It is above the minimum tensile load according to AWS and Japanese and NES standard of 3.0 KN at the 1440 number of continuous welds.

The maximum tensile strength and extension at maximum load are 4.38 KN and 2.83 mm (Figure 8.6 (a, b)) at 120 number of spot weld. This was not accepted due to expulsion evaluated at this position. The acceptable maximum tensile strength and extension at maximum load are 4.21 KN and 2.63 mm at 480

continuous spot welds. The failure mode was PF. It was evaluated by the dint of the expulsion. As the number of spot welded increases, the mode of failure of the nuggets was first expulsion then pullout failure followed by partial interfacial failure with the decreasing strength of the welded nuggets.

Under cross tension test as shown in figure 8.6 (c, d), the minimum cross tension strength is 1.9 KN and the minimum extension at the maximum load is 26 mm. The trend shows that it is almost constant over the entire number of welds (1440).

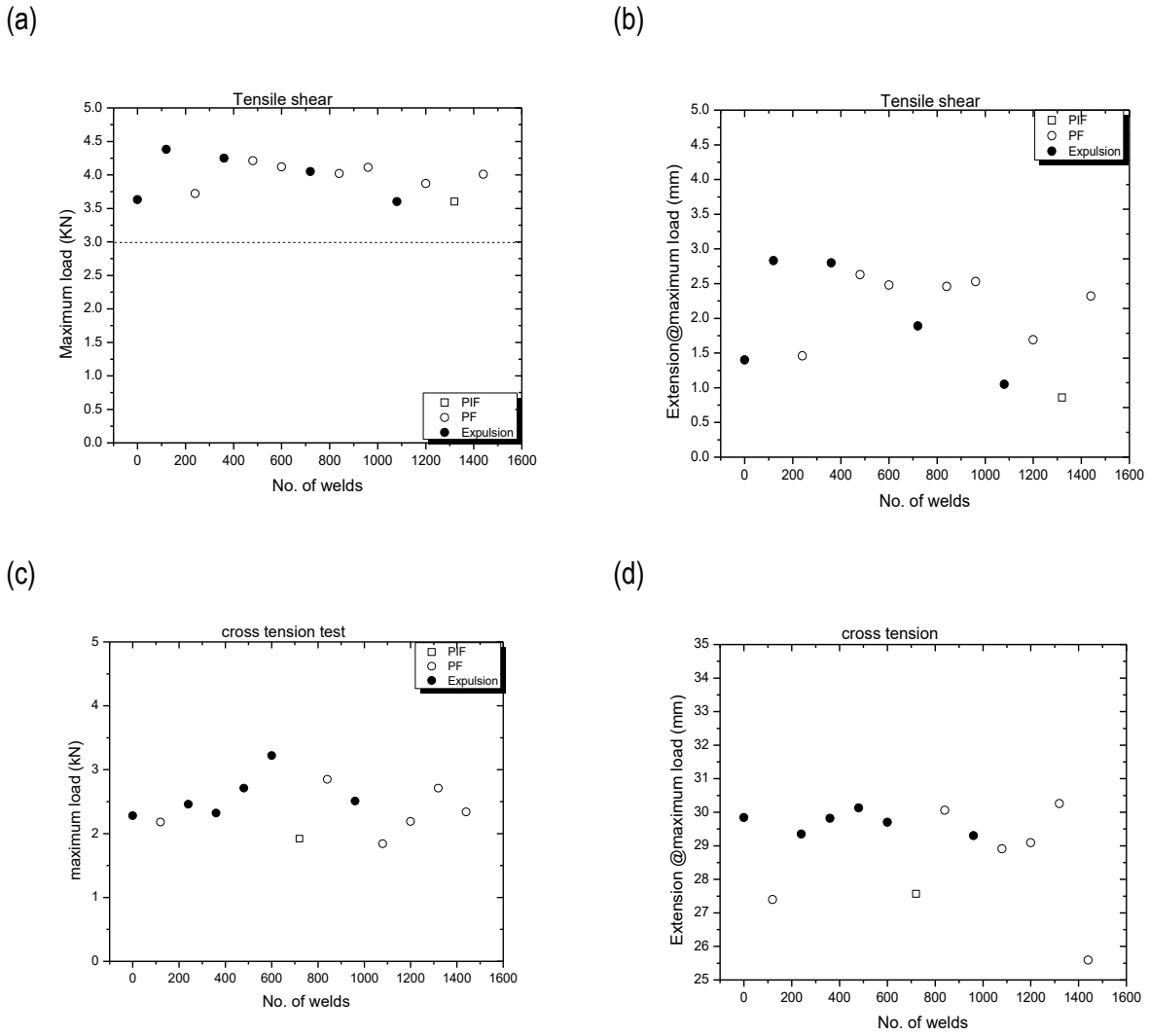

Figure 8.6. Effect of the maximum load and extension at the maximum load on the number of spot welds subjected to TSS and CT tests.

As shown in figure 8.6 (c, d), the cross-tension strength of the initial weld and the final weld (1440 number of continuous spot welds) remains approximately same. The maximum cross tension strength and extension at the maximum load is 3.22 KN at 600 number of spot weld and 30.13 mm at 480 number of spot weld

respectively. The strength and extension at the maximum load was evaluated in the form of PF with some sort of expulsion. Moreover, with the lapse of number of spot welds, the cross-tension strength first showed an increase up to 600 number of continuous welds and then drops rapidly to 2.51 KN at 960 continuous welds. This happened because during expulsion the mode of failure was pullout failure but at 720 continuous welds, the mode of failure was partial interfacial failure with no expulsion.

8.2.3 Electrode condition

During endurance test, the electrode gets eroded as the number of continuous spot welds increases as shown by stereo images in figure 8.7. After 1440 number of continuous welds, the centre portion of face of truncated electrode get eroded because of the following:

1) Since the heat generated during continuous spot welds were constant made the electrode life not degradation first otherwise they may have fail to develop the standard nugget diameter.
2) Formation of brass on the top face of electrode (reaction of zinc coating with that of cu electrode at the elevated temperature ~1700^{0}c). The width of top face of electrode increases leads to the lower energy density made the spot undersized.
3) Since Cu electrode is softer than that of zinc metal, therefore after repetition of spot welding, electrode get eroded.
4) Figure 8.7 shows the initial and final condition of electrode. As compare to mushrooming effect on the electrode, degradation is the dominating phenomenon because of secondary coated IF steel.

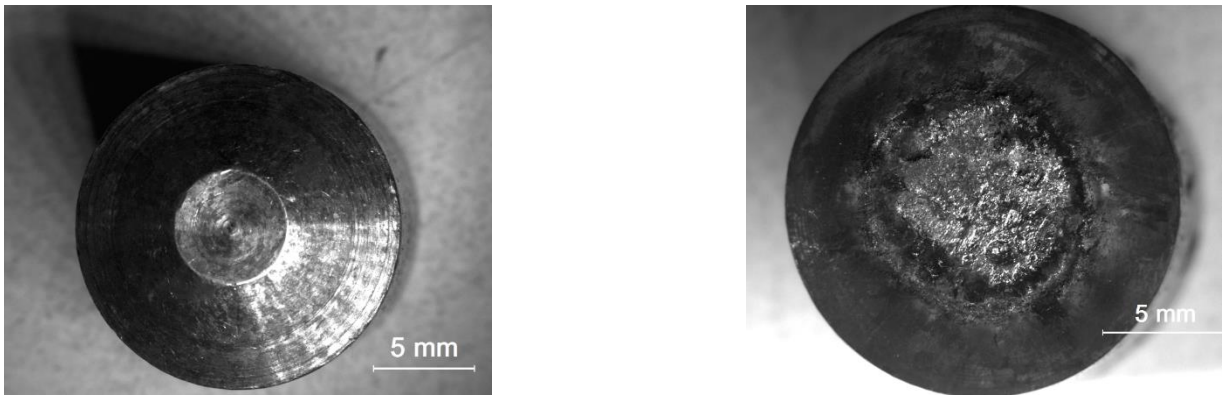

(a) Initial condition (b) Final condition

Figure 8.7. Stereo image of the electrode in (a) initial condition and (b) after 1440 number of spot welds.

Approach 2: Resistance seam welding

Materials used in this experiment were 1) Interstitial Free (IF) steel having primary coating of galvannealed (12 µm) and secondary coating of organic (3 µm). For performing endurance test, weld lobe was constructed to define the range of welding parameters such as welding current and welding time. In this case welding current of 11 kA, welding speed of 1.5 m/min and a constant electrode force of 3 Kg/cm^2 were used. For endurance test, weldability of steel sheets was evaluated by performing continuous seam welding of 30-meter weld length. This was done to prepare the tensile shear test specimens and peel test specimens for evaluating the effect of mechanical properties on the joint strength and failure location starting from initial when no weld condition to 30 meter of weld lengths at an interval of 5 meter. Moreover, micro structure analysis was performed as a function of weld length to evaluate the quality of welds and zinc intrusion. Electrical performances in the form of heat generated for each case were assessed to correlate the relation between heat input in kJ/cm to the nugget diameter. Electrode images using camera and imprints using carbon paper at every five meter of weld lengths were performed to estimate the degradation and changes in the width of the electrode trade wheel.

8.3 Construction of the weld lobe

The effects on the weld nuggets starting from weld current of 8 kA where no faying surface was developed as shown by TS test up to 13 kA where copper ingression was first noticed during welding from the eroded surface of the electrode due to formation of the brass. Moreover, heavy copper ingression took place at the welding current of 14 kA to 16 kA. The arcing between electrode and sheet or between two steel sheets due to high current is called as expulsion which was initiated from 13 kA down to 12 kA.

In the present study only two parameters were consistently varied (such as welding speed and welding current) with constant electrode force of 3 gf/cm^2. The desired nugget diameter can only be obtained by adjusting welding current intensity versus welding time properly [12, 13] with fixed electrode force. A graphical explanation of the ranges of welding parameters over which acceptable seam welds are formed at a constant electrode force is known as a “Seam Weld Lobe Curve” [59].

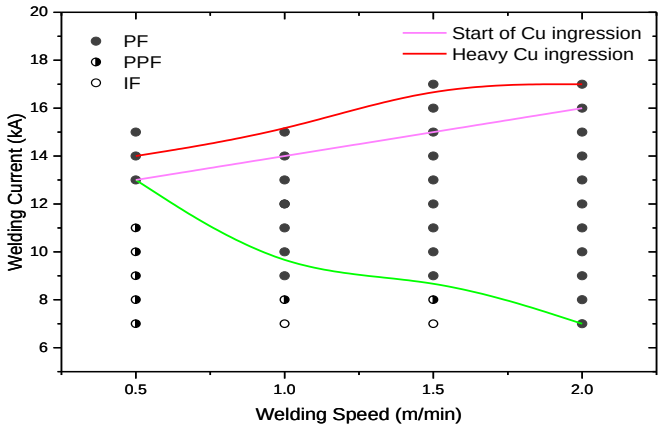

Figure 8.8 Weld Lobe at constant electrode force of 3 Kg per cm^2.

The weld lobe (Figure 8.8) of secondary coated IF steel based on welding current and welding speed gives an indication of good welding parameters and the tolerance of the weld schedule in the manufacturing environment [134], [135]. The weld currents between 6.5 to 11.0 kA resulted in undersize weak nugget. The upper limit of the weld lobe was established as the nugget weldment are large, resulting in severe expulsion decreasing the weld strength. Pouranvari et al. [27] investigated that although expulsion does not reduce the load carrying capacity of spot welds rather it decreases their energy absorption capability which was attributed to the change of failure location due to excessive electrode indentation. Moreover, copper ingression also limits the upper limit of weld lobe as it was heavily ingested at 16 kA for every welding speed (Figure 8.10). When the welding parameters such as welding current and welding time are high, the spot weld will also have intensive heat. This will affect the nugget size and strength of the weld joint [131],[132]. In the present study, weld strength was used as a criterion to assess the weld quality.

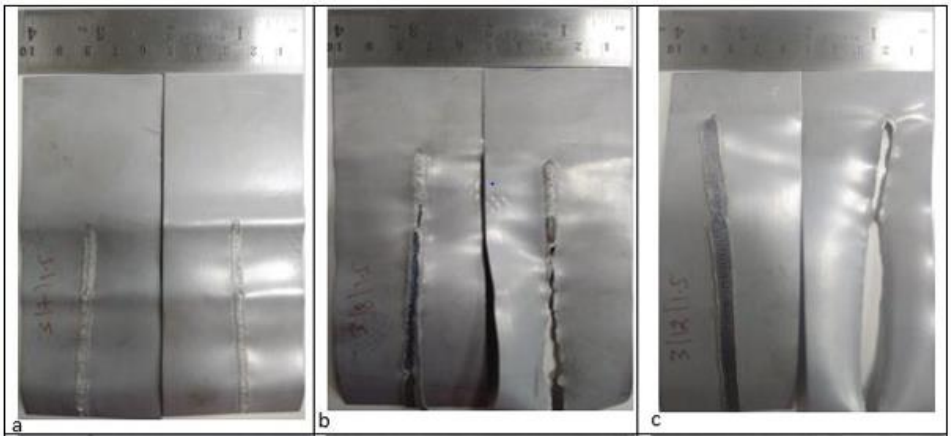

Figure 8.9. The images of seam weldments at constant electrode force of 3 Kg/cm^2 and welding speed of 1.5 meter per minute after peel test as (a) Interfacial failure at 7 kA (b) Partial pull out failure at 8 kA and (c) Pull out failure at 12 kA.

Figure 8.10. The images of Weldment during seam welding under constant electrode force of 3 Kg/cm^2 and welding speed of 1.5 meter per minute as: (a) heavy copper ingression at 16 kA (b) light copper ingression at 14 kA and (c) neither copper ingression nor expulsion at 11 kA.

During Peel test following mode of failure occurs: In interfacial Failure as shown in figure 8.9 (a), the joint fails through the weld nugget centerline and the fracture surface is relatively smooth. Cracks usually initiate from a sharp notch and then propagate through the weld nugget. IF mode is accompanied by little plastic deformation and has a detrimental effect on the crashworthiness of the vehicles and results in weak weldability [43]. As seen from the weld lobe, the interfacial failure evaluated at 7.0 kA of weld current with 1.0 and 1.5 meter per minute of the welding speed. In partial pull out Failure (PPF) mode (Figure 8.9 (b)), a fraction of the weld nugget is removed. The crack first propagates in the weld nugget, then redirects perpendicularly to the centerline towards one of the sheets. In pullout failure (PF), withdrawal of the weld nugget from one sheet, (Figure 8.9 (c)), fracture may initiate from the base metal (BM). Spot welds that fail by PF mode have higher peak loads and energy absorption levels than those that fail through IF or PIF failure modes [87]. PF is the most preferred failure mode due to wide range of plastic deformation and energy absorption. It results in crashworthiness. Hence process parameters should be adjusted so that the pullout failure mode is established [44]. As seen in the weld lobe increasing welding current and welding speed increases the possibility of pullout failure.

8.4 Endurance test

8.4.1 Dynamic contact resistance (DCR)

The initial tests were carried out to estimate the range of adequate nugget formation. Nugget growth can be estimated as a function of weld time and current. It comprises of four sequential stages: incubation period, rapid growth, reduced growth and expulsion [136]. Figure 8.11 shows the DCR curves for different weld length values from initial condition to thirty meter of continuous seam welding with a constant weld speed of 1.5 meter per minute and constant electrode force of 3 Kg/cm^2 and 11 kA of welding current DCR decreases from initial condition to the condition after 15 meter of continuous seam weld, increases for 20 meter and then again decreases for 25 meter to 30 meter for secondary coated IF steel. This is justified by the increase in width of weldment as shown in figure 8.12 (a) from 5.40 mm to 5.5 mm after 15 meter of continuous seam welds. The weldment width then decreases to 5.00 mm after 20 meter of welds and again

increase to 6.00 mm after 25 meter of weld. Finally, after 30 meter of weld length, the weldment width was 5.84 mm (Figure 8.11). This is due to the non-uniformity of heat dissipation as the weld length increases because of formation and breaking of brass deposition on electrode width [136].

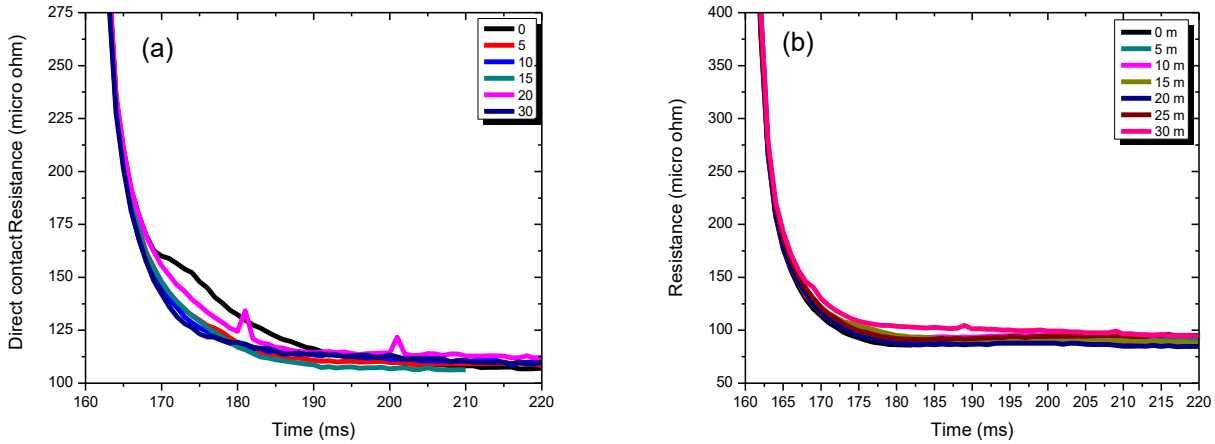

Figure 8.11. Dynamic contact resistance curves for the continuous seam weld length of (a) T coated IF steel and (b) GA coated IF steel for the 30 meter of continuous weld length.

The variation of DCR with the increase in weld length of continuous seam. The range of β- curve for secondary coated IF steel in specific weld length is slightly more than that of GA coated IF steel. Therefore, there is no wide variation in DCR behavior for both of the coated steels. The initial contact resistance is varied between 800 and 850 micro ohms for the entire weld length up to 30 meter for T coated IF steel and varied between 775 and 825 micro ohms for the entire weld length up to 30 meter for GA coated IF steel.

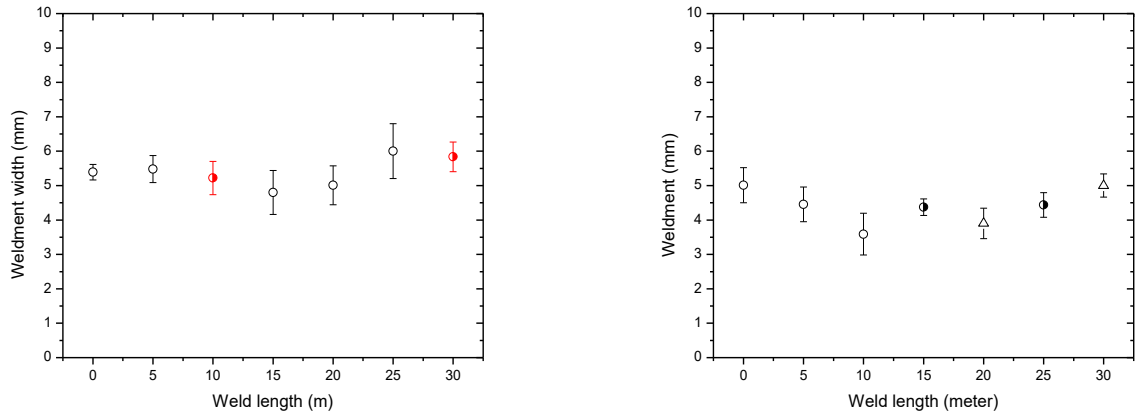

Figure 8.12. Effect of the continuous weld length on the width of seam weldment in mm of (a) secondary coated IF steel and (b) GA coated IF steel

8.4.2 Heat input

The heat transfer takes place due to bulk resistance and contact resistance depending on the process parameters such as current, electrode force and time, the material's thermally dependent physical properties and the weld efficiency factor. The resistance produced leads to the generation of heat through joule's law of heating as described in equation 1.1. Figure 8.13 (a) shows the variation of heat input in kJ/cm as the function of the weld length. Heat inputs were calculated by the following equation:

$$Heat\ Input = \frac{Energy}{Length} = \frac{Energy \times 60}{Velocity \times time} \quad \text{..... (4.4)}$$

Where energy in kJ is calculated through equation (8.1), velocity in mm/min of electrode wheel, total time in millisecond and the heat input in kJ per cm.

The maximum variation of heat input for entire weld length of T coated if steel is 0.42 kJ/cm (10.9 %). The maximum variation of heat input for entire weld length of GA coated IF steel is 0.32 kJ/cm (10.4 % variation).

Following points are to be noted:

1) There is almost constant heat input for the entire weld length for both of T coated and GA coated IF steel.
2) More heat input is required to weld secondary coated IF steel as their mean heat input in kJ/cm for the entire weld length up to 30 meter was 4.06 and that of GA coated IF steel was 3.22 with an error in fraction of 0.42 and 0.32 respectively.

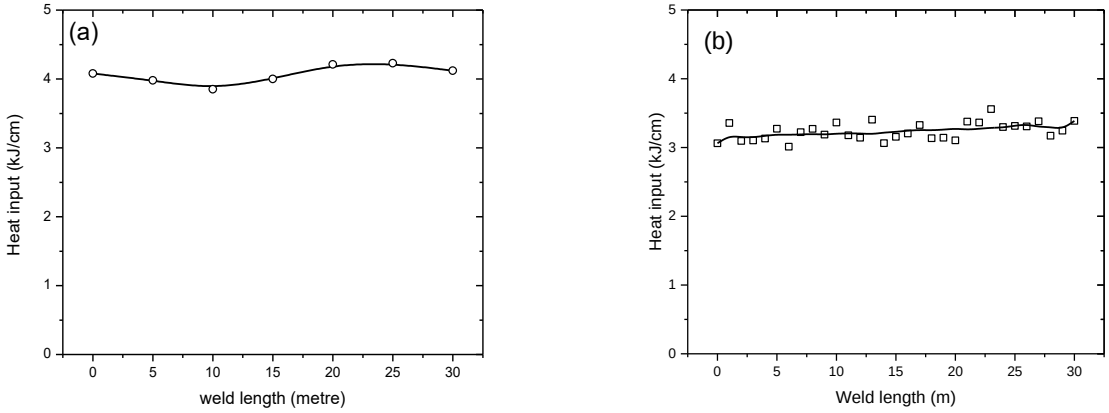

Figure 8.13. Effect of the continuous weld length on heat input in kJ/cm of (a) secondary coated IF steel and (b) GA coated IF steel at 11 kA of welding current, 3 kg/cm^2 of electrode force and 1.5 meter per minute of welding speed.

8.4.3 Mechanical Performance

Seam weld mechanical performance is generally considered under static/quasi-static, fatigue and impact loading conditions. Excessive loads on the vehicle, are some of the cases which can cause overload failure [61].It is noticeable that during service, seam welds can experience both shear loading due to the relative displacement or rotation of the adjacent sheets and tensile loading due to the separating forces applied between the adjacent sheets in a direction normal to the sheets [57]. The tensile–shear (TS) are the most widely used tests for evaluating the seam weld mechanical behaviors. Figure 4.16 shows the graphs of maximum load of the weldment, extension at the maximum load and energy of the weldment of T coated IF steel and GA coated IF steel.

Table 8.1. Mechanical performance of steel as a function of weld lengths

Secondary coated IF steel			Primary coated IF steel (GA-IF steel)		
Weld Length (meter)	**Failure location**	**Tensile load (kN)**	**Weld Length (meter)**	**Failure location**	**Tensile load (kN)**
0	BM	7.07	0	BM	6.845
5	BM	7.13	5	BM	6.735
10	BM	6.97	10	BM	6.52
15	HAZ	6.91	15	BM	6.27
20	BM	7.045	20	HAZ	4.095
25	BM	7.08	25	HAZ	5.565
30	BM	7.115	30	IF	3.16

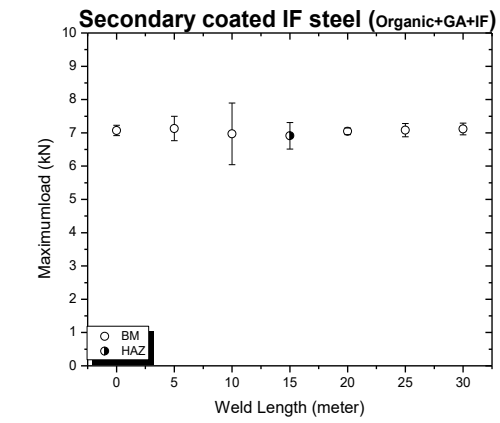

(a)

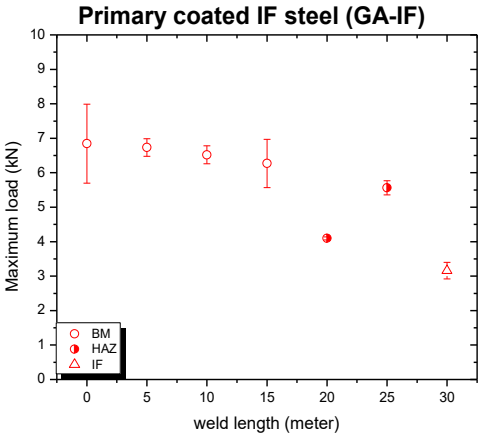

(b)

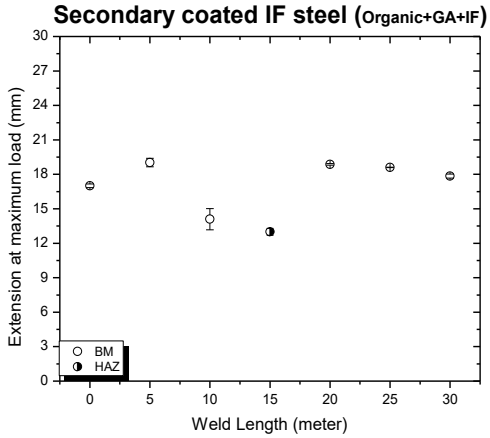

(c)

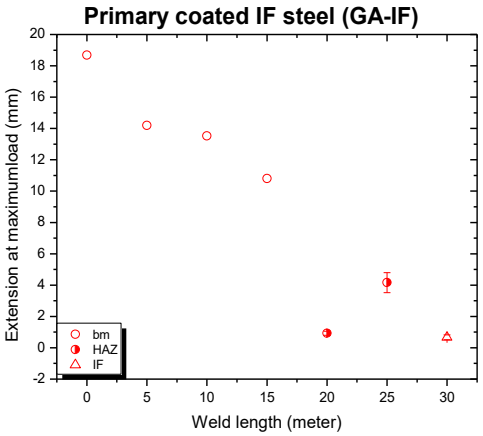

(d)

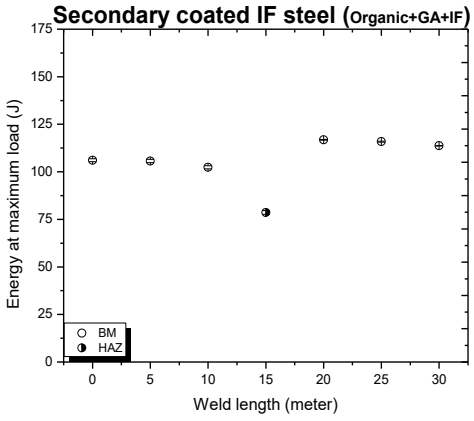

(e)

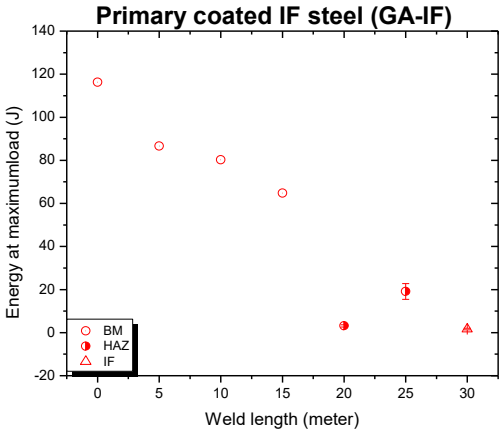

(f)

Figure 8.14. Effect of weld length in meter on mechanical properties of the weldments such as maximum load, extension at maximum load and energy at maximum load of the joint at the welding current of 11 kA, welding speed of 1.5 m/min and electrode force of 3.0 kg/cm^2 under tensile shear test, considering 3 meter per minute strain rate.

Figure 8.14 (a) indicates the effect of weld length on tensile shear force in resistance seam welding of secondary coated IF steel. As the length of weldment increase, the failure location shifted from base metal to heat affected zone with the decrease in strength from 7.1 kN to 6.7 kN at 15 meter of weldment. After 15 meter of weld, the load bearing ability increases to 7.05 kN at 20 meter with failure location of base metal and then made a constant till 30 meter. But after 30 meter of welds, failure location was changed to heat affected zone. Moreover, in this analysis two samples were made at the particular weld length but there was no acceptable variation in this two samples testing. As shown in the graph in the form of overlapping denotation.

Figure 8.14 (b) indicates the effect of weld length on tensile shear force in resistance seam welding of GA coated IF steel. Analysis started with the preparation of two sample at particular weld length, in first sample represented by black colour. As the length of weldment increases, the failure location shifted from base metal to heat affected zone with following variation in the strength from 4.7 kN, 7.02 kN, 6.8 kN at 0, 5, 10 meter of weldments respectively. At 15 and 20 meter of welds, the failure locations were heat affected zone and the tensile strength was 3.5 and 4.1 kN respectively. Figure 8.14 (c) indicates the effect of weld length on the extension at maximum load in resistance seam welding of T coated IF steel. The highest extension at maximum load is 19.37 mm for weldment failed at the base metal at 5 meter. The extension at maximum load were 10 and 16 mm for the failure location at heat affected zone, when weld length were 15 meter and 30 meter respectively as shown in table 4.5

Figure 8.14 (d) indicates the effect of weld length on extension at maximum load in resistance seam welding of GA coated If steel. The highest extension at maximum load is 18.65 mm for weldment failed at the base metal at 5 meter. The extension at maximum load were 1.2, 0.6 and 0.8 mm for the failure location at heat affected zone, when weld length were 5, 15 and 20 meter respectively.

Figure 8.14 (e) indicates the effect of weld length on energy at maximum load in resistance seam welding of secondary coated IF steel. The highest energy at maximum load is 123.3 joule for weldment failed at the base metal at 5 meter. The energy at maximum load were 62.0 and 95.4 joule for the failure location at heat affected zone, when weld length were 15 meter and 30 meter respectively as shown in table 8.2

Figure 8.14 (f) indicates the effect of weld length on energy at maximum load in resistance seam welding of GA coated If steel. The highest extension at maximum load is 115.75 joule for weldment failed at the base metal at 5 meter. The extension at maximum load were 5.36, 1.10 and 3.45 joule for the failure location at heat affected zone, when weld length were 5, 15 and 20 meter respectively as shown in table 8.2

Table 8.2. Variation of extension and absorbing energy as a function of continuous weld length.

Secondary coated IF steel				Primary coated IF steel (GA-IF steel)			
Weld Length (m)	Failure location	Extension at maximum load	Energy at maximum load	Weld Length (m)	Failure location	Extension at maximum load	Energy at maximum load
0	BM	17.005	106.0743	0	BM	18.69	116.272
5	BM	19.025	105.6978	5	BM	14.2	86.63
10	BM	14.095	102.3445	10	BM	13.52	80.279
15	HAZ	13	78.6045	15	BM	10.8	64.803
20	BM	18.87	116.8727	20	HAZ	0.925	3.123
25	BM	18.6	115.8735	25	HAZ	4.16	19.1155
30	BM	17.845	113.71	30	IF	0.665	1.697

8.4.4 Microstructure

An optical microstructure and SEM micrograph of the BM microstructure are shown in Figure 8.15. The microstructure of the BM contains equiaxed ferrite grains with an average grain size of about 15 μm. The higher the CE, the higher the hardenability of the steel, the more difficult the steel is to weld. Due to low carbon content of the IF steel, its hardenability is expected to be relatively low than that of other steels and thus, the hardness of the weld zone should not be very high.

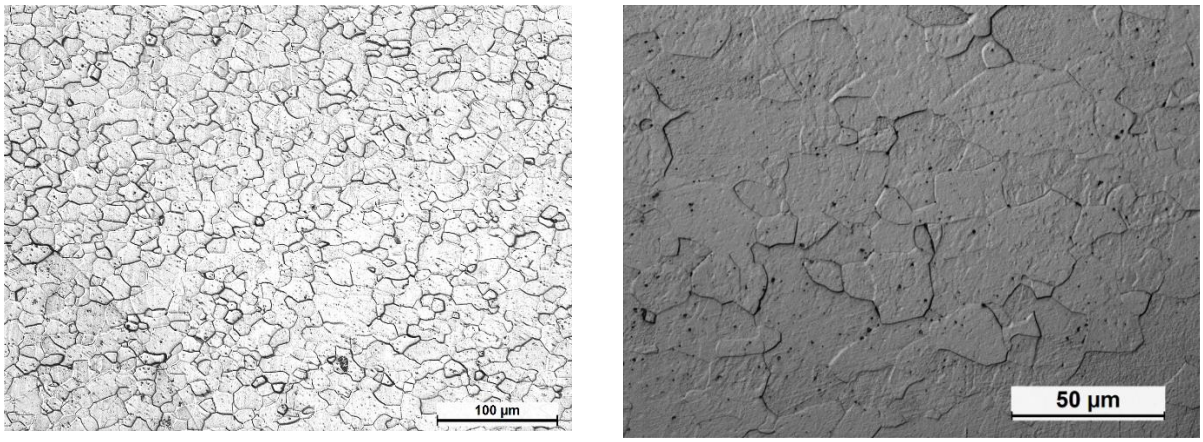

Figure 8.15. BM microstructure captured by (a) optical microscopy and (b) SEM of IF steel.

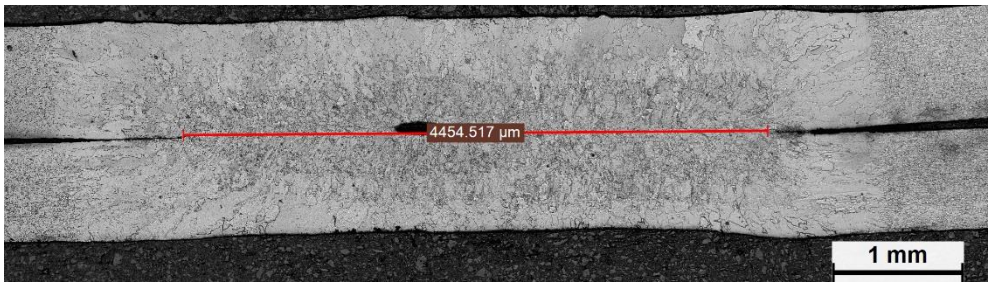

Initial condition

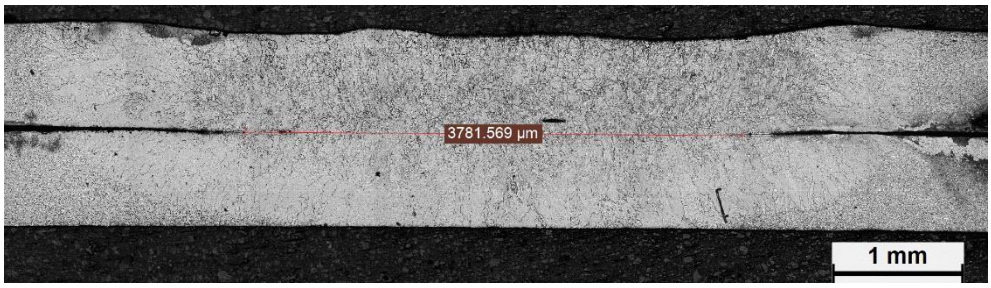

After 10 meter

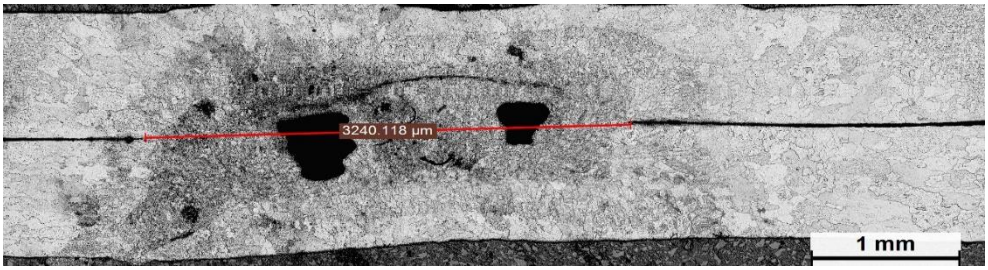

After 20 meter

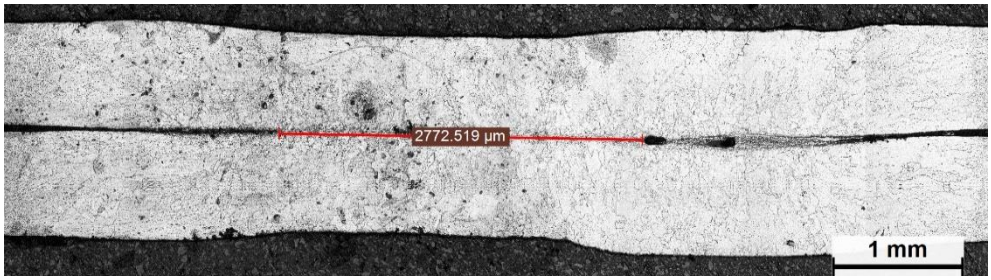

After 30 meter

Figure 8.16. Effect in the quality of weld microstructure as the function of weld lengths on secondary coated IF steel.

Fusion zone consists of lathe martensite having small crack in it initially, the crack gets enlarged as the weld length increases to 20 meter of continuous weld. Zinc intrusion in a fusion zone also embedded after 10 meter of continuous weld length.

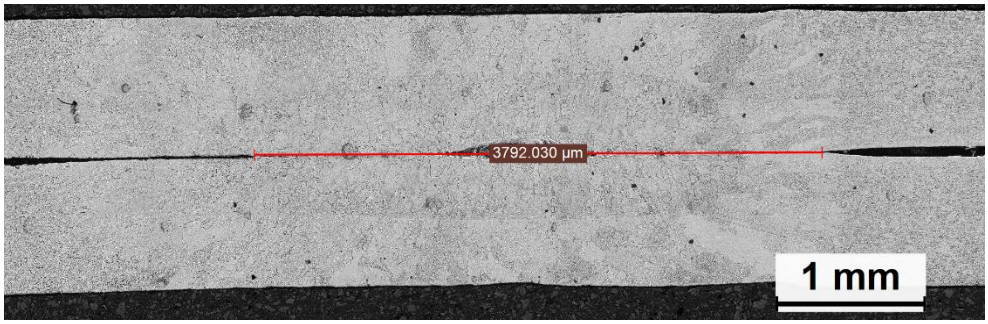

Initial condition

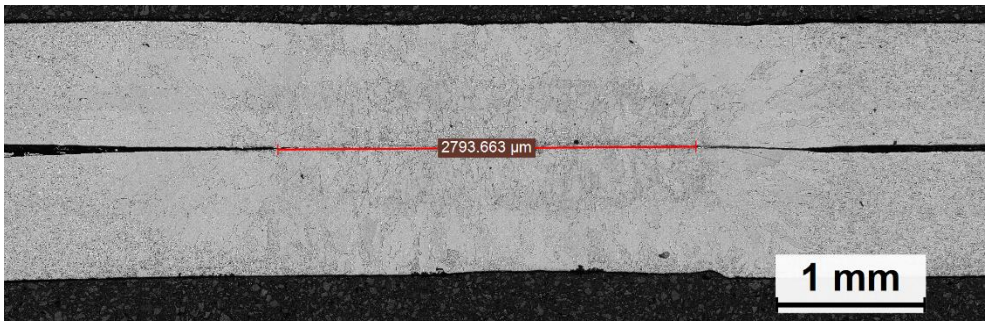

After 10 meter

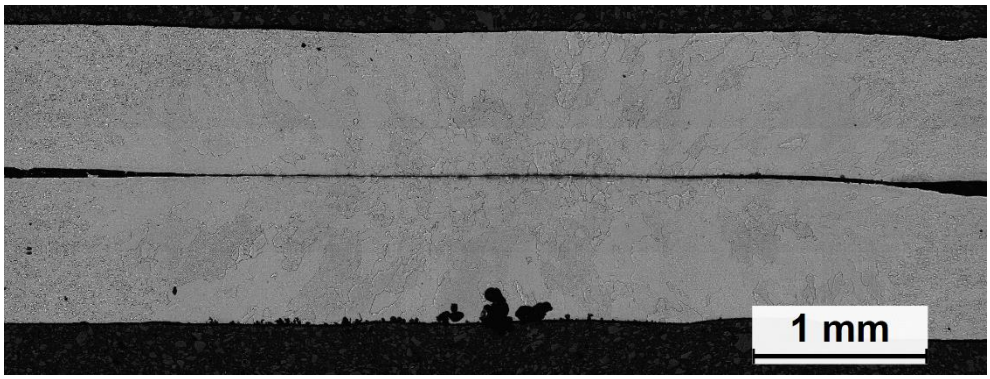

After 20 meter

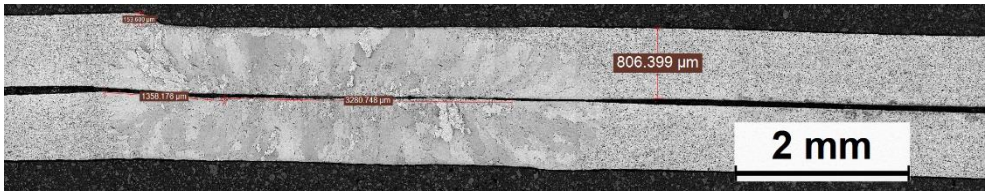

After 30 meter

Figure 8.17. Effect in the quality of weld microstructure as the function of weld lengths on GA coated IF steel.

The growth of nugget width can also be judged initially up to the 30 meter of weld length. Initially, the nugget width was fully developed, after 10 meter of weld length it get reduced as the heat generated get

reduced due to the low electrode density due to formation of mushrooming on the width of the electrode. In case of secondary coated IF steel, the quality of microstructure as shown in figure 8.16 is degraded as compare to the GA coated IF steel because of more heat input generated in the secondary coated steel (23% more). In addition to the weld quality, nugget formation gets diminished as the continuous seam weld length increases because of less heat generated. This less heat gets minimum when coating of steel impinges on the electrode because of heat not concentrating on target rather it scattered.

8.4.5 Electrode condition

Electrode deterioration by deformation and chemical reaction during resistance seam welding of zinc coated steels is a well-known problem. The zinc coatings used for protection of corrosion on Interstitial free steel accelerates the deterioration of copper based alloy of resistance seam welding electrodes compared to welding bare steels. Zinc is more electrically and thermally conductive than steel [137]. It is also softer than steel, and it conforms better to electrode tips when they are pressed against the Zn-coated surfaces during the resistance welding operation. Compared to electrode use on the bare steels, resistance welding electrodes are undoubtedly exposed to higher temperatures with the zinc coated steels. Temperatures high enough to melt the Zn (> 420°C), and possibly even to vaporize it (> 906°C), are typically observed [138][139][140]. The combination of relatively higher temperatures and contact with liquid Zn are responsible for their accelerated deterioration.

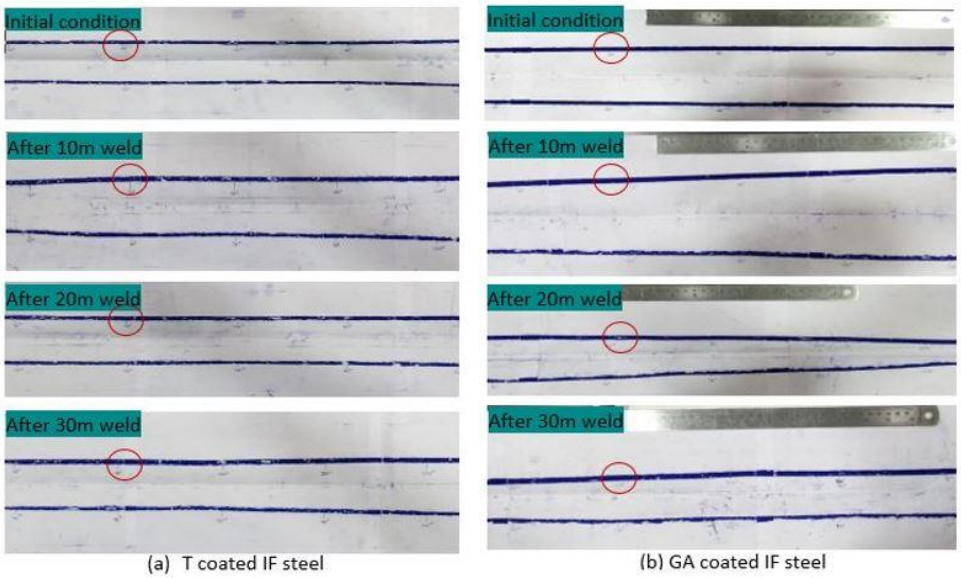

Figure 8.18. Electrode imprints of continuous seam welding after every ten meter of welding process of a) Secondary coated IF steel and b) Galvannealed IF steel.

In Figure 8.18 and 8.19 initial and after every ten meter of electrode imprint are reported. For the condition of the electrode to be exposed, specific location was decided and marked with red circle to know the changes pertains after every ten meter of welds. Initially, electrode was in ideal condition, after twenty meter of continuous seam welds, there was deterioration in the form of pits on the periphery of electrode and after ten meter scratches in the form of pits get reduced due to the formation of brass layer on the outer periphery of electrodes as shown in figure 8.19 (a). There were same effect in case of GA coated IF steel (figure 8.19 (b)) [141].

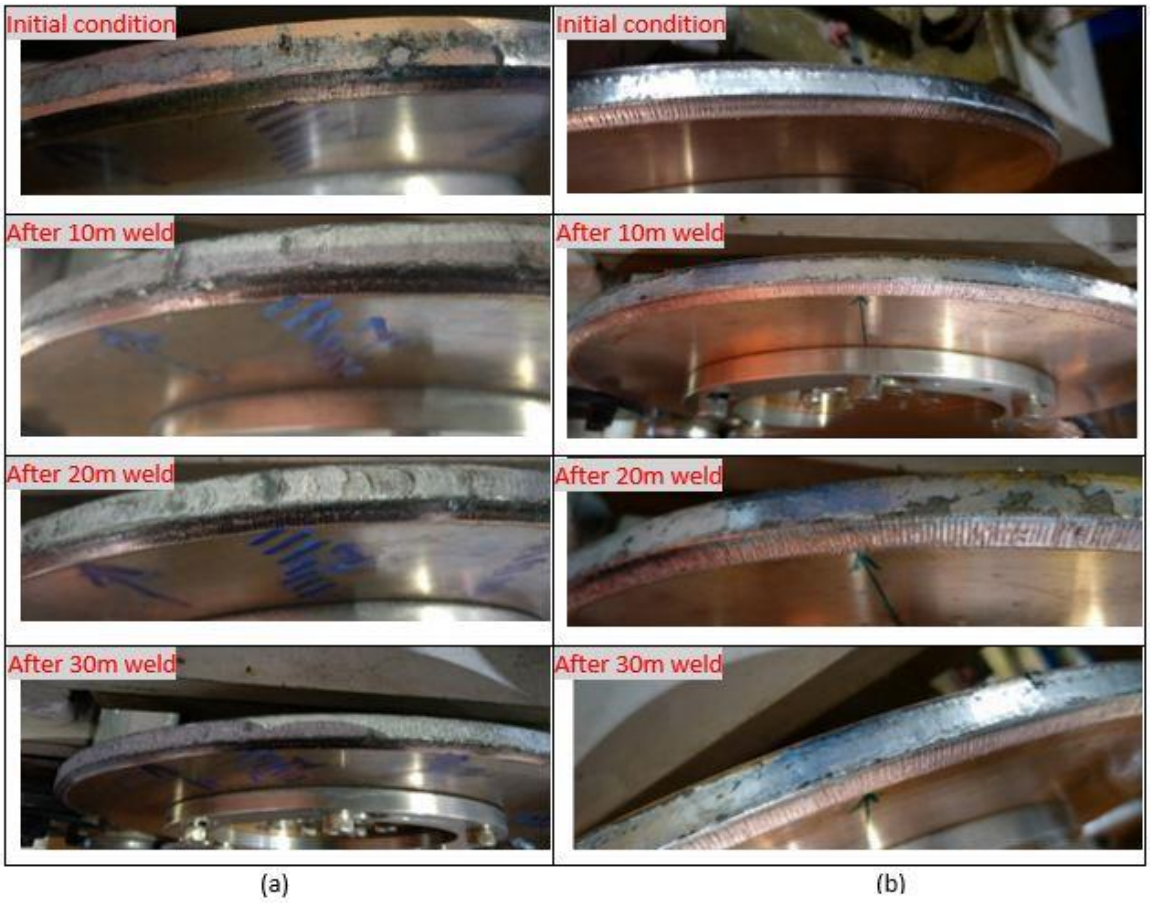

Figure 8.19. Electrode condition of continuous seam welding after every ten meter of welding process of a) secondary coated IF steel and b) Galvannealed IF steel.

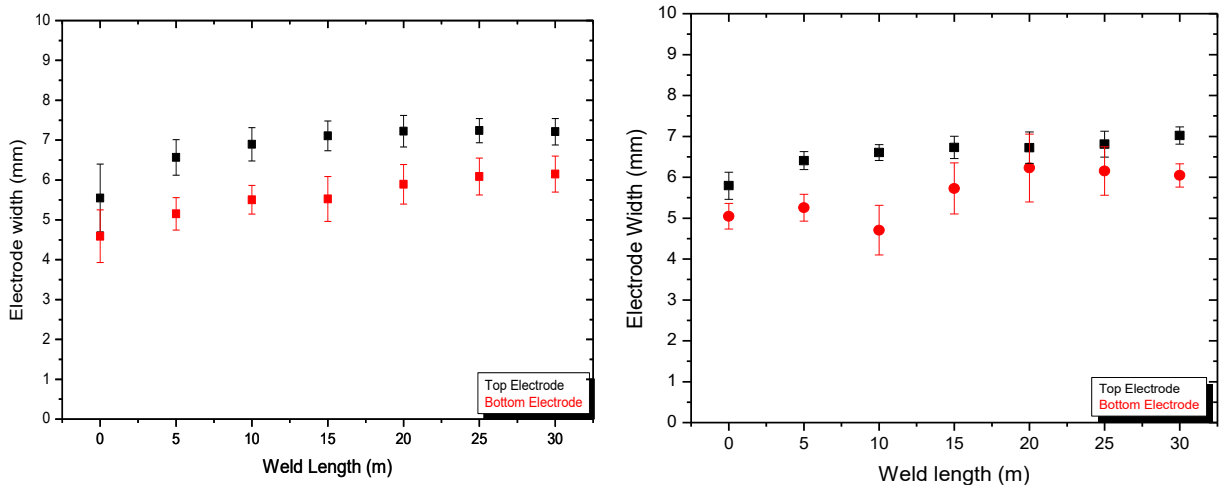

Figure 8.20. Variation in the width of electrode after continuous seam welding of (a) secondary coated IF steel and (b) GA coated IF steel.

The process of electrode deterioration occurs through a combination of deformation and chemical attack or alloying between the Zn and Cu electrode alloys [138][142]. With the increase in continuous seam weld length, electrode width increases. The extent of increase is different for secondary coated and GA coated IF steel. For secondary coated IF steel welds (figure 8.20 (a)) top and bottom electrode wheel increases from 5.6 mm and 4.6 mm to 7.1 mm and 5.5 mm respectively up to 15 meter of continuous welds. From 20 meter of welds, there were no wide variation in electrode width up to 30 meter. On the contrary, for GA coated IF steel (figure 8.20 (b)), the width of the top electrode increases from 5.78 mm to 6.71 mm at 15 m of continuous weld. The width gets reduced after 20 meter of continuous weld. The deposited zinc layer on the electrode wheel start getting separated [143]. The percentage increase in the width of electrode when welded with these two steels were 31 percent and 21 percent respectively.

Chapter 5: Conclusions

The following conclusions may be drawn from the RSW and RSeW investigation with respect to electrode life estimation:

1. Based on existing weldability window, endurance test was carried at 7.75 kA of welding current, 300 ms of weld time and 3.2 kN of electrode force in an automated zig assisted welding machine. It was found that ~ 1440 spots were welded with no significant deterioration of weld quality. The weld nugget diameter (was higher than $4.25\sqrt{t}$ condition) with satisfactory TSS and CTS value.
2. The energy input per welding was calculated from dynamic contact resistance (DCR) and was found to be consistent at ~2.4±0.12 kJ. Consequently, the nugget diameter was at ~ 5.4±0.5 mm for all the spot weld. The maximum load bearing capacity of the welds were at 4±0.25 kN which is mare to an acceptable
3. RSeW electrode life determined for 0.8 mm thick secondary coated IF-GA sheets. It has been found that the continuous welding is possible up to 30 m without compromising the weld quality. The nugget width and load bearing capacity of the weld has been found constant at 5.4±0.4 mm and 7±0.1 kN respectively for entire length of weld.
4. RSeW electrode life determined for 0.8 mm thick IF-GA sheets (without any secondary coating) has lower electrode life. The nugget width remains constant at 4.4±0.5 mm for the 30 m of welding; however, up to 15 m of welding the load bearing capacity remains constant at 6.6±0.2 kN then it shows a decreasing trend.
5. Application of thin organic coating (secondary coating) over GA coating increases the process heat input from 3.2±0.1 kJ/cm to 4.1±0.1 kJ/cm which is a 28% increase. Higher bulk resistance of organic coating increases the overall contact resistance which ultimately produces more amount of heat. This higher heat input is responsible for 23% increase in weld nugget in secondary coated product over conventional GA coated product.
6. During continuous welding, the electrode faces width increases 31% for secondary coated product and 21% for conventional GA coated product. Higher heat generation in welding of secondary coated product increases the deterioration rate of electrodes by enhancing the electrode face temperature which eventually fasten the brass formation and mushrooming process.

Further work

This work has developed a ANN based approach. C, Mn and Si content of steels, YS, UTS, %El and coating types were used as inputs and critical nugget diameter was the output.

The model laid a solid platform for calculating critical nugget diameter experimentally for each of the automotive steel grade. Moreover, this could be trained for two or more spot welded joints for similar and dissimilar materials and validate accordingly.

The methodology developed represents a general approach which can be used in many other steel grades and types of coating.

The work on electrode life estimation has been done through two different welding processes resistance spot welding and resistance seam welding through truncated electrode and circular electrode. In case of spot welding, this can also be extended to use different electrode geometries.

The hardenability of electrode life could be examined as the function of continuous weld followed by the intrusion of zinc in the developed nugget.

References

[1] Aslanlar S. "The effect of nucleus size on mechanical properties in electrical resistance spot welding of sheets used in automotive industry" J. Mater. Des.,27, pp. 125–6, 2006.

[2] M. Marya and X. Gayden, “Development of Requirements for Resistance Spot Welding Dual-Phase (DP600) Steels Part 2: Statistical Analyses and Process Maps,” Weld J, pp. 197–204, 2005.

[3] K. E., Easterling K., “Mathematical Modelling of Weld Phenomena, Institute of Materials, London, Feulvarch,” pp. 183–200, 1993.

[4] M. Pouranvari, H. R. Asgari, S. M. Mosavizadch, and P. H. Marashi, “Effect of weld nugget size on overload failure mode of resistance spot welds,” April, 2007.

[5] Y. T. and T. I. H. Oikawa, G. Murayama, T. Sakiyama, “Resistance spot weldability of high strength steel (HSS) sheets for automobiles,” Nippon Steel Tech. Rep., vol. 95, pp. 39–45, 2007.

[6] C. L. Jenney, A. O’Brien, and Welding Handbook Committee., Welding handbook. Volume 1, Welding science and technology.

[7] Handbook for resistance spot welding", 2005, Miller Electric Manufacturing Co., Appleton, WI.

[8] S. A. D. and T. Debroy, “Current issues and problems in welding science,” Science (80)., vol. 257, pp. 497–502, 1992.

[9] Zhang, H.; Senkara, J. Resistance Welding: Fundamentals and Applications, 2nd ed; CRC Press: New York, NY, USA, 2012; p. 197. 21.

[10] Fundamentals of American Welding Society. 1980. Welding Handbook Volume 1.

[11] Zhang, H., Senkara, J, “Resistance Welding: Fundamentals and applications”, Taylor & Frances, Boca Raton, 2006. .

[12] G. S. Gaikwad and K. H. Inamdar, “A Review on Effect of Process Parameters of Resistance Welding,” pp. 828–835.

[13] M. J. M, M. Pouranvari, and S. M. Mousavizadeh, “Failure mode of m130 martensitic steel resistance-spot welds,” vol. 47, no. 6, pp. 771–776, 2013.

[14] S. S. Mishra, “Research on Resistance Spot Welding of Dissimilar Metal Sheets : An Overview,” no. April 2016, 2017.

[15] P. Marashi, M. Pouranvari, S. Amirabdollahian, A. Abedi, and M. Goodarzi, “Microstructure and failure behavior of dissimilar resistance spot welds between low carbon galvanized and austenitic stainless steels,” vol. 480, pp. 175–180, 2008.

[16] X. Wan, Y. Wang, and P. Zhang, “Effects of Welding Schedules on Resistance Spot Welding of DP600 Steel,” ISIJ Int., vol. 54, no. 10, pp. 2375–2379, 2014.

[17] M. Pouranvari, S. M. Mousavizadeh, S. P. H. Marashi, M. Goodarzi, and M. Ghorbani, “Influence of fusion zone size and failure mode on mechanical performance of dissimilar resistance spot welds of AISI 1008 low carbon steel and DP600 advanced high strength steel,” Mater. Des., vol. 32, no. 3, pp.

1390–1398, 2011.

[18] M. Pouranvari and S. P. H. Marashi, “Failure mode transition in AHSS resistance spot welds. Part I. Controlling factors,” Mater. Sci. Eng. A, vol. 528, no. 29–30, pp. 8337–8343, 2011.

[19] M. M. and X. Q. GAYDEN, “Development of requirements for resistance spot welding dual-phase (dp600) steels part 1 — the causes of interfacial fracture,” no. November, 2005.

[20] B. M. Brown, “Comparison of AC and DC rsesistance welding of automotive steels,” Weld. J., vol. 66, pp. 18–23, 1987.

[21] D. C. and G. A. G. W. Li, “A comparative study of single-phase AC and multiphase DC resistance spot welding.‟, , 2005, 127, 583-589.,” J. Manuf. Sci. Eng. ASME, vol. 127, pp. 583–589, 2005.

[22] M. I. Khan, M. L. Kuntz, and Y. Zhou, “Effects of weld microstructure on static and impact performance of resistance spot welded joints in advanced high strength steels,” vol. 13, no. 3, pp. 294–304, 2008.

[23] A. M. Slovaca, “Effect of electrode force on fracture type of dqsk steel resistance spot welds,” vol. 19, no. 2, pp. 149–153, 2013.

[24] F. L. and P. Dong, Sci. Technol. Weld. Join. 4 (1999) 285–289.

[25] K. L. Chatterjee and W. Waddell, Weld. Met. Fab. 64 (1996) 110– 114.

[26] X. Sun, E. V. Stephens, and M. A. Khaleel, “Effects of fusion zone size and failure mode on peak load and energy absorption of advanced high strength steel spot welds under lap shear loading conditions,” Eng. Fail. Anal., vol. 15, no. 4, pp. 356–367, 2008.

[27] M. Pouranvari et al., “Effect of expulsion on peak load and energy absorption of low carbon steel resistance spot welds Effect of expulsion on peak load and energy absorption of low carbon steel resistance spot welds,” vol. 1718, 2013.

[28] E. K. and T. E. E. W. Kim, T. W. Eagar, “Parametric analysis of resistance spot welding lobe curve," SAE International, Warrendale, PA, USA, 1988,SAE Tech. Pap. 880278, 1988.

[29] Y. I. and Kiy. Bessyo, “Cracking Parameter to heat of affected High Strength zone cracking Steels related by Yoshinori Ito and Kiyoshi Bessyo,” pp. 55–63.

[30] M. Pouranvari, S. P. H. Marashi, and D. S. Safanama, “Failure mode transition in AHSS resistance spot welds . Part II : Experimental investigation and model validation,” vol. 528, pp. 8344–8352, 2011.

[31] M.Pouranvari “Effects of fusion zone size and failure mode on peak load and energy absorption of advanced high-strength steel,” no. January, 2007.

[32] M. Pouranvari, S. P. H. Marashi, and S. M. Mousavizadeh, “Failure mode transition and mechanical properties of similar and dissimilar resistance spot welds of DP600 and low carbon steels,” vol. 15, no. 7, pp. 625–632, 2010.

[33] Tumuluru M "Resistance spot weld performance and weld failure modes for dual phase and TRIP steels. Failure Mechanisms of Advanced Welding Processes A", In: Woodhead Publishing Series in Welding and Other Joining Technologies, Edited by: X. Sun, ISBN.” (2010)

[34] T. M. and N. J. D. Uijl, S. Smith, C. Goos, E. van der Aa and T. van der Veldt, “Failure modes of resistance spot welded advanced high strength steels’,, September 2008,,” in Proc. 5th Int. Semin.

on ‘Advances in resistance welding’, Toronto, Canada, 2008, pp. 78–104.

[35] N. J. D. U. and S. Smith, “Resistance spot welding of advanced high strength steels for the automotive industry,” in Proc. 4th Int. Semin. on ‘Advances in resistance welding,’ 2006, pp. 30–60.

[36] S. P. K. and T. L. J. E. Gould, “Predictions of microstructures when welding automotive advanced high-strength steels,” Weld. J. (Miami, Fla), vol. 85, pp. 111-s–116-s., 2006.

[37] R. Rathbun, D. Matlock, and J. Speer, “Fatigue behavior of spot welded high-strength sheet steels,” Weld. J., vol. 82, no. 8, pp. 207–218, 2003.

[38] M. Babu, N. K., Brauser, S., Rethmeier and C. Cross, “Characterization of microstructure and deformation behaviour of resistance spot welded AZ31 magnesium alloy.,” Mater. Sci. Eng., vol. 549, no. A, pp. 149–156, 2012.

[39] M. Pouranvari and S. P. H. Marashi, “Critical review of automotive steels spot welding: process, structure and properties,” Sci. Technol. Weld. Join., vol. 18, no. 5, pp. 361–403, 2013.

[40] P. Marashi et al., “Relationship between failure behaviour and weld fusion zone attributes of austenitic stainless steel resistance spot welds Relationship between failure behaviour and weld fusion zone attributes of austenitic stainless steel resistance spot welds,” vol. 0836, 2013.

[41] M. Pouranvari, S. P. H. Marashi, S. M. Mousavizadeh, M. Pouranvari, S. P. H. Marashi, and S. M. Mousavizadeh, “Failure mode transition and mechanical properties of similar and dissimilar resistance spot welds of DP600 and low carbon steels Failure mode transition and mechanical properties of similar and dissimilar resistance spot welds of DP600 and low carbon stee,” vol. 1718, 2013.

[42] M. Pouranvari, E. Ranjbarnoodeh, M. Pouranvari, and E. Ranjbarnoodeh, “Failure mode of HSLA / DQSK dissimilar steel resistance spot welds Failure mode of HSLA / DQSK dissimilar steel resistance spot welds,” vol. 9233, 2013.

[43] Peng ZHANG, Xiaodong WAN, Yuanxun WANG1, “Characteristics of welding crack defects and failure mode in resistance spot welding of DP780 steel,” Sci. direct, vol. 23, no. 10, pp. 1104–1110, 2016.

[44] M. Pouranvari, S. P. H. Marashi, and S. M. Mousavizadeh, “Dissimilar resistance spot welding of DP600 dual phase and AISI 1008 low carbon steels: correlation between weld microstructure and mechanical properties,” Ironmak. Steelmak., vol. 38, no. 6, pp. 471–480, 2011.

[45] A. N. A. E. and C. J. A. Joaquin, “‘Reducing shrinkage voids in resistance spot welds,’” Weld. J., vol. 86, pp. 24–27, 2007.

[46] M. Pouranvari et al., “Effect of weld nugget size on overload failure mode of resistance spot welds Effect of weld nugget size on overload failure mode of resistance spot welds,” vol. 1718, 2013.

[47] M. Pouranvari, S. P. H. Marashi, and D. S. Safanama, “Failure mode transition in AHSS resistance spot welds . Part II : Experimental investigation and model validation,” Mater. Sci. Eng. A, vol. 528, no. 29–30, pp. 8344–8352, 2011.

[48] M. Pouranvari and S. P. H. Marashi, “Failure mode transition in AHSS resistance spot welds . Part I . Controlling factors,” Mater. Sci. Eng. A, vol. 528, no. 29–30, pp. 8337–8343, 2011.

[49] M. Pouranvari, “Susceptibility to interfacial failure mode in similar and dissimilar resistance spot welds

of DP600 dual phase steel and low carbon steel during cross-tension and tensile-shear loading conditions," vol. 546, pp. 129–138, 2012.

[50] S. P. H. Marashi, "Failure Mode Transition in AISI 304."

[51] M. Pouranvari and S. P. H. Marashi, "Failure of resistance spot welds : tensile shear versus coach peel loading conditions Failure of resistance spot welds : tensile shear versus coach peel loading conditions," vol. 9233, pp. 103–111, 2013.

[52] M. Pouranvari and S. P. H. Marashi, "Failure of resistance spot welds : tensile shear versus coach peel loading conditions Failure of resistance spot welds : tensile shear versus coach peel loading conditions," vol. 9233, 2013.

[53] Radakovic, D. J., and Tumuluru, M. Factors influencing fracture mode in resistance spot weld shear-tension testing of advanced high strength steels. Paper presented at FABTECH International & AWS Welding Show, 2006, Atlanta, Ga."

[54] M. TUMULURU, "The Effect of Coatings on the Resistance Spot Welding Behavior of 780 MPa Dual-Phase Steel," Weld. Res., vol. 86, pp. 161–169.

[55] C. J. and Y. S. J. Bohr, "Resistance spot welding of advanced high strength steel, a comparative study of joint efficiency," Proc. 5th Int. Semin. 'Advances Resist. welding', Toronto, Canada, pp. 147–166, 2008.

[56] M. A. K. and D. J. X. Sun, E. V. Stephens, R. W. Davies and Spinella, "Effects of fusion zone size on failure modes and static strength of aluminum resistance spot welds," Weld. J. (Miami, Fla), vol. 83, pp. 308-S–318-S., 2004.

[57] M. P. and S. P. H. Marashi, "Failure of resistance spot welds: tensile shear versus coach peel loading conditions," Ironmak. Steelmak., vol. 39 pp. 104–11, 2012.

[58] L. E. Svensson, "Prediction of mechanical properties of steel spotwelds," Proc. 7th Int. Conf. Pine Mt. GA, USA 'Trends Weld. Res., vol. ASM intern, pp. 41–46, 2005.

[59] ANSI/AWS/SAE D8.9–97: Recommended practices for test methods for evaluating the resistance spot welding behavior of automotive sheet steels materials, Miami, FL, American Welding Society, 1997."

[60] "Method of inspection for spot welds", JIS Z 3140, Japanese Industrial Standards Committee, Tokyo, Japan, 1989.

[61] A. A. E. and A. K. S. Daneshpour, A. H. Kokabi and Motarjemi, "Crack initiation and kinking behaviours of spot welded coach peel specimens under cyclic loading," Sci. Technol. Weld. Join., vol. 12, pp. 696–702, 2007.

[62] X. Sun, E.V. Stephens, M.A. Khaleel, Eng. Failure Anal. 15 (2008) 356–367.

[63] J.M.Sawhill, Jr, H. Watanabe, and J.W. Mitchell, "Spot Weldability of Mn-Mo-Nb, VN and SAE 1008 Steels," Weld. J., pp. 217–224, 1977.

[64] "D.J. Radakovic and M. Tumuluru: "Predicting resistance spot weld failure modes in shear tension tests of advanced high-strength automotive steels," Welding Journal, 87, 96-s-105-s, 2008.

[65] Y. J. Chao, “Failure mode of spot welds: interfacial versus pullout,” Sci. Technol. Weld. Join., vol. 8, pp. 133–137, 2003.

[66] L. G. H. J. and X. G. M. Marya, K. Wang, “Tensile- shear forces and fracture modes in single and multiple weld specimens in dual-phase steels,” J. Manuf. Sci. Eng. Trans., vol. 128, pp. 287–298, 2006.

[67] R. A. Smith, “Fracture and fatigue-elasto-plasticity, this sheet and micro-mechanisms,” in proc. 3rd Eur. Colloquium on ‘Fracture’, (ed. J. C. Radon),Oxford, Pergamon Press, pp. 49–56, 1980.

[68] M. Kuo and J. Chiang, “Weldability Study of Resistance Spot Welds and Minimum Weld Button Size Methodology Development for DP Steel,” SAE Tech. Pap. Ser., vol. 1, no. 724, 2010.

[69] V. Naprednega et al., “Failure-mode transition in resistance spot welded dp780 advanced high-strength steel : effect of loading conditions,” vol. 48, no. 1, pp. 67–71, 2014.

[70] P. R. Spena, M. De Maddis, F. Lombardi, and M. Rossini, “Investigation on Resistance Spot Welding of TWIP Steel Sheets,” vol. 85, no. 9999, pp. 1–10, 2015.

[71] D. Zhao, Y. Wang, D. Liang, and P. Zhang, “Modeling and process analysis of resistance spot welded DP600 joints based on regression analysis,” vol. 110, pp. 676–684, 2016.

[72] M. Pouranvari and E. Ranjbarnoodeh, “Resistance spot welding characteristic of ferrite-martensite DP600 dual phase advanced high strength steel-part III: Mechanical properties,” World Appl. Sci. J., vol. 15, no. 11, pp. 1521–1526, 2011.

[73] M. Tamizi, M. Pouranvari, and M. Movahedi, “Welding metallurgy of martensitic advanced high strength steels during resistance spot welding,” Sci. Technol. Weld. Join., vol. 22, no. 4, pp. 327–335, 2017.

[74] J. Liang, H. Zhang, X. Qiu, and Y. Shi, “Characteristics of the Resistance Spot Welding Joints in Dissimilar Thickness Dual-phase Steels,” ISIJ Int., vol. 55, no. 9, pp. 2002–2007, 2015.

[75] V. H. B. Hernandez, M. L. Kuntz, M. I. Khan, and Y. Zhou, “Influence of microstructure and weld size on the mechanical behaviour of dissimilar AHSS resistance spot welds,” vol. 13, no. 8, pp. 769–776, 2008.

[76] H. Zhang, A. Wei, X. Qiu, and J. Chen, “Microstructure and mechanical properties of resistance spot welded dissimilar thickness DP780 / DP600 dual-phase steel joints,” vol. m, pp. 443–449, 2014.

[77] X. Yuan, C. Li, J. Chen, X. Li, X. Liang, and X. Pan, “Journal of Materials Processing Technology Resistance spot welding of dissimilar DP600 and DC54D steels,” vol. 239, pp. 31–41, 2017.

[78] M. S. Khan, S. D. Bhole, D. L. Chen, E. Biro, and G. Boudreau, “Welding behaviour , microstructure and mechanical properties of dissimilar resistance spot welds between galvannealed HSLA350 and DP600 steels Welding behaviour , microstructure and mechanical properties of dissimilar resistance spot welds between galvann,” no. August 2015, 2009.

[79] M. Pouranvari, S. P. H. Marashi, M. Pouranvari, and S. P. H. Marashi, “Key factors influencing mechanical performance of dual phase steel resistance spot welds Key factors influencing mechanical performance of dual phase steel resistance spot welds,” vol. 1718, 2013.

[80] S. Singh, R. Chhibber, K. Singh, and M. Shome, “Journal of Materials Processing Technology

Resistance spot welding of galvannealed high strength interstitial free steel," J. Mater. Process. Tech, vol. 246, pp. 252–261, 2017.

[81] C. Ma, D. L. Chen, S. D. Bhole, G. Boudreau, A. Lee, and E. Biro, "Microstructure and fracture characteristics of spot-welded DP600 steel," vol. 485, pp. 334–346, 2008.

[82] S. S. Nayak, V. H. B. Hernandez, Y. Okita, and Y. Zhou, "Microstructure – hardness relationship in the fusion zone of TRIP steel welds," Mater. Sci. Eng. A, vol. 551, pp. 73–81, 2012.

[83] M. Goodarzi, S. P. H. Marashi, and M. Pouranvari, "Journal of Materials Processing Technology Dependence of overload performance on weld attributes for resistance spot welded galvanized low carbon steel," vol. 209, pp. 4379–4384, 2009.

[84] M. Pouranvari, "Young researchers and elite club, dezful branch, islamic azad university, dezful, iran," 2013.

[85] M. Pouranvari and S. P. H. Marashi, "Minimum fusion zone size required to ensure pullout failure mode of resistance spot welds during tensile-shear test," pp. 197–202, 2010.

[86] Techniques for improving the weldability of trip steel using resistance spot welding G SHI AND S A Westgate TWI Ltd, Cambridge, United Kingdom.

[87] M. Pouranvari and S. P. H. Marashi, "Factors affecting mechanical properties of resistance spot welds," Mater. Sci. Technol., vol. 26, no. 9, pp. 1137–1144, 2009.

[88] M. Pouranvari, "Influence of welding parameters on peak load and energy absorption of dissimilar resistance spot welds of DP600 and AISI 1008 steels," Can. Metall. Q., vol. 50, no. 4, pp. 381–388, 2012.

[89] U. T. Steels, "Resistance Spot Weldability of Galvanize Coated and Uncoated TRIP Steels," 2016.

[90] H. K. Zeytin, H. E. Emre, and R. Kaçar, "Properties of Resistance Spot-Welded TWIP Steels," vol. 9, pp. 1–13, 2017.

[91] F. Nikoosohbat, S. Kheirandish, M. Goodarzi, M. Pouranvari, and S. P. H. Marashi, "Microstructure and failure behaviour of resistance spot welded DP980 dual phase steel," Mater. Sci. Technol., vol. 26, no. 6, pp. 738–744, 2010.

[92] M. Pouranvari, P. Marashi, M. Goodarzi, and H. Bahmanpour, "Metallurgical Factors Affecting Failure Mode of Resistance Spot Welds," no. January, 2008.

[93] L. To et al., "Effect of tempering on the microstructure and mechanical properties of resistance-spot-welded," vol. 49, no. 1, pp. 133–138, 2015.

[94] M. Pouranvari, "Analysis of Fracture Mode of Galvanized Low Carbon Steel Resistance Spot Welds," pp. 36–40, 2011.

[95] M. Pouranvari, "Effect of Welding Current on the Mechanical Response of Resistance Spot Welds of Unequal Thickness Steel Sheets in Tensile-Shear Loading Condition," pp. 63–67, 2011.

[96] P. R. I. Uporovnem, T. O. Kastem, V. Naprednega, and F. V. T. Jekla, "Dependence of the fracture mode on the welding variables in the resistance spot welding of ferrite-martensite dp980 advanced high-strength steel",vol. 46, no. 6, pp. 665–671, 2012.

[97] D. S. Safanama, S. P. H. Marashi, and M. Pouranvari, “Similar and dissimilar resistance spot welding of martensitic advanced high strength steel and low carbon steel : metallurgical characteristics and failure mode transition Similar and dissimilar resistance spot welding of martensitic advanced high strengt,” vol. 1718, 2013.

[98] M. Pouranvari and S. P. H. Marashi, “Similar and dissimilar RSW of low carbon and austenitic stainless steels: effect of weld microstructure and hardness profile on failure mode,” Mater. Sci. Technol, vol. 25, no. 12, pp. 1411–1416, 2009.

[99] A. N. D. J. C. Baker, “Spot Weldability of High-Strength Sheet Steels,” pp. 19–30.

[100] Welding Metallurgy of Dissimilar AISI 430 / DQSK Steels Resistance Spot Welds,June, 2015.

[101] H. C. Lin, C. A. Hsu, C. S. Lee, T. Y. Kuo, and S. L. Jeng, “Effects of zinc layer thickness on resistance spot welding of galvanized mild steel,” J. Mater. Process. Technol, vol. 251, no. August 2017, pp. 205–213, 2018.

[102] S. P. H. Marashi, “Resistance spot welding of dissimilar austenitic / duplex stainless steels : Microstructural evolution and failure mode analysis,” J. Manuf. Process., vol. 28, pp. 186–196, 2017.

[103] N. Charde and R. Rajkumar, “Investigating spot weld growth on 304 austenitic stainless steel (2 mm) sheets,” vol. 8, no. 1, pp. 69–76, 2013.

[104] M. J. Peet, H. S. Hasan, and H. K. D. H. Bhadeshia, “Prediction of thermal conductivity of steel,” Int. J. Heat Mass Transf., vol. 54, no. 11–12, pp. 2602–2608, 2011.

[105] S. Koley, T. Ray, I. Mohanty, S. Chatterjee, and M. Shome, “Prediction of electrical resistivity of steel using artificial neural network,” Ironmak. Steelmak,pp. 1–9, 2017.

[106] W. K. Lauenroth and R. K. Steinhorst, “Neural Networks in Materials Science,” vol. 41, no. 2, pp. 181–232, 2014.

[107] M. H. Beale, M. T. Hagan, and H. B. Demuth, Neural Network Toolbox 7. 2010.

[108] P. Potocnik, “Neural Networks : MATLAB examples,” 2012.

[109] Keeler, S. and Kimchi, M. 2014 Advanced High Strength Steel Application Guidelines Version 5.0. WorldAutosteel.

[110] R. S. and R. K. R. A. Chakraborty,Mater. Charact., vol. 60, pp. 882– 887.

[111] R. Rana, S.B. Singh, and O.N. Mohanty: Corros. Eng. Sci. Technol., 2011, vol. 46, pp. 517–20.

[112] A. Bak and S. Gu ndu z: J. Automob. Eng., 2010, vol. 224, pp. 29–40.

[113] M. Takahashi: ISIJ Int., 2015, vol. 55, pp. 79–88.

[114] W.R. Osorio, L.C. Peixoto, and A. Garcia: J. Mater. Corros., 2010, vol. 61, pp. 407–11.

[115] R. Higgins, Materials for engineers and technicians. 2010.

[116] K. Weman, welding process handbook, oxford. 2003.

[117] Swift KG, Booker JD. Process selection. 2nd ed. Oxford: Butterworth- Heineman; 2003.

[118] A. Khosravi, A. Halvaee, and M. Hossein, “Weldability of electrogalvanized versus galvanized interstitial free steel sheets by resistance seam welding,” J. Mater, vol. 44, pp. 90–98, 2013.

[119] N. T. W. and W. Waddell, “High speed resistance seam welding of uncoated and coated steels”, ECSC Agreement No. 7210.KA/809,” Br. Steel Corp., pp. 1–5.

[120] M. Murali D. Tumuluru, Hong yang, Zhang, “Procedure Development and Practice Considerations for Resistance Welding, ASM Handbook, Welding,” vol. 6A, pp. 463–485.

[121] T. C. J. Saleem, A. Majid1, K. Bertilsson1, J. Saleem, A. Majid, K. Bertilsson, and T. Carlberg, "3-Dimensional Finite Element Simulation of Seam Welding Process," Elektronika Ir Elektrotechnika, ISSN 1392-1215, 19, 2013, 73-78,” pp. 1392–1215.

[122] Inoue Tomohiro, Suzuki Masahito, Okabe Takatoshi, and Matsui Yutaka, Development of Advanced Electric Resistance Welding (ERW) Line pipe ‘Mighty Seam TM’ with High Quality Weld Seam Suitable for Extra-Low Temperature Services, JFE Technical Report No. 18,” pp. 18–22, 2013.

[123] J. D. and Y. Zhou, Metall. Mater. Trans. A 34A,1501– 1511, 2003.

[124] G. P. K. and Y. Z. J. Dong, IEEE Trans. Electron. Pack. Manufac. 25,pp. 355–361, 2002

[125] J. J. M. and J. E. G. K. M. Pickett, Proc. Sheet Metal Weld. Conf. 5; AWS-Detroil Section, Detroit, MI, USA, Oct. (1992) Paper A2.

[126] X. Hu, G. Zou, S. J. Dong, M. Y. Lee, J. P. Jung, and Y. Zhou, “Effects of Steel Coatings on Electrode Life in Resistance Spot Welding of Galvannealed Steel Sheets,” vol. 51, no. 12, pp. 2236–2242, 2010.

[127] J. Peng, S. Fukumoto, L. Brown, and N. Zhou, “Image analysis of electrode degradation in resistance spot welding of aluminium,” vol. 9, no. 4, pp. 331–336, 2004.

[128] H. R. M. Costa, J. S. Dias, R. A. A. Aguiar, R. A. A. Lima, and D. M. Lopes, “The effect of process parameters on the lifetime of copper electrodes used in spot welding of interstitial free steel sheets,” Ann. “Dunarea Jos” Univ. Galati, Fascicle XII, Weld. Equip. Technol., vol. 27, no. January 2017, pp. 55–61, 2016.

[129] S. Emmer, Z. Gabrisova, J. Kovacik, P. Sejc, M. Lis, and J. Kulasa, “Microstructure changes of the tungsten insert in CuCrZr compound electrode during resistance spot welding of galvanized sheets,” 2017.

[130] S. Babu, M. Santella, and W. Peterson, “Modeling Resistance Spot Welding Electrode Life,” Oak Ridge Natl. Lab., no. November, pp. 1–16, 2000.

[131] Aslanlar S, Ogur A, Ozsarac U "Welding time effect on mechanical properties of automotive sheets in electrical resistance spot welding," Mater Des 29:1427–1431, 2008

[132] Satonaka KK, Okamoto S (2004) Prediction of tensile-shear strength of spot welds based on fracture modes. Weld World 48: 39–45.”

[133] M. Pouranvari, S. P. H. Marashi, M. Pouranvari, and S. P. H. Marashi, “Factors affecting mechanical properties of resistance spot welds Factors affecting mechanical properties of resistance spot welds,” vol. 0836, 2013.

[134] Ruuki part of SSAB, http://www.ruukki.com/~/media/Files/Steel- products/Cold-rolled-metal-colour-

coated-instructions/Ruukki- Resistance-welding-manual.pdf.

[135] Xinmin L, Xiaoyun Z, Yansong Z, Guanlong C, "Weld quality inspection based on online measured indentation from servo encoder in resistance spot welding," IEEE Trans Instrum Meas 56:1501–1505, 2007.

[136] S. Singh, R. Chhibber, K. Singh, and M. Shome, “Journal of Materials Processing Technology Resistance spot welding of galvannealed high strength interstitial free steel,” vol. 246, pp. 252–261, 2017.

[137] Properties and Selection: Nonferrous Alloys and Special-Purpose Materials, 10th Edition, Properties of Pure Metals, ASM International, Materials Park, Ohio,” in ASM Handbook, vol. 2, 1990.

[138] N. A. Freytag, “A Comprehensive Study of Spot Welding Galvanized Steel,” Weld. J., vol. 44, no. 4, pp. 145-s-156-s, 1965.

[139] P. H. and S. C. Kelley, “A Comparison of the Resistance Spot Weldability of Bare, Hot-Dipped, Galvannealed, and Electrogalvanized DQSK Sheet Steels,” SAE Pap. 880280, 1988.

[140] K. I. Johnson, “Spot Welding Electrode Life Tests on Galvanized Steel Sheet,” Weld. Inst. Res. Report, P/74/75.

[141] T. K. Pal, M. Shome, and J. Maity, “GMA Brazing of Galvannealed,” February, 2013.

[142] W. R. Upthegrove and J. F. Key, “A High Speed Photographic Analysis of Spot Welding Galvanized Steel,” Weld. J., vol. 51, no. 5, pp. 233-s-244-s., 1972.

[143] and R. J. H. J. D. Parker, N. T. Williams, “Mechanisms of electrode degradation when spot welding coated steels,” Sci. Technol. Weld. Join., vol. 3, no. 2, pp. 65–74.